MICROPOROUS CERAMIC MEMBRANES FOR GAS SEPARATION PROCESSES

S R Tennison

University of Bath

Contract JOE3-CT95-0018

PUBLISHABLE REPORT

January 1996 to July 1998

Research funded in part by
THE EUROPEAN COMMISSION
in the framework of the
Non Nuclear Energy Programme
JOULE III

INDEX

1. PARTNERSHIP

Co-ordinator
Mr S R Tennison
c/o MAST International Ltd
62 Farleigh Road
Addlestone
Surrey KT15 3HR

Co-ordinating Institution
Professor Barry Crittenden
School of Chemical Engineering
University of Bath
Claverton Down
Bath BA2 7AY

Professor Brian McEnaney
School of Materials Sciences
University of Bath
Claverton Down
Bath BA2 7AY

Ir Paul Pex
ECN
Westerduinweg 3
Petten 1755 ZG
Netherlands

Dr Nick Kanellopoulos
NCRS Democritos - MESL
GR 15310
Aghia Paraskevi Attikis
Greece

Dr David Nicholson
Imperial College of Science and Technology
Department of Chemistry
London SW7 2AZ
UK

Professor Jorg Karger
University of Leipzig
Fakultat fur Physik und Geowissenschaften
Abteilung Grenzflachenphysik
Linnerstrasse 5
Leipzig D-04103

Dr Brendan Laverty
BG Gas Research Centre
Ashby Road
Loughborough
Leicestershire LE11 3QU

Dr. Alain Methivier
Institute Francais du Petrole
Applied Physico Chemistry and Analysis Division
1 et 4 Avenue du Bois- Preau
BP311 - 92506 Rueil Malmaison
CEDEX France

Mr Simon Davies
Kvaerner Process Systems AS
PO Box 13
Billingstadsletta 38
1361 Billingstad
Norway

Dr Tim Naylor
The Smart Chemical Company Ltd
University of Greenwich
Wellington Street
Woolwich
London SE18 6PF
UK

Ir. Jaap J de Wit
Continental Engineering bv
Process Technology/Systems Development Division
Joan Muyskenweg 22
1096 CJ Amsterdam
The Netherlands

Dr Nikos Papayannakos
National Technical University of Athens
Department of Chemical Engineering
9 Heroon Polytechniou Street
GR 15773 Zografos
Athens Greece

Professor Ingo Romey
University of Essen
FB12 - Technik der Energieversorgung und Energiewirtschaft
D-45117 Essen
Germany

Dipl.Ing Gunther Haupt
Siemens AG
Coal Conversion, Oil Gasification, IGCC Technology
Dept. KWU FTP2
PO Box 3220
D-91058 Erlangen, Germany

Dr Jean-Alain Dalmon
Centre National de La Recherche Scientifique
Institut de la Recherches sur la Catalyse CNRS
2 Avenue Albert Einstein
69626 Villeurbanne
CEDEX France

Professor Ron Hughes
University of Salford
Chemical Engineering Unit
Salford
Greater Manchester M5 4WT
UK

2. OBJECTIVES

Microporous ceramic membranes have long been recognised as having significant potential in process and petrochemical environments as a means of improving their operability and efficiency. During the last decade the number of studies in this field has grown enormously in terms of both the types of membrane and the processes to which they have been applied. This is reflected in the numbers of papers and overviews that have been published. Despite this no microporous membrane has yet found its way into commercial application. This reflects several factors -

- The production of defect free and reproducible membranes is very difficult on even the small laboratory scale and it is clear that until this is fully resolved no company is likely to undertake the even more difficult process of scaling them up to commercial production until applications with clear commercial potential are found..
- The membranes are expensive given that the microporous separating layer is normally supported on a multilayer mesoporous ceramic or porous metal that is expensive in its own right even before the cost and complexity of the microporous layer is added. In the case of the palladium membranes the additional cost of the metal must also be taken into account. This inevitably limits the processes where the membranes might be applied.
- The mode of operation of the microporous membranes is extremely complex and despite major efforts is still poorly understood. This makes the optimisation and design of processes where these membranes might be used difficult and therefore a realistic assessment of the potent benefits almost impossible.

This project, which reflected the combination of three separate projects aimed at membrane fundamentals and ceramic membranes in ammonia synthesis and IGCC processes, was set up to try and address the last two of these points with the intention of providing a justification for the first.

The timing of such a programme seemed ideal in that for the first time a reasonable selection of microporous and palladium membranes were available in tubular form, that were compatible with genuine process condition testing, and where an accurate cross comparison of their performance could be achieved in a range of process applications. Some new insights into the mode of operation of the microporous membranes had also been achieved in an earlier EEC funded programme that offered the

prospect of establishing a good description of their mode of operation to carry forward the flowsheeting .and process design studies.

To achieve these very challenging goals the following team was established with the indicated responsibilities:-

University of Bath, UK	Project co-ordinator low temperature membrane process testing gravimetric adsorption and diffusion studies
ECN, Holland	High temperature membrane testing, modelling
MESL, Democritos	Membrane testing, modelling
Imperial College	Molecular simulation - adsorption and transport
University of Leipzig	pulse field gradient NMR diffusion studies
BG Technology	silica alumina membranes, membrane testing, multicomponent adsorption modelling
Institute Francais du Petrol	High temperature membrane testing
Kvaerner Process Systems	Natural gas flowsheeting
Smart Chemical Company	Zeolite A membranes
Continental Engineering bv	Ammonia and methanol flowsheeting
Uniervsity of Essen	IGCC Flowsheeting, FCC recovery flowsheeting
Siemens AG	IGCC flowsheeting
Uniervsity of Salford	palladium membrane production and testing
IRC Lyon	Silicalite membrane production, Quasi elastic electron scattering for diffusion measurement
MAST Carbon Ltd	carbon membranes

The detailed objectives of the programme are described below with the outcome of the various topics discussed in section 3.

Task 1 Fundamental Studies

Task 1 has its primary objective the development of a clear understanding of the mode of action of microporous ceramic membranes and the provision of the supporting data on the adsorption and transport properties of the membranes as database for use in the membrane flowsheeting module that is one of the main deliverables from the overall project

Task 1.1 Non equilibrium Molecular Dynamics Studies (NEMD)
Partners:- Imperial College

Imperial College will investigate the transport of molecules in confined spaces using both equilibrium and non equilibrium molecular dynamics..

Task 1.2 Diffusion by Step Adsorption
Partners:- Bath University

The diffusion constants will be measured by step adsorption techniques. These "step" measurements, which give the transport diffusivity over long distance scales, will be carried out at Bath using high pressure gravimetry. The diffusion constants are then extracted by conventional methods from the time dependence *of the weight uptake.*

Task 1.3 Diffusion by Pulse Field Gradient NMR (PFGNMR)
Partners University of Leipzig
The PFGNMR technique provides data on diffusion over a much shorter length scale than the step adsorption techniques and, as such can provide more detailed evidence for the effects of membrane and adsorbed phase structure on diffusivity.

Task 1.4 High Pressure Relative Permeability Testing
Partners Democritos
The equipment provides a sensitive test of the relative contributions of molecular and co-operative flows to the overall membrane performance.

Task 1.5 Adsorption isotherm data
Partners University of Bath, British Gas, IFP
The interpretation of all of the diffusion and transport results requires accurate adsorption isotherms for all of the species of interest. These will be measured at Bath University for the silica, silica/alumina, zeolite and carbon materials and also at IFP for the high temperature zeolitic systems. The task at Bath is effectively carried out simultaneously with task 1.2 as the isotherms are measured each time an incremental pressure step is used in the isotherm determination.

Task 1.6 Multicomponent Adsorption
Partners Bath (Materials Science) and British Gas
The original task envisaged the determination of the multicomponent isotherms using a volumetric method which required ~50ml of adsorbent. It has become apparent during the course of the project that such quantities would not be available and that even mg quantities of some of the materials is difficult. The experimental part of the objective has therefore been discontinued. By agreement with the CEC effort will therefore be concentrated on theoretical methods.

Task 1.8 Pore Diffusion Model
Partners Imperial College, University of Bath, Leipzig and Democritos
IC, Leipzig, Bath and Democritos will collaborate to develop a realistic model for the pore adsorption and transport. This will be implemented as a computer programme (compiled FORTRAN) for implementation in stand alone form and subsequently as a component of the integrated membrane model. This will incorporate the recommended multi-component adsorption algorithm from task 1.7 and will include the required isotherm and diffusion data from tasks 1.5, and 1.1-1.3.

Task 1.9 Fluid Dynamics and Finite Element Modelling
Partners Democritos and NTUA
Democritos and NTUA will collaborate to extend their existing models for flow in the membrane/support matrix (finite element) and flow in the monolith/module (fluid dynamics) to provide guidance on the impact of membrane and module structure on the overall performance of the separation system. The primary aim is to provide guidance on the extent to which these structural parameters will degrade the performance of the "real" systems relative to the performance observed in the simple tubular membranes that will be used in the test programs.

Task 1.10 Membrane Model
Partners ECN, University of Bath, Imperial College, Democritos
The main outcome of the fundamental studies will be an integrated membrane model that can be used for the evaluation/interpretation of pilot plant data and can subsequently be incorporated into the flowsheeting models for the process flow sheet evaluation. This will be an integrated model capable of extracting fundamental membrane parameters from multi-component pilot plant test data. The model will be developed by ECN in collaboration with Bath, IC and Democritos and will be implemented in compiled FORTRAN for general use in PC's and other computers.

Task 1.11 Palladium membrane Model
Partners University of Salford and ECN
The transport properties of palladium membranes are reasonably well defined. Salford/ECN will supply a model for the transport processes in these membrane systems for implementation in the integrated membrane models.

Task 2 - Membrane Production
This task encompasses the production and QC of the membranes that will be used in all of the process and fundamental test programs. The membranes to be tested in each specific process application will be identified and prioritised in the preliminary process evaluations in task 4. The membranes will be produced in a fixed tubular form, as far as is possible, to minimise problems with the use of differing reactor designs in the test programs. The membranes to be produced encompass examples of all of the known and available microporous systems (carbon, silica, silica-alumina, zeolite A and silicalite) along with a non porous palladium system.

Task 2.1 Silica Membranes
Partners ECN
ECN have considerable experience in the production of microporous silica membranes gained in a previous programme. Initial membranes will be available within 60 days of the start of the programme. Initial testing will be at Bath for the H2-hyrocarbon separation programme. Subsequently membranes will be produced as required.

Task 2.2 Silica Alumina
Initial samples will be produced for testing in task 3.1.1. Samples will be available within 90 days of the start of the programme(subject to supply of the commercial alumina support tubes).

Task 2.3 Carbon Membranes
Partners University of Bath (MAST)
Membranes will be produced by MAST under subcontract to Bath University. Initial samples will be available for the ammonia recovery tests within 60 days of the project start date.

Task 2.4 Zeolite Membranes
Partners Smart Chemical Company, CNRS Lyon, IFP
Two types of zeolite membranes will be produced and tested. SCC will produce Na exchanged zeolite A membranes. CNRS Lyon will produce silicalite membranes. The "A" membranes have the smaller pore sizes but have yet to be tested at high temperatures. The smaller pore size should allow higher selectivities and may therefore offer the opportunity of higher selectivities. Zeolite A will be evaluated for natural gas treatment and Silicalite initially for high temperature hydrogen removal. Additional high temperature testing may be undertaken on "A" when its high temperature characteristics have been checked. In addition IFP will provide further silicalite membranes for in-house evaluation only

Task 2.5 Palladium Membranes
Partners University of Salford (Johnson Matthey)
These will be purchased from Johnson Matthey by ECN and also produced by Salford. Initial evaluation at Salford will confirm the preferred membrane for the initial water gas shift and steam reforming trials and all subsequent membranes will be tested at Salford prior to pilot plant testing (2.5.3) . Salford will also undertake further membrane development to try and improve the resistance to poisons of the current systems.

Task 2.6 Powder Production
Partners University of Bath, Smart Chemical Company, ECN, British Gas

The fundamental studies at Bath and Leipzig will require specially prepared powder samples of all of the membrane materials. Each of the partners responsible for the production of the membranes (with the exception of the Pd systems) will also provide10 - 20 gram quantities of the membrane in powder form for these studies. These will be required 1 month into the programme.

Task 2.7 Comparative QC of all Microporous Ceramic Membranes
Partners ECN
ECN will be responsible for the comparative QC testing of all of the microporous ceramic membranes. The tests will include bubble point and permeability, to assess the pore structure of the membrane layer and the extent to which the membrane are free from larger (meso/macro) pore defects, along with microscopy for the determination of membrane thickness.

Task 3 - Membrane Testing
The purpose of this part of the project is two fold :-

a) to provide fundamental performance data to assist in the development of the membrane models. These tests will be carried out under broadly similar conditions to the required process conditions but will be modified to provide improved fundamental data.
b) *to provide process engineering data for use in the process screening and process design studies. In these tests the conditions will be specifically selected to mimic the anticipated process conditions*

Task 3.1 Low Temperature Testing
Throughout the low temperature testing the performance of the membranes will be evaluated using the microporous membrane models developed in task 1.10 in conjunction with the adsorption isotherm (1.5) and diffusion (1.2 and 1.3) databases to confirm the acceptability of these models for use in the more detailed process flowsheeting studies to be carried out in task 4.1 and 4.3. The low temperature testing comprises 4 sub tasks:-

Task 3.1.1 Environmental Testing
Partners Democritos (Atlantis)
To demonstrate the potential for removing aromatics from air streams in for instance printing works using microporous membranes

Task 3.1.2 Hydrogen recovery from fluid cat cracker off-gas and other refinery plant.
Partners University of Bath
To demonstrate the recovery of high value hydrocarbon components from fluid cat cracking plant for us in ethylene steam cracking plants using microporous membranes
Task 3.1.3 Ammonia recovery in process recycle streams
Partners University of Bath
To demonstrate the potential of microporous membranes for the recovery of ammonia from ammonia synthesis loops using microporous membranes

Task 3.1.4 Natural Gas Processing
Partners BGas, KPS
To demonstrate the potential of microporous ceramic membranes for the high pressure removal of carbon dioxide from produced natural gas.

Task 3.2 Medium Temperature Testing - Water gas Shift Reaction
Partners ECN. Salford
This task involves the implementation of a complete membrane-reactor system where the water gas shift catalyst will be contained within the membrane tube. Initial tests will concentrate on palladium as it is considered unlikely that the microporous systems will have adequate selectivity. This will be reviewed after the preliminary screening analysis (task 4.2). Following the initial test programme at Salford,

which appeared to show a severe inhibition of the membrane performance by water vapour and carbon monoxide, the actual "membrane reactor" testing was removed from the programme (with the agreement of the CEC) in favour of a more detailed examination of the impact of test conditions on membrane performance.

Task 3.3 High Temperature Testing

This task comprises 2 sub tasks, hydrogen removal from hydrocarbons and steam reforming. The steam reforming work is scheduled for year 2 of the programme.

Task 3.3.1 Hydrogen removal from hydrocarbons - equilibrium shifting. IFP

To demonstrate the potential of microporous membranes for the removal of hydrogen from high temperature hydrocarbon stream in for instance butane dehydrogenation processes

Task 3.3.2 Hydrogen recovery in steam reforming - ECN and Salford University

To demonstrate the use of palladium membranes in hydrogen production in the context of stand alone or IGCC processes.

Task 4 Flowsheeting Studies

This task covers two main areas -

a) *the development of the integrated membrane model for both the ceramic and palladium systems, based on the membrane flux/transport models developed in task 1, and their implementation as a module within a conventional flowsheeting programme*
b) *The evaluation of the commercial potential of the membrane systems in a variety of processes. The latter task will have two stages -a preliminary study which will be based on literature data for the various membranes and very simplistic process studies and a final detailed process optimisation study using the membrane flowsheeting module and the actual membrane performance data developed in task 3.*

Task 4.1 Module Model Development

Partners ECN, Bath, Democritos, B Gas, Continental, TUA, Essen,

To enable the detailed flowsheeting studies to be undertaken it will be necessary to extend the integrated membrane model (task 1.10) to a module capable of being implemented within conventional European process flowsheeting packages. By agreement with the CEC the complexity of the module has been reduced as it was clear that it would not be possible to extend this beyond the inclusion of the micropore model into the flowsheeting package in the time available

Task 4.2 Preliminary Screening Analysis

The task includes three separate subtasks with different partners responsible for each deliverable although ECN will be responsible for the overall task.

Task 4.2.1 Membrane Performance Characteristics

Partners ECN, Bath, B Gas, SCC, CNRS Lyon, Salford

preparation of a detailed report on the performance characteristics of the membranes available within the project and a comparison with other membranes reported in the literature

Task 4.2.2 Plant Opportunities

Partners Essen, ECN, Continental, IFP, BG, Kvaerner,

Essen will co-ordinate a review of the opportunities for improved processes from reductions in energy consumption and process capital costs through the use of ceramic membranes across the fields of hydrogen production (methanol, ammonia, hydrogen, IGCC etc.- Essen/ECN/Continental), hydrogen/hydrocarbon separation (Bath, IFP), environmental processes (Democritos and gas processing (British Gas, KPS).

Task 4.2.3 Preliminary Process Screening and Analysis

Partners **Continental, Essen, ECN, Siemens, Bath, IFP, BG,KPS, Democritos**

Continental will be responsible for a preliminary overview of the potential energy savings that could be available from the use of ceramic membranes in hydrogen generation processes. The study will be carried out in conjunction with Essen, ECN and Siemens and will involve plant optimisation studies treating unit operations as black boxes and optimising overall plant energy consumption through thermodynamic pinch point analysis. The membrane will be treated as a simple splitter using preliminary selectivity/flux data.

Task 4.3 **Final Process Analysis and Flow Sheeting Studies**

Partners **Continental, Essen, Siemens, British Gas, Kvaerner and Bath.**

The final output from the project will be a detailed analysis of the energy and capital savings and the environmental benefits that can be achieved in the processes selected in task 4.2 through the use of ceramic membrane technologies. The analysis will be dependent upon the data generated in task 3 and the viability of the flowsheeting models developed though tasks 1 and 4. Continental, Essen and Siemens in conjunction with ECN will undertake quantitative assessments of these savings for the water gas shift, steam reforming and ammonia synthesis applications. BGas and GMS-Kvaerner will provide a similar estimate for the natural gas processing industry and Bath/IFP for the hydrogen recycle process.

3. TECHNICAL DESCRIPTION

In describing the outcomes from this project it should be borne in mind that this was a fundamental project and therefore, by definition, distant in time from real commercial applications. Nonetheless the project has achieved its main objective of determining where development projects are required to build on the results obtained, where further research work is still required to confirm potential and where there appears to be little scope for further research and development. The work of the project can be split into three main areas:-

1. **Fundamentals** - in this topic the area the primary targets was to establish a better understanding of the mode of operation of the membranes to support the process flowsheeting studies and to develop the flowsheet models for the membrane.
2. **Membrane production and testing** - this was an essential part of the project as the evaluation of the membranes was critical to the flowsheeting topics. However the preparation of new membranes was not one of the objectives. Nonetheless improved membrane production techniques have evolved during the project which will impact on future commercial development.
3. **Flowsheeting** - the main aim of the project was the development of reasonably detailed flowsheets for a variety of membrane applications that could demonstrate the potential commercial viability of the overall processes from both a CAPEX and OPEX standpoint and through this provide guidance on where future development efforts should be targeted.

3.1 Fundamentals

The primary task of the fundamentals section of the programme was to supply a detailed understanding of the mode of action of the membrane systems under investigation and, in particular, to provide the membrane models for use in the flowsheeting section of the project. Whilst it was intended that these would incorporate all aspects of membrane performance, as shown in Figure 1, from single pore, through pore networks and up to complete modules this proved impossible in the time available. Nonetheless considerable progress has been made and a good foundation has been provided for further work in the microporous membrane field. In the case of the palladium membranes a detailed model was developed that was subsequently coded for use in the ASPEN flowsheeting package and used in the detailed flowsheet optimisation studies.

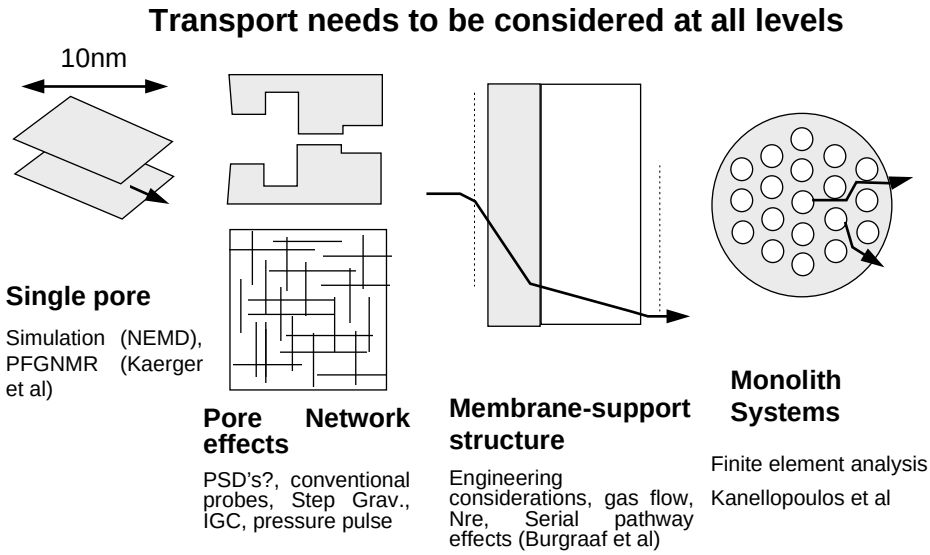

Figure 1 Aspects of Membrane Model Development

3.1.1 Theoretical Studies - Microporous Membranes

3.1.1.1 Micropore membrane modelling

In the case of the microporous membranes the fundamental performance is determined in the first instance by what goes on at the single pore level and one of the objectives was then to establish whether a single model could be applied across a wide range of different ceramic membranes (silica, zeolite A, carbon, silica-alumina and silicalite) where the underlying pore structures are very different. The two main factors influencing performance at this level are summarised in Figure 2 and comprise the multicomponent adsorption and desorption of the diffusing species into and out of the pores and the multicomponent diffusion of the species through the pores. Whilst binary adsorption has been the subject of a large number of studies, including a major JOULE programme, the ability of the accepted methods to reliably model binary mixture adsorption across a range of materials, let alone multicomponent adsorption has never been fully tested. So, whilst in this project Bath University has determined the single component isotherms for the critical gases and membrane materials, their extension to multicomponent mixtures for use in such models remains in question. However in a previous CEC funded programme on carbon membranes it was demonstrated that the ideal adsorbed solution theory could predict binary adsorption of carbon dioxide with methane or nitrogen[1,] and of binary mixtures or methane and ethane[2] if the gravimetric isotherms were corrected from excess to total[3].

Figure 2 Separating and Support Layer Effects

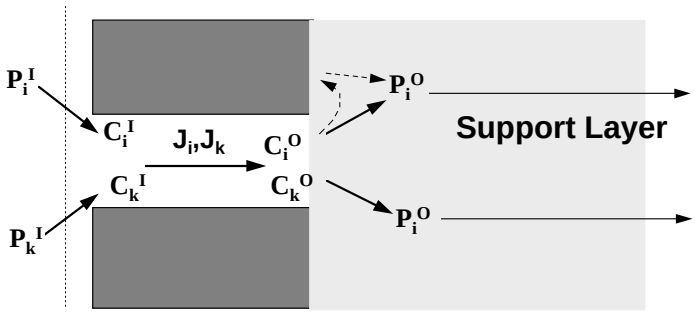

The second factor, multicomponent micropore diffusion, is even less well understood with other authors citing a wide range of transport mechanisms that might operate either in isolation or in combination. In a previous EEC project we demonstrated conclusively that effective separation at low

1 Cracknell_RF, Nicholson D, Tennison_SR, Bromhead_J, Adsorption-Jnl Int Ads Society, 1996, Vol.2, No.3, pp.193-203
2 Cracknell RF, Nicholson D, Quirke N, Molecular Simulation, 1994, Vol.13, No.3, pp.161-175
3 Cracknell RF, Nicholson D, Adsorption-Jnl Int Ads Soc, 1995, Vol.1, No.1, pp.7-16

temperatures was only likely in pores whose size was up to 2-3 time that of the diffusing molecules as above this the selectivity fell rapidly (this is of the order of 0.8nm for simple molecules) whilst in smaller pores the selectivity would in general be inhibited by molecular sieving . At higher temperatures, where molecular sieving was the primary separation mechanism, the smaller pores could be tolerated and could even be beneficial, although the selectivity was then in general reduced by adsorption effects.

If the flux through the pore for a single component is simply defined by Ficks law:-

$$-J_i = D_i \frac{dC_i}{dX}$$

where C_i is the adsorbed phase concentration gradient for component *i*, the critical question id the form of the diffusion coefficient *D*. Whilst this is called a "diffusion constant" in reality it is far from constant and it is the variation with *D* with pore structure and operating conditions that is one of the main targets of the simulation and experimental part of the programme

The challenge in the project was to search for some unifying transport theory that could account for all molecules and operating conditions. A theoretical framework for micropore transport was developed previously by Imperial College[4] and subsequently extended in this project which was then supported by both molecular simulation studies (NEMD) of pore transport and the direct determination of the diffusion characteristics using pulse field gradient NMR (PFGNMR) (Leipzig University) and quasi elastic neutron scattering (QENS) (CNRS Lyon). These have demonstrated the complexity of the behaviour and have shown that all of the materials investigated have unique performance characteristics. A particularly significant finding of this study has been the abnormal transport behaviour of the silicalite which showed severely inhibited hydrogen diffusion due to the trapping of the hydrogen in the pentacil channels of the zeolite structure. This may well the explanation for the relatively poor performance of the silicalite membranes in the high temperature hydrogen removal processes. In contrast some of the other membrane materials (carbon, zeolite A etc) appeared to show the reverse behaviour whereby the hydrogen diffused independently of the more strongly adsorbing hydrocarbon species. This implies the presence of parallel transport pathways which would tend to reduce efficiency in low temperature hydrogen separation processes but could make them more efficient in high temperature separations. Whilst all of these findings tend to imply that a single model for diffusion in microporous membranes is highly unlikely, as it will need to be modified by experimentation for these material specific effects, the NEMD studies have shown that there are some underlying fundamental principles that should be common to all microporous systems. In particular these have shown that the previous assumption of a direct link between the self diffusivity and the transport diffusivity via the Darken equation is probably seriously in error with the real transport diffusivity significantly exceeding the estimated value, an effect that we believe has been observed for the first time using a newly developed QENS technique that allows the simultaneous determination of these two parameters. These observation may also provide an explanation for the enhanced transport behaviour occasionally observed in zeolite membranes. Unfortunately the complexity of this area precluded the development of the micropore transport model that was one of main aims and this remains one of the main target areas for future research.

These studies are discussed in more detail in the following sections.

3.1.1.1.1 Model Development and Transport Theory

Two models that were developed specifically for silicalite membrane systems were have been considered within the project. Both IRC Lyon and IFP have developed models specifically for the high temperature hydrogen - butane separation. In the IRC Lyon model the separation of two components, one with a strong adsorption which depends on the temperature, the other with a negligible interaction, the transport

4 Nicholson, D. Supramolecular Science, in press (1998).

through the membrane has been represented by two equations corresponding respectively to the gas-phase and surface flows.

The Maxwell-Stefan equation stands for the gas-phase transport:

$$\sum_{j=1}^{n} \frac{x_j . N_{i,gaz} - x_i . N_{j,gaz}}{D_{ij}^e} + \frac{N_{i,gaz}}{D_i^e} = -\frac{P}{R.T}\frac{\partial x_i}{\partial r} - \frac{x_i}{R.T.P}\left(\frac{B_0 . P}{\mu . D_i^e} + 1\right)\frac{\partial P}{\partial r}$$

The surface transport, based on a Langmuir-type isotherm is accounted for by:

$$N_{i,sur} = -D_{i,eff}^{sur} c_s \frac{k_i}{(1 + k_i P x_i)^2}\frac{\partial x_i}{\partial r}$$

where the butane adsorption is described by the Langmuir isotherm and parameters like diffusivities *D* have been taken from the literature or calculated but whithin this formalism are held constant. Tye hydrogen is assumed to be non adsorbing and to simply occupy the spaces left by the butane. The set of equations has then been solved using the orthogonal collocation method. Figure 3 shows that a rather good agreement is observed between experimental results and modelling.

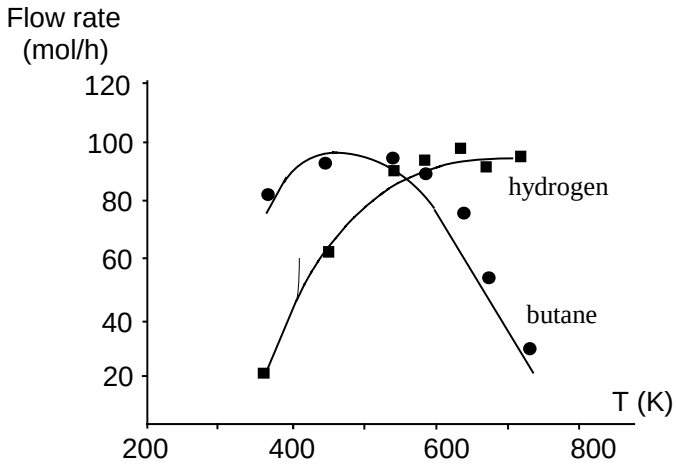

Figure 3 Observed and Calculated Silicalite Membrane Performance - IRC Lyon

IFP have developed a related model that is based excluisvely on the Stefan Maxwell diffusion equations but allows for a more comprehensive description of the hydrogen and butane adsorption. In this instance the C4 adsorption is defined by a two site langmuir model whilst the hydrogen is assumed to follow Henry's law. In this instance whilst reasonable agreement was achieved for the single component systems the performance of the model for hydrogen-butane mixtures was relatively poor. This suggests that the udnerlying assumptions, that diffusion and adsorption in the single component systems can be directly applied to the binary systems is not correct.

Whilst both of the above models utilised the Stefan Maxwell approach to transport in the micropores, with the further addition of surface transport in the IRC model, they both assumed that the diffusion constants for the components were constant and did not change from the values measured for the single components, and that the single component adsorption could be directly transferred to the binary systems.

In the work undertaken at Imperial we have sought to remove the simplifying assumptions that are inherent in these two models. A general expression for the isothermal steady state flux of a single component through a single pore, in the absence of external driving forces, can be written

$$J = -\frac{\rho D_o}{kT}\frac{\partial \mu}{\partial r_\alpha} - \frac{\rho B_o}{\eta}\frac{\partial p}{\partial r_\alpha} \qquad (1)$$

Here, J represents the number of molecules flowing in the r_α-direction through unit cross section of the pore in unit time, ($r_\alpha \equiv x$ in slit pores and z in cylindrical pores). The terms on the right hand side, represent the mass and momentum transport contributions to the flux respectively. The former is driven by the chemical potential gradient. The molecular density at r_α averaged over the pore cross section, is ρ. The diffusion coefficient D_o in equation (1) can be shown to be the sum of two parts: the self diffusion coefficient D_s and a cross correlation diffusion coefficient D_ξ ,

$$D_o = D_s + D_\xi \qquad (2)$$

The self diffusion coefficient is essentially the diffusion coefficient that would be measured by a tracer, or by experiments such as potential field gradient NMR (PFGNMR) or quasi elastic neutron scattering (QENS) and is related to the correlation of the velocity of a molecule at time t with the velocity of the same molecule at some earlier time. The cross correlation diffusion coefficient is related to a similar correlation between distinct molecules. In a single component bulk fluid, or when specular reflection of molecules occurs at the pore wall, this term becomes zero. However a single component fluid inside a pore is in effect, a two component system, and D_ξ is not zero when the wall reflection modifies molecular trajectories. The second term on the right hand side of (1) is a viscous term; in the present context ($\partial p/\partial r_\alpha$) is the gradient in the r_α-component of the pressure tensor for the fluid inside the pore.

The isothermal Gibbs-Duhem equation, relates p to μ.

$$Nd\mu = Vdp \qquad (3)$$

In slit geometry B_o is given by $H^2/12$, or in cylindrical geometry by $R^2/8$. It arises from the solution of the Navier-Stokes problem. The viscosity coefficient η may be regarded simply as a phenomenological coefficient, so the form of B_o says nothing about the behaviour of η with concentration or fluid temperature. Since η is certainly density dependent in liquids, it is to be expected that there will be an underlying spatial dependence normal to the walls because of the density gradient caused by the adsorbent field. Davis and co-workers [5,6] have proposed a method for the determination of a mean η, appropriate for confined spaces, by assuming that the viscosity at the local density corresponds to that of a bulk fluid at the same density.

Equation (1) can be recast as a Fickian diffusion equation using the thermodynamic relationship: $\mu=\mu^0+kT \ln f$, between the fugacity f of the external gas phase that is in equilibrium with the adsorbate, and the chemical potential, the resulting equation reads :-

$$J = \left[D_o + \frac{\rho kT B_o}{\eta} \right] \left(\frac{\partial \ln f}{\partial \ln \rho} \right) \left(\frac{\partial \rho}{\partial x} \right) \qquad (4)$$

where the effective (or total) Fickian diffusion coefficient, D is

$$D = \left[D_o + \frac{\rho kT B_o}{\eta} \right] \left(\frac{\partial \ln f}{\partial \ln \rho} \right) \qquad (5)$$

5 Bitsanis, I, Vanderlick, T. K., Tirell, M. and Davis, H. T., J. Chem. Phys., 89, 8126, (1988).
6 Cracknell, R.F., Nicholson, D. & Quirke, N. Phys.Rev.Lett. 74, 2463 (1995).

The term $\partial \ln f / \partial \ln \rho$ in (5) is the Darken factor which can be obtained from the inverse slope of the adsorption isotherm (ρ vs *f*). In the low concentration Henry law limit, this becomes unity. Also from the above argument, the second term in the square bracket in equation (5) is expected to be negligible at low concentration, and the contribution from cross-correlations, D_ξ , is likewise expected to vanish in this limit. Thus $D \rightarrow D_s$, the self diffusion coefficient, as $\rho \rightarrow 0$. The diffusive part of *D* is thus given by the product of D_o and the Darken coefficient. On the grounds that the D_ξ and viscous contributions to flux are expected to be small in micropores, it is conventional to define a transport diffusion coefficient (sometimes known as the Darken diffusion coefficient) by the equation,

$$D_{trans} = D_s \left(\frac{\partial \ln f}{\partial \ln \rho} \right) \qquad (6)$$

However the simulation studies carried out for this project strongly suggest that this assumption is invalid for the pore models employed. The critical issue is then to find a fundamentally sound way of estimating the variation in D_{trans} with the operating conditions. This is addressed in section 3.1.1.1.3. This theoretical background has been extended to binary processes to provide the foundation for the micropore membrane transport, and a paper detailing the first part of this work has been published in *J. Membrane Sci.*[7].

3.1.1.1.2 Binary Transport Model Development

The development of a binary diffusion equation is outlined in this section. The object was to obtain expressions for mixture transport in single pores that could be written in terms of single component properties. A subsequent stage of the model development would be to incorporate the single component equations into a network model, and then to use the results from this model as input to a flowsheeting program. Further details of the equation development can be found in [8].

The extension of this basic model, described above, to multicomponent systems introduces several new problems. For a binary mixture, comprising components 1 and 2, the equations derived by Mason and co-workers[9,10] from the statistical mechanical theory of membrane transport can be expressed in the form:

$$\begin{aligned} -J_1 &= L_{11} \nabla \mu_1 + L_X \nabla \mu_2 + \alpha_1 L_{o1} \nabla p \\ -J_2 &= L_X \nabla \mu_1 + L_{22} \nabla \mu_2 + \alpha_2 L_{o2} \nabla p \end{aligned} \qquad (3)$$

where $L_{oi} = r_i B_o / h$ and *h* is a mixed shear viscosity coefficient. The coefficients a_1, a_2 account for possible separation effects in viscous flow, they can be expressed in terms of the "osmotic" coefficients a'_1, a'_2, introduced by Mason and del Castillo[9]. The primed coefficients $a'_i \neq 1$ allow for the possibility of semipermeable behaviour, such as might occur if one species is restrained by repulsive forces from passing through the pore ($a'_i = 0$).

The phenomenological coefficients can be expressed in terms of the diffusion coefficients, D_{1M}, D_{2M}, and

---

7 Nicholson, D., J. Membrane science, 129, 209, (1997).

8 D. Nicholson, The transport of adsorbate mixtures in porous materials: Basic equations for pores with simple geometry, J. Membrane Sci., 129 (1997) 209

9 E. A. .Mason and L. F. del Castillo, The role of viscous flow in theories of membrane transport, J.Membrane Sci. 23 (1985) 199.

10 E. A. Mason and H. K. Lonsdale, Statistical mechanical theory of membrane transport, J.Membrane Sci. 51 (1990) 1

$D_X = D_{12} = D_{21}$. The coefficients D_{iM}, relate to the diffusion of species *i* within the pore in the presence of the other species, and D_X describes the interdiffusion of species 1 with species 2. The phenomenological coefficients in equation (3) can be expressed in terms of the adsorbate densities and the above coefficients by the equations:

$$kT\, L_{11} = \frac{\rho_1 D_{1M}\ (\rho_1 D_{2M} + \rho\, D_X\ )}{\rho_1 D_{2M} + \rho\, D_X + \rho_2 D_{1M}} \tag{4}$$

$$kT\, L_X = \frac{\rho_1 \rho_2 D_{1M}\ D_{2M}}{\rho_1 D_{2M} + \rho\, D_X + \rho_2 D_{1M}} \tag{5}$$

The expressions for L_{22} and a_2 are obtained by interchanging the subscripts. It is to be noted that these equations all have the same denominator, and that $a_1 = a_2 = 1$ in the absence of any semi-permeability ($a'_1 = a'_2 = 1$). The diffusion coefficients are accessible from molecular dynamics calculations through time correlations.The assumption of local equilibrium can be expressed through the Gibbs-Duhem equation for the binary mixture at constant temperature

$$\rho_1 \nabla \mu_1 + \rho_2 \nabla \mu_2 = \nabla\, p \tag{6}$$

which can be used to eliminate the pressure terms from equation (3) to give:

$$\begin{aligned} -J_1 &= \left(L_{11} + \frac{\alpha_1\ \rho_1^2 B_o}{\eta} \right) \nabla\, \mu_1 + \left(L_X + \frac{\alpha_1\ \rho_1 \rho_2 B_o}{\eta} \right) \nabla\, \mu_2 \\ -J_2 &= \left(L_X + \frac{\alpha_2\ \rho_1 \rho_2 B_o}{\eta} \right) \nabla\, \mu_1 + \left(L_{22} + \frac{\alpha_2\ \rho_2^2 B_o}{\eta} \right) \nabla\, \mu_2 \end{aligned} \tag{7}$$

It is to be noted that the reciprocal relations do not apply in (7) if $a_1 \ldots a_2$. These equations can also be written in Fickian form:

$$\begin{aligned} -J_1 &= \frac{kT}{\rho_1} \left[L_{11} + \frac{\alpha_1 \rho_1^2 B_o}{\eta}\ \right] \left(\frac{\partial \ln f_1}{\partial \ln \rho_1} \right) \nabla\, \rho_1 + \frac{kT}{\rho_2} \left[L_X + \frac{\alpha_1 \rho_1 \rho_2 B_o}{\eta}\ \right] \left(\frac{\partial \ln f_2}{\partial \ln \rho_2} \right) \nabla\, \rho_2 \\ -J_2 &= \frac{kT}{\rho_1} \left[L_X + \frac{\alpha_2 \rho_1 \rho_2 B_o}{\eta}\ \right] \left(\frac{\partial \ln f_1}{\partial \ln \rho_1} \right) \nabla\, \rho_1 + \frac{kT}{\rho_2} \left[L_{22} + \frac{\alpha_2 \rho_2^2 B_o}{\eta}\ \right] \left(\frac{\partial \ln f_2}{\partial \ln \rho_2} \right) \nabla\, \rho_2 \end{aligned} \tag{8}$$

where ($M \ln f_i / M \ln r_i$) are the Darken factors that relate to the individual component isotherms in the adsorbate mixture.

Under conditions of mechanical equilibrium (Lp=0), only the diffusion contributions to the flux, J_{iD}, remain from equation (3). The ratio of the fluxes under these conditions is:

$$\frac{J_{1D}}{J_{2D}} = -\frac{D_{1M}}{D_{2M}} \tag{9}$$

This result, which was also obtained by Mason and del Castillo by a different route, shows that the total flux is not zero under a zero pressure gradient.

When the condition of constant pressure (mechanical equilibrium) is imposed in the Gibbs-Duhem equation,

$$\rho_1 \nabla \mu_1 + \rho_2 \nabla \mu_2 = 0 \qquad (10)$$

The mean force on a particle of species *i*, F_i is $-Lm_i$. According to the Stokes equation, F_i is also proportional to the mean streaming velocity $\langle u_i \rangle$

$$F_i = -\nabla \mu_i = 3\pi\eta\sigma_i \langle u_i \rangle \qquad (11)$$

where F_i and $\langle u_i \rangle$ are components in the direction of flow and *h* is the mixture viscosity introduced in equation (3).Substitution of (11) into (10) leads to

$$\rho_1\sigma_1 \langle u_1 \rangle + \rho_2\sigma_2 \langle u_2 \rangle = 0 \qquad (12)$$

and since $J_{iD} = r_i \langle u_i \rangle$, this can be written as

$$\frac{J_{1D}}{J_{2D}} = -\frac{\sigma_2}{\sigma_1} \qquad (13)$$

Equation (13) is consistent with equation (9) if the Stokes-Einstein equation is used for D_{iM},

$$D_{iM} = \frac{kT}{3\pi\eta\sigma_i} \qquad (14)$$

This result can be confirmed by considering the total flux, $J_{1D} + J_{2D}$ under the condition Lp=0. Using equations (4) and (5) with equation (3), one finds, after some algebra,

$$-kT\ (J_{1D} + J_{2D}) = \rho_1 D_{1M} \nabla \mu_1 + \rho_2 D_{2M} \nabla \mu_2 \qquad (15)$$

If (11) is introduced into this equation, there results:

$$(J_{1D} + J_{2D}) = J_{1D}\left(\frac{D_{1M}\ 3\pi\eta\sigma_1}{kT}\right) + J_{2D}\left(\frac{D_{2M}\ 3\pi\eta\sigma_2}{kT}\right) \qquad (16)$$

which is again consistent with equation (14).

The phenomenological coefficients in the Fickian equations (8) can now be expressed solely in terms of the mixed viscosity *h*, the cross diffusion coefficient D_X, the geometric factor B_o and the osmotic coefficients a'_i. The latter are expected to be of the order of unity unless the pore width is close to one molecular diameter, or specific electrostatic effects operate on one species.

The next step is to obtain a relationship between the mixed viscosity and single component properties – the single component viscosities in the first instance. Of the several equations that have been proposed to relate mixed viscosity to individual pure component viscosities, the most successful was found [8] to be

$$\eta^{\rho} = \eta_1^{\rho_1}\eta_2^{\rho_2} \qquad (17)$$

In the limit when one or other of the component concentrations tends to zero, *h* tends to the viscosity of the remaining component, and a limiting expression for the phenomenological coefficients can be found, for example

$$kT \lim_{\rho_2 \to 0} L_{11} = \rho_1\left(\frac{kT}{3\pi\eta_1\sigma_1}\right) \qquad (18)$$

Using equation (14) gives

$$\lim_{\rho_2 \to 0} L_{11} = \frac{\rho_1 \, D_{o1}}{kT}$$

where D_{o1} is the diffusion coefficient of pure component 1 in the pore at a concentration r_1. Combining equations (14) and (17) gives an expression for the diffusion coefficients in a binary mixture in terms of those of the pure components,

$$D_{iM} \, \sigma_i = (D_{o1} \, \sigma_1)^{x_1} \; (D_{o2} \, \sigma_2)^{x_2} \qquad (19)$$

Little information is available for guidance on the construction of a model for the cross coefficients $D_{12} = D_{21} = D_X$, in pore fluids. Schoen and Hoheisel [11] studied bulk fluids and proposed a relationship for D_X which may be written in the form:

$$D_X = D_X^o \; E \qquad (20)$$

D_X^o is a weighted mean of the self diffusion coefficients of 1 and 2 in the mixture, within a thermodynamic factor that is close to unity. In the pore, the equivalent expression is

$$\rho \, D_X^o = \rho_1 \, D_{2Ms} + \rho_2 \, D_{1Ms} \qquad (21)$$

The factor E appearing in equation (20) is expressed in terms of a ratio of Lennard-Jones interaction parameters, e_1, e_2 for the components by

$$E = \left(\frac{1}{\varepsilon} + \varepsilon - 1 \right) \quad \text{where} \quad \varepsilon = (\varepsilon_1 / \varepsilon_2)^2 \qquad (22)$$

Equations (20) and (21) imply a relationship between L_{11}, L_{22} and L_X , when E=1, this is

$$\rho_1 \, \rho_2 \, L_{11} \; L_{22} - 2 \, L_X \quad (\rho_1^2 \; L_{22} + \rho_2^2 \; L_{11} \;) + 3 \, \rho_1 \, \rho_2 \; L_X^2 = 0 \qquad (23)$$

The only simulation data available to test this equation were obtained for hard sphere fluids[12]. The phenomenological coefficients obtained in these simulations were used in equation (22) to recalculate the mole fractions of the adsorbate and the calculated values were in good agreement with those reported for the simulations. This suggests that (20) and (22) are acceptable approximations. However further simulation studies of mixtures of interacting molecules in pores are needed to investigate these equations more fully.

The results from (20), (21) and (22) can be now be inserted into equations (4) to (6) to give expressions for the mixture phenomenological coefficients that depend only on molecular parameters, adsorbate concentrations, and single component diffusion coefficients:

---

[11] M Schoen, and C. Hoheisel, The mutual diffusion coefficient D_{12} in binary liquid model mixtures. Molecular dynamics calculations based on Lennard Jones (12-6) potentials, .Mol. Phys., 52, (1984) 33, 1029.

12 S-H. Suh, and J. M. D. Macelroy, Molecular dynamics simulation of hindered diffusion in microcapillaries, Mol. Phys., 58 (1986) 445; J. M. D. Macelroy and S-H. Suh, Computer simulation of moderately dense hard-sphere fluids and mixtures in microcapillaries, Mol. Phys., 60 (1987), 475.

$$kT\,L_{11} = \frac{\rho_1 (D_{o1}\sigma_1)^{x_1}(D_{o2}\sigma_2)^{x_2}\,[\rho_1\sigma_1(1+E)+\rho_2\sigma_2 E]}{(\rho_1\sigma_1+\rho_2\sigma_2)\,\sigma_1(1+E)} \tag{24}$$

$$\alpha_1 = \frac{\alpha_{1'}\rho_1\sigma_1 + \alpha_{1'}(\rho_1\sigma_1+\rho_2\sigma_2)E + \alpha_{2'}\rho_2\sigma_2}{(\rho_1\sigma_1+\rho_2\sigma_2)(1+E)} \tag{25}$$

$$kT\,L_X = \frac{\rho_1\rho_2 (D_{o1}\sigma_1)^{x_1}(D_{o2}\sigma_2)^{x_2}}{(\rho_1\sigma_1+\rho_2\sigma_2)(1+E)} \tag{26}$$

With the aid of (14) and (17), L_{oi} defined in equation (3) can also be expressed in terms of the pure component coefficients D_{oi}:

$$L_{oi} = \frac{\rho_i\, B_o}{\eta} = \left(\frac{3\pi}{kT}\right)\rho_i B_o (D_{o1}\sigma_1)^{x_1}\,(D_{o2}\sigma_2)^{x_2} \tag{27}$$

Equations (24) to (27) can now be substituted into (8), the Fickian equation for the fluxes, to give:

$$-J_1 = \frac{(D_o 1\sigma_1)^{x_1}(D_o 2\sigma_2)^{x_2}}{(\rho_1\sigma_1+\rho_2\sigma_2)(1+E)\sigma_1}$$

$$\_\{\ (\ \rho_1\sigma_1(1+E)+\rho_2\sigma_2 E + [\alpha_{1'}\rho_1\sigma_1+\alpha_{1'}(\rho_1\sigma_1+\rho_2\sigma_2)\,E+\alpha_{2'}\rho_2\sigma_2]\,\rho_1\sigma_1 3\pi B_o\ )\left(\frac{\partial \ln f_1}{\partial \ln \rho_1}\right)\nabla\rho_1$$

$$+(\rho_1\sigma_1 + [\alpha_{1'}\rho_1\sigma_1+\alpha_{1'}(\rho_1\sigma_1+\rho_2\sigma_2)\,E+\alpha_{2'}\rho_2\sigma_2]\ \rho_1\sigma_1 3\pi B_o)\left(\frac{\partial \ln f_2}{\partial \ln \rho_2}\right)\nabla\rho_2\ \}$$

$$-J_2 = \frac{(D_o 1\sigma_1)^{x_1}(D_o 2\sigma_2)^{x_2}}{(\rho_1\sigma_1+\rho_2\sigma_2)(1+E)\sigma_2}$$

$$\_\{\ (\rho_2\sigma_2 + [\alpha_{1'}\rho_1\sigma_1+\alpha_{2'}(\rho_1\sigma_1+\rho_2\sigma_2)\,E+\alpha_{2'}\rho_2\sigma_2]\ \rho_2\sigma_2 3\pi B_o)\left(\frac{\partial \ln f_1}{\partial \ln \rho_1}\right)\nabla\rho_1$$

$$+(\ \rho_2\sigma_2(1+E)+\rho_1\sigma_1 E + [\alpha_{1'}\rho_1\sigma_1+\alpha_{2'}(\rho_1\sigma_1+\rho_2\sigma_2)\,E+\alpha_{2'}\rho_2\sigma_2]\,\rho_2\sigma_2 3\pi B_o\ )\left(\frac{\partial \ln f_2}{\partial \ln \rho_2}\right)\nabla\rho_2\ \}$$

(29a,b)

Here $x_i = r_i / r$ and x_2 are mole fractions of the adsorbate components. The Darken factors in these equations relate directly to the mixed adsorption isotherm. An alternative would be to express the component fluxes directly in terms of the fugacity gradients which relate more directly to permeabilities. Onsager reciprocity does not hold in this equation. Equations (26) and (27) show that the ratio of the differential fluxes does not depend on the transport coefficients.

3.1.1.1.3 Simplified Equations

In developing an approach based on this that could be used within a membrane model for multicomponent gases a simplified form of the above model has been proposed that incorporates several major and controversial simplifications. The key assumptions are:

1. Pore network is replaced by a single pore.

2. The flux equations are expressed in terms of single component diffusion coefficients.

3. In the form presented the isotherms correlating partial pressure with adsorbed phase density are represented by Langmuir isotherms although extension to more complex forms is not problematical.

4. The viscous component is dominant under the conditions of interest. This assumption is supported by NEMD simulation.

5. Mixed viscosity is related to component viscosities by

$$\eta = \eta_1^{x_1} \eta_2^{x_2}$$

Attempts have been made to estimate the diffusivity using various correlations for single component viscosities. The most successful was the Stokes Einstein. However these correlations were only reasonably successful under a limited set of circumstances. In particular where there is no apparent inhibition to transport due to the pore becoming blocked by other molecules as indicated in the figure

When this occurs, the Stokes Einstein relationship provided a poor correlation. Unfortunately this may well prove to be the case for cylindrical cross sections and silicalite membranes in particular.

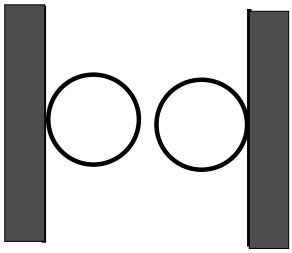

Stokes Einstein correlation good

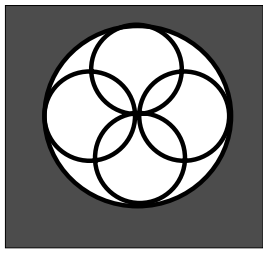

Stokes Einstein correlation BAD

Using the above development with the Stokes Einstein assumption leads to the expression:

$$kT\, L_{oi} = A \rho_i (D_{o1} \sigma_1)^{x_1} (D_{o2} \sigma_2)^{x_2} \qquad (30)$$

Where, $A = 3\,\delta\, R^2/8$ for cylinders according to the Stokes-Einstein equation. However simulation suggests that in micropores A is larger than this. We don't have any detailed expression for the dependence of A on pore size. Though simulation data, suggest that this is likely to be oscillatory rather than monotonic.

On the basis of assumption (iv) we ignore the L_{ij} terms. This is highly unconventional, but is in keeping with the tentative results from simulation.

5. The Gibbs-Duhem relation gives:

$$\nabla p = \rho_1 \nabla \mu_1 + \rho_2 \nabla \mu_2 = \rho_1 kT \nabla \ln f_1 + \rho_2 kT \nabla \ln f_2 \qquad (31)$$

where *f* is the fugacity (pressure!) in the external gas phase, and ñ is the (absolute) concentration in the adsorbed phase (number of molecules per unit volume).

Omitting the diffusion contribution leaves:

$$\begin{aligned} -J_1 &= A(D_{o1}\sigma_1)^{x_1}(D_{o2}\sigma_2)^{x_2}\rho_1(\rho_1\nabla\ln f_1+\rho_2\nabla\ln f_2) \\ -J_2 &= A(D_{o1}\sigma_1)^{x_1}(D_{o2}\sigma_2)^{x_2}\rho_2(\rho_1\nabla\ln f_1+\rho_2\nabla\ln f_2) \end{aligned} \quad (32)$$

From which the flux ratio is

$$J_1/J_2 = \tilde{n}_1/\tilde{n}_2. \quad (33)$$

The total flux is

$$-(J_1+J_2) = A(D_{o1}\sigma_1)^{x_1}(D_{o2}\sigma_2)^{x_2}(\rho_1+\rho_2)(\rho_1\nabla\ln f_1+\rho_2\nabla\ln f_2) \quad (34)$$

Assumption (iii) gives

$$\frac{\rho_1}{\rho_s} = \theta_1 = \frac{b_1 f_1}{1+b_1 f_1+b_2 f_2} \quad (35)$$

This is the mixed Langmuir isotherm, $\tilde{n}_s$ is the saturation density for $(\tilde{n}_1 + \tilde{n}_2)$.
Note that this is an absolute isotherm.

The densities can be now be expressed as fugacities (pressures):Also

$$\begin{aligned} \rho_1+\rho_2 &= \rho_s(\theta_1+\theta_2) \\ &= \frac{\rho_s(b_1 f_1+b_2 f_2)}{1+b_1 f_1+b_2 f_2} \end{aligned} \quad (36)$$

$$x_1 = \frac{\rho_1}{\rho_1+\rho_2} = \frac{b_1 f_1}{b_1 f_1+b_2 f_2} \quad (37)$$

It is readily deduced from this and from equation (33) that the limiting separation factor is (approximately) given by the ratio of the Langmuir adsorption constants.

The self diffusion coefficients are also functions of concentration. However it may be a reasonable approximation to take these as constant over the pressure range of interest.

The total flux can now be written as a function of f_1 and f_2 only,

This could be written as :

$$-J = \alpha_1\nabla f_1+\alpha_2\nabla f_2 \quad (38)$$

where $\acute{a}_i(f_1, f_2)$ is found from the preceding equation. The flux is found by integration between in going (f_i^0) and outgoing pressures (=0 if the gas is swept away at the outgoing side of the membrane).

$$Jl = \int_0^{f_1^0}\alpha_1 d f_1+\int_0^{f_2^0}\alpha_2 d f_2$$

$$-J = -J_1 + J_2$$

$$= A(D_{ol}\sigma_1)^{x_1}(D_{o2}\sigma_2)^{x_2}\rho_s^2 \frac{(b_1\int_1 + b_2\int_2)}{(1+b_1\int_1+b_2\int_2)^2}(b_1\nabla\int_1 + b_2\nabla\int_2$$

Where l is the length of the membrane. In this form the theory requires as input, the Langmuir constants, b_1, b_2 and $\tilde{n}_s$, and estimates of the (assumed constant) self diffusion coefficients at the operating density with the diffusivities at higher pore concentrations given by the viscosity correlations.

3.1.1.1.4 Modelling single component transport

To provide these diffusivity correlations a Stokes-Einstein model was investigated. This was chosen on two grounds: (i) Evidence in the literature suggested that D_ξ should be relatively small. (ii) D_s is accessible experimentally and can be easily calculated. The model exploits the simple relationship between D_s and η: $Ds=kT/3\pi\eta\sigma$ and assumes that $D_s \sim D_o$. The subsequent EMD calculations described in the previous section have shown that "true" viscosities are very much larger than the corresponding bulk values, and that D_ξ can be relatively large. Nevertheless the model is quite successful for slit pores, as illustrated in Figure 4although it fails badly for cylindrical pores. Since the molecular mechanisms contributing to D_ξ are not fully understood, it is not possible to say whether the limited success of the S-E model has any significance at the molecular level.

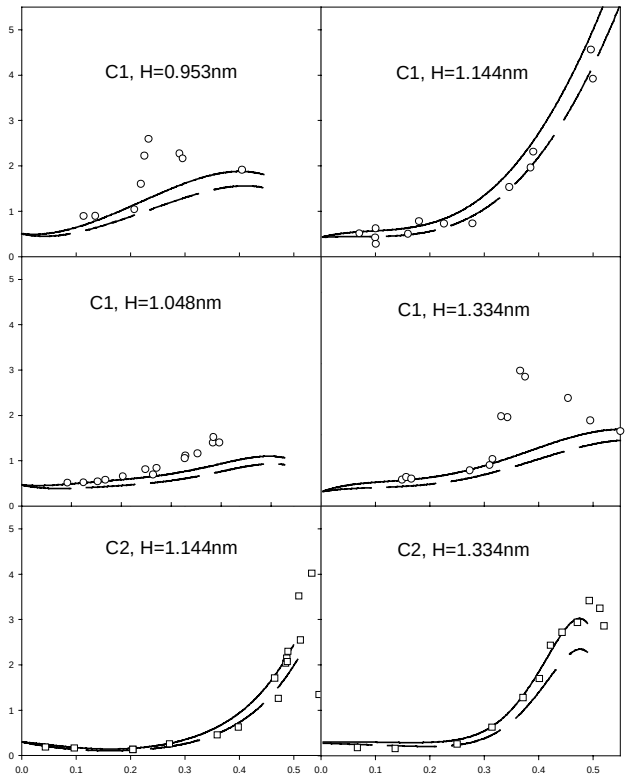

Figure 4 Total diffusion coefficient vs. Density for methane at 296K and ethane at 298K in graphitic slit pores. The points are from NEMD simulation and the full lines from the Stokes Einstein model. The broken line is for the closely related Zwanzig model.

3.1.1.1.5 Modelling of binary mixture transport

The extension of the above model introduces new problems. A key requirement for further progress is to obtain simulation data for mixture transport in micropores. Software for this purpose was developed during the project, but has not yet yielded any presentable data. It may be preferable to settle the unresolved questions surrounding single component transport, before taking the simulation studies to this stage.

3.1.1.1.6 *Simulation Studies*

The primary objective of Imperial College was to provide a better understanding of the molecular level processes relating to adsorption, separation and transport in highly confined spaces. Molecular simulation was the key approach in these studies. The main focus has been on transport processes, especially the further development and application of the non-equilibrium molecular dynamics method.

This novel technique was initiated in a previous CEC sponsored project [BRITE BREU-CT92-0568]. During the present project efforts were made to improve and extend the methodology.

3.1.1.1.6.1 Pore Models

Although a distribution of pore sizes and interconnectivity will be present in real materials, most simulation studies, as in this work, have concentrated on single pore models, since this affords the best opportunity to study fundamental molecular processes. Previous work suggests that major qualitative changes are unlikely to result when more complex pore models are constructed. Two types of model pore have been chosen for detailed investigation.

3.1.1.1.6.1.1 Graphite Pores.

Porous carbons are complex materials. However it is commonly held that the most of their essential adsorption behaviour can be modelled by graphitic slit pores, since slit pores with exposed graphitic basal planes as their adsorbing surfaces, are the most prominent feature of porous carbons. In this work the standard 10-4-3 model has been used to represent the single graphitic surface. The 10-4-3 potential models the solid as a continuum, and the potential field varies only in a direction normal to the surface. It thus takes no account of potential variation parallel to the surface planes (corrugation). The pores were modelled by two surfaces in parallel. The pore size, *H*, is the separation between the planes, measured from the centres of the first layer of carbon atoms. It is important to note that "pore size" here refers to this physically well-defined parameter. Internal or "chemical" pore sizes, as determined from adsorption measurements, are less easy to define precisely, and are significantly smaller (by ~ one molecular diameter) than physical size in the micropore size range.

3.1.1.1.6.1.2 Pseudo Atom Model

The pseudo atom model starts from an array of interaction centres (sites). Planes of atoms are used to build simple geometries (slits, cylinders, spheres). The chemical character of the pseudo atoms is specified by 12-6 parameters (ε_s, σ_s). Potentials are calculated by placing a probe species over one of the atoms in the array and summing over all interactions. Any probe at the same distance from the surface is given the same potential, regardless of its lateral position over the atoms. Thus in this form the pseudo atom potential is also essentially a continuum model in which the potential only varies normal to the surface. The parameters (ε_s, σ_s) are found by calibrating the model against a real material using heat of adsorption at zero coverage. The model has the advantage that comparisons between different geometries and surface chemistries can easily be made, and has been used, for example, to examine selectivity in methane/CO_2 mixtures [13] as a function of adsorbent properties and pore geometry. Furthermore extensions to heterogeneous surface models are readily accommodated within this framework.

In this project the parameters for modelling silica surfaces have been carefully re-examined using experimental data for argon in VPI5 for calibration. We take the chemical radius of the VPI5 pore to be 0.605nm, giving a physical radius *R* of (0.727nm) [$R=R'+0.4253I_{(Ar\text{-}O)}-I_{(Ar\text{-}Ar)}/2$]. The experimental value of $q_{st}(0)$ is 15.99kT at 77K. A single layer pseudo atom adsorbent model with parameters, ε_s/k=395K, σ_s=0.270nm, gave $q_{st}(0)$=15.96kT for Ar at 77K, and R=0.729. A 12-6 potential was used to model both atom species, for Ar we used ε/k=120K, σ=0.3405nm. The chosen value of σ_s is a reasonable estimate for oxygen.

3.1.1.1.6.1.3 NEMD simulation

The total diffusion coefficient, *D*, was found using a non-equilibrium molecular dynamics method. Details of the method were presented in the first year report and have been described in publications

13 Nicholson, D. and Gubbins, K. E., J. Chem. Phys., 104, 8126, (1996).

[6,14,15], so only a brief summary is given here. The simulation box was divided into three equal sections in the flow direction and constant chemical potentials were maintained in the two end sections by normal MC creation and destruction trials. Molecular dynamics time steps were performed on all the molecules in the system, such that the ratio of stochastic trials to dynamic steps was fairly large (~30 to 60). This establishes a concentration gradient between two constant density end sections. The flux is obtained by counting the total number (N_+ -N_-) of particles lost and gained in each end section. The rate of change of (N_+ -N_-) is then divided by the concentration gradient to obtain the total (effective) diffusion coefficient. It should be noted that this results in an integral rather than a differential diffusion coefficient.

Gaussian constraint was used to maintain a thermostat. Between 300 and 500 particles in total were used and the simulations were run for a minimum of 1.4 x 10^6 time steps. On Silicon graphics R4000, P133 processors and i860 processors, run times varied from 2 to 15 days, depending on the processor and size of the calculation. The best times (P133) may be improved by a factor of 4 on the Power PC processors, purchased for this project, and by a factor of 16 on SG R10000 processors recently acquired in this Department. A comparable performance can now be achieved with 300-400MHz PC's.

In most cases good linearity was obtained in the plots of (N_+-N_-) against time, but there is considerable fluctuation at high densities where it was observed that the adsorbate fluid tended to produce structural peaks in the flow direction. If the concentration gradient is too low, plots of number against time become extremely noisy and often display sections where extended periods of back flow occur. These runs were repeated with new parameters in order to reduce noise.

The majority of the calculations were carried out using diffuse boundary reflection conditions in which the velocity components that are independent of the adsorbent field are randomised after wall collision, in such a way as to maintain detailed balancing (Hamiltonian is conserved). In the cylinders it is necessary to transform the molecular co-ordinates into a local orthogonal frame at the point of collision.

3.1.1.1.6.1.4 EMD simulation

In earlier work equilibrium molecular dynamics was used to obtain the self diffusion coefficient. This is a relatively standard procedure requiring substantial but not excessive resources. Attempt to find D_o directly from streaming velocity autocorrelation were not initially successful because of the uncertainties caused by oscillating long time tails. The problem was revisited at the beginning of 1998 following the acquisition of a new desk top machine with large disk, memory and fast (300MHz) processor (not funded from this project). A careful study of earlier work [16] showed that both D_o, and the components of the shear viscosity coefficient, can be obtained by increasing the run length and the number of time origins sampled by a factor of about 10. The very large files generated can be readily accommodated on the high capacity disks that are now standard.

3.1.1.1.6.2 Results from simulation

3.1.1.1.6.2.1 Overview

Simulation studies have concentrated on investigating the density dependence of the transport coefficients in pores in the micropore size range for adsorbates at ambient temperatures (298K). Methane and ethane were chosen as adsorbates, and modelled as spherical molecules. Pore models included the graphitic slit pores and the siliceous cylindrical pores described above. Molecule-molecule interactions were through a Lennard-Jones potential with parameters ε/k=148K (243K) and σ=0.3812nm, (0.3950nm) for the methane (ethane) respectively. The dimensions of the pores are listed in Table 1 and Table 2

14 Nicholson, D. Carbon, in press (1998).
15 Nicholson, D. Supramolecular Science, in press (1998).
16 Schoen, M. and Hoheisel, C. Mol. Phys. 56, 653 (1985).

which also show the internal widths in terms of the molecular diameters. The third and 6th columns in Table 1 give an approximate estimate of the number of adsorbate layers

All the pore models studied had smooth continuum surfaces, and diffuse reflection was assumed.

Table 1 Graphite slit pore properties.

	C1			C2		
H/nm	H/σ	H'/σ	$1+H_{max}/\sigma$	H/σ	H'/σ	$1+H_{max}/\sigma$
0.953	2.5	0.9	1.6			
1.048	2.75	1.15	1.8			
1.144	3.0	1.4	2.1	2.89	1.3	2.0
1.334	3.5	1.9	2.6	3.38	1.8	2.5

Table 2 Silica cylindrical pore properties.

(Methane only)

R/nm	R/σ	R'/σ
0.585	1.53	1.01
0.68	1.78	1.26
0.78	2.03	1.52

It is readily apparent from these that in the region of interest, with pores of between ~0.4 and 0.8nm there is room for at most two atom layers and in most cases less than two complete layers. This brings into question models that assume variations between surface and gas phase diffusivity as there is effectively only one molecular layer at the pore wall.

3.1.1.1.6.2.2 Summary of Results NEMD

3.1.1.1.6.2.2.1 Methane in graphitic slit pores at 296K [17]

Figure 5 summarises the data for this system. The graphs show diffusion coefficient (in reduced MD units) against reduced density. Conversion from reduced units is given by the factor $D=D^*\text{x}1.06\text{x}10^{-7}\text{m}^2\text{s}^{-1}$. The open points are total diffusion coefficient, from NEMD. The closed points are the transport diffusion coefficients calculated from equation (6), with D_s from EMD.

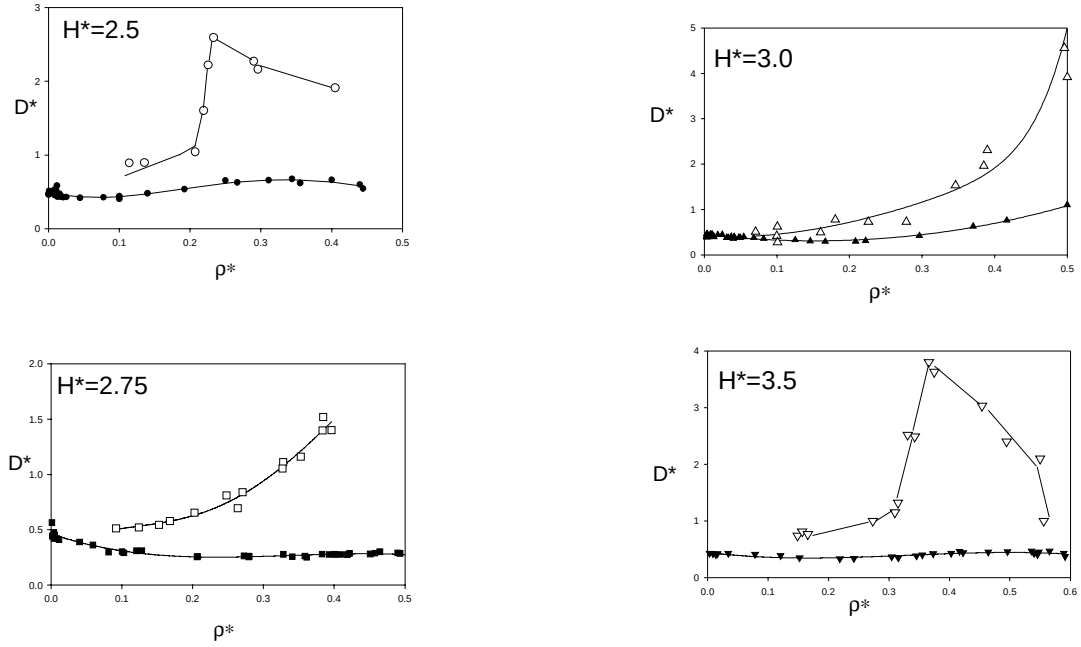

Figure 5 Reduced diffusion coefficients as a function of reduced density at 296K for methane in graphitic slit pores

The adsorption isotherms for this system (Figure 6) are all simple monotonic type 1 with no transitions or other features (although they do not fit well to the Langmuir or even the Langmuir Freundlich equation). A reduced fugacity of 1 on the horizontal scale corresponds to 370bar. Adsorbate density is with respect to the "physical" volume of the pore, so the pores approach maximum filling at around 20 to 30 bar.

17 Nicholson, D., Adams, R. W., Cracknell, R. F. and Papadopoulos, G.K. Proceedings of the 4th IUPAC Symposium on Characterisation of Porous Solids, Royal Society of Chemistry Special Publication No. 213, eds. B. McEnany, T.J. Mays, J. Rouquerol, F. Rodriguez-Reinoso, K.S.W. Sing and K.K.Unger, 57-64 (1997).

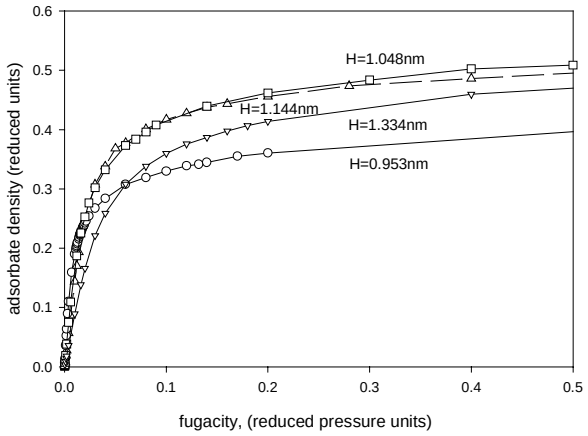

Figure 6 Adsorption isotherms for methane in graphitic slit pores at 296K

3.1.1.1.6.2.2.2 Ethane in graphitic slit pores at 298K[6]

In the bulk phase 12-6 ethane is below its critical temperature (305K) at 296K. The isotherms (Figure 7) therefore exhibit a different character, having an initially sigmoid shape (on a linear pressure scale).

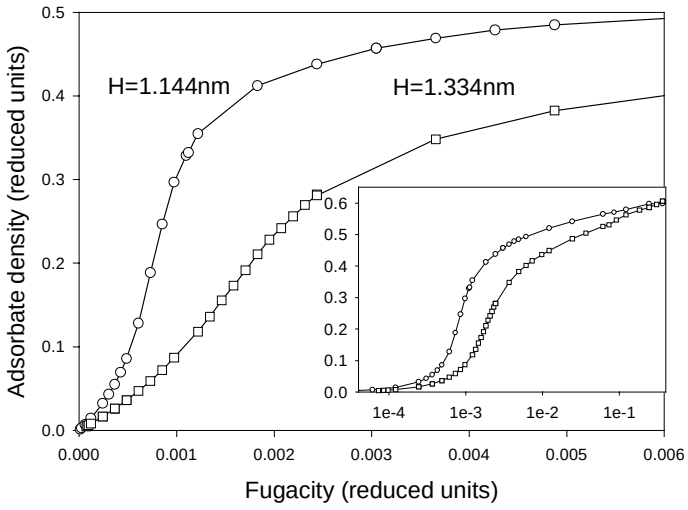

Figure 7 Ethane Isotherms at 298K in graphitic slit pores

The abscissa is fugacity (~ pressure) in reduced units which needs to be multiplied by a factor of 537 to convert to atm., so for example, a density of $\rho^*=0.4$ would be reached at an adsorptive pressure of ~1atm. in the smaller pore, and ~3 atm. in the larger pore. The smaller pore fills to a higher density at lower pressures because of the intense potential field experienced by ethane. The inset graph shows that it is only at extremely high pressure that the adsorbate density in the wider pore exceeds that in the narrower pore. It can be seen from column 7 of Table 1 that this can be attributed to misfit in packing into the larger pore.

The diffusion coefficients in reduced units are shown as a function of density in Figure 8; conversion to $m^2\ s^{-1}$ can be made by multiplying these by 1.32×10^{-7}. The self diffusion coefficients are about half the magnitude of those for methane at the same density, as expected at the lower reduced temperature. The sigmoid shape of the isotherms gives rise to a decrease in the Darken factor over the region where adsorption rises steeply. This in turn causes the transport diffusion coefficient to fall below the self diffusion coefficient in this range of density. It was found that the total diffusion coefficients from NEMD follow the same trend, which helps to confirm the consistency of the technique as well as being in agreement with the general behaviour expected from equation (1). At adsorbate densities beyond the inflection, the isotherm slope begins to decrease (the "knee" of the isotherm) and the total diffusion coefficients start to rise steeply. There is some indication that a steep "transition" occurs in the narrower pore, as noted for methane for H=0.953nm and 1.334nm. At very high adsorbate densities, D passes through a maximum. Density profiles taken in the direction of flow suggest that the adsorbate has become structured along the gradient, resembling a disordered solid rather than a liquid. The scatter of points in this high density region gives an indication of the very large error bars, and the difficulty of performing NEMD at these densities. It is interesting to note that a maximum also appears in the transport diffusion coefficients. Since the Darken factor increases rapidly here (as the isotherm slope flattens) this is indicative of very low self diffusion coefficients.

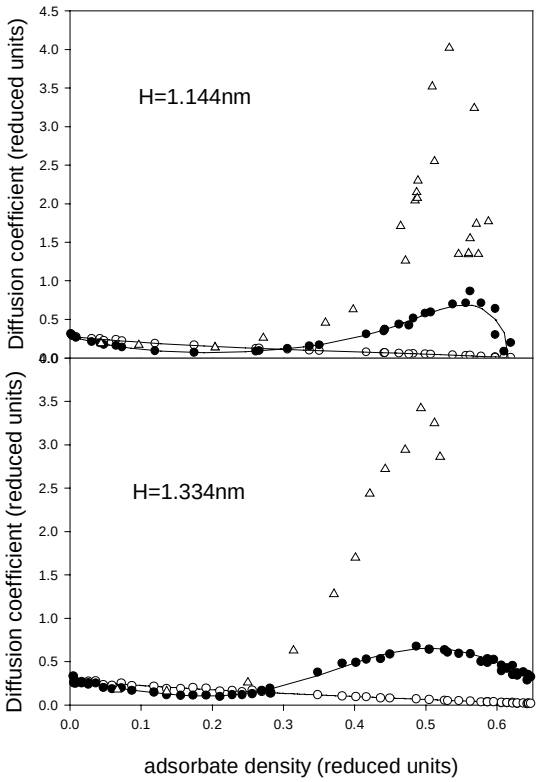

Figure 8 Diffusion coefficients for ethane in graphitic slit pores. Open triangles are the total D. Filled points D_{trans}, open circles are Ds

3.1.1.1.6.2.2.3 Methane in cylindrical pores

The isotherm and diffusion coefficient results for cylindrical pores are summarised in Figure 9 and Figure 10

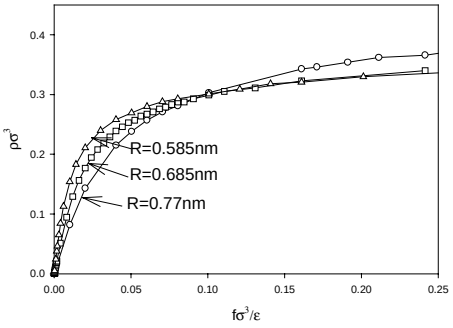

Figure 9(above) Adsorption isotherms for methane in siliceous cylindrical pores at 298K

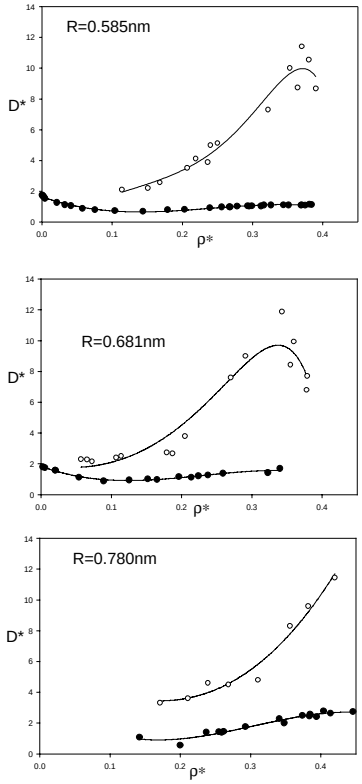

Figure 10 (right) Diffusion coefficients for methane in siliceous pores at 298K. Open points show he total diffusion coefficient from NEMD. Filled points are the transport diffusion coefficients from Ds

Three pore sizes were studied. The general trends are similar to those described for the slit pores, however it is apparent that the highest values of the total *D* are about a factor of three higher than those found in slit pores. Simulations with graphitic, rather than oxide parameters confirm that this is probably a geometric, rather than an energetic effect, suggesting that co-operative or cross correlation enhancement of the flow is greater in cylindrical geometry than in slit geometry.

3.1.1.1.6.2.3 EMD calculation of D_o and η slit pores

These calculations have been made for two of the slit pores previously studied by NEMD. The results are summarised in Figure 11 and Figure 12. The figures show the earlier NEMD results (open circles) and the total diffusion coefficients obtained from EMD and GCMC. In the latter, equation (5) was used. D_o was obtained from the mean square displacement of centre of mass and streaming velocity autocorrelation, η from autocorrelation of the stress tensor, and the Darken factor from GCMC simulations. The viscosity is calculated as three off-diagonal components of a nine component tensor; in slit pores, two of these components should be identical, whilst the third (the *xy*-component where *x* and *y* are parallel to the pore walls) turns out to be much smaller, but plays no part in transport in the *x*-direction. The route to the total diffusion coefficient is therefore entirely different from, and independent of, the NEMD method. The first thing to note is that the total diffusion coefficients are of the same order of magnitude from both calculations, supporting the conclusion that *D* is much larger than D_{trans}, even in highly confined spaces. Secondly it can be seen that the largest part of *D* comes from D_o. In accord with the formal theory, the viscous component increases with pore width and can be a substantial part of *D* when $H=3.5\sigma$. Closer examination of the viscosity coefficient shows that by far the largest contribution arises from the adsorbent field contribution to the stress tensor. Bulk fluid viscosities at the mean adsorbate density are substantially lower. If these were used in equation (5), the viscosity contribution to

D would be a factor of 4 or more higher (depending on density, pore width etc) – which explains the moderate success of the Stokes-Einstein modelling of *D*.

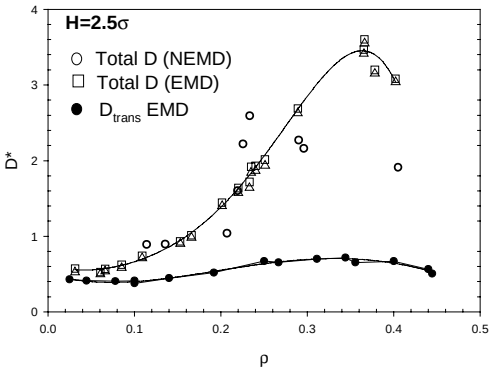

Figure 11 Methane diffusion coefficients from NEMD and EMD at 296K in graphitic slit pore, H- 2.5σ

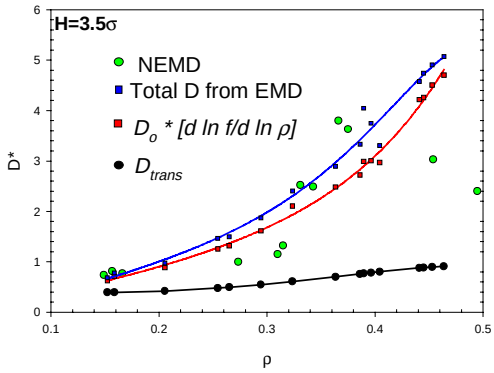

Figure 12 Methane diffusion coefficients from NEMD and EMD at 296K in graphitic slit pore, H=3.5σ

Thirdly it may be noted that the total diffusion coefficient, calculated by the EMD/GCMC route is not in quantitative agreement with NEMD results, and indeed is even qualitatively different in that it exhibits no transitions, and that *D* tends to be substantially larger at high densities. The reasons for this discrepancy are not clear. Several possibilities can be considered:

(i) NEMD calculates a *D* that is a mean value with respect to density. The error involved can be estimated using the new EMD data. The calculations suggest that the correction terms are not large enough to account for the discrepancy.

(ii) there are substantial error bars involved in both calculations, however the underlying trends appear to be both systematic and outside the estimated error bars.

(iii) The existence of a density gradient may alter the transport coefficients, but again only small corrections would be expected.

(iv) the largest discrepancies occur at very high densities. The pressures needed to achieve such densities would be >7atm. Distribution functions obtained during the simulations indicate that the adsorbate has an ordered solid-like structure under these conditions which may lead to uncertainties in both methods.

3.1.1.1.6.2.4 Transport at very low densities in cylindrical pores

The limiting behaviour of the transport coefficient of an ideal gas inside a cylindrical pore space with diffusely reflecting walls is well known, and is given by the Knudsen diffusion coefficient. It is therefore of interest to investigate this limit as a means of (a) testing and validating the software (b) comparing the results from more realistic models with this known limit. The problem turns out to require very large resources and some revision of techniques. It was found that the limiting diffusion coefficient at very low concentration is below the Knudsen value, as anticipated from earlier work, but rises rapidly to a value much greater than the Knudsen limit when molecules can interact dynamically. It is of interest that this enhanced diffusion apparently occurs within the Henry law adsorption range, so that this equilibrium behaviour reflects lack of significant intermolecular interaction. The suggested mechanism for this effect is one where molecules undergoing close encounters tend to pull each other away from the adsorbent walls, thereby generating long trajectories.

3.1.1.2 Pore Network Effects

The extension of the single pore models to full pore networks has been investigated by Democritos. It is not possible at this stage to quantitatively assess the precise impact of the extension from single micropores to complete networks on overall performance as the calculations have been limited to mesoporous structures. Nonetheless it is possible to see that complex pore shapes and interconnectivities will impact severely on pore transport properties. If the intention in the future is to measure the pore diffusivity through a technique such as PFGNMR it will be necessary to modify these values to take account of the pore network effects. More work will be necessary in the network modelling field to allow this.

3.1.1.2.1 PORE STRUCTURAL CHARACTERISATION BY GAS PERMEABILITY MEASUREMENTS

The permeability of micro- and mesoporous membranes is an important parameter in the evaluation of these membranes for gas separations. Consequently a number of theoretical approaches have been employed to predict gas permeability and to understand how it is related to the pore structure of the membrane. The most popular approach has been the network model in which the pore space is represented as a graph of sites connected by bonds[18]. In such a graph, the sites correspond to pore bodies while the bonds correspond to the pore throats connecting the pore bodies. A modification of the general network model is the capillary network model where the sites have zero volume and are connected by long capillary tubes representing the pore throats[19]. This model is particularly useful when simulating slit-like geometry, or crystalline materials such as zeolites. On the other hand, it fails to represent accurately granular materials based on regular or random packing of spheres. Since for the purpose of the present work we are mainly interested in the former type of materials we are only focused on the capillary network models.

3.1.1.2.1.1 Construction of Capillary Networks and Effective Medium Models

Consider a three dimensional regular network of capillaries with radii r, randomly selected from a distribution function $f(r)$, defined in the range $[r_a, r_b]$. Such a network is constructed by taking each bond connecting the node at the origin of the network with nodes located at all edges, center-phases and center-edges of the cubic unit cell. The nodes (sites) themselves are not assigned any pore volume or resistance. The above unit cell construction when repeated in space leads to a regular network with its maximum connectivity, z, of 26. Lower connectivities are obtained by setting r=0 at the appropriate bonds each time, in order to maintain network regularity. Following this procedure three dimensional regular networks of connectivity 18, 12, 8, 6 and 4 can be constructed.

. An alternative approach to the sophisticated yet computer intensive network models is the single-bond Effective Medium Approximation (EMA)[20,21,22]. According to this method, a disordered medium is replaced by a hypothetical homogeneous effective one, having the same conductance, between all neighboring sites. This conductance is determined by requiring the average of all potential fluctuations with respect to a distribution of conductances in the original disordered medium to be zero. This leads to an integral equation which can be readily solved numerically or in certain cases analytically.

---

[18] Fatt I., Petrol., Trans. AIME **207**, 144 (1956)

[19] Nicholson D. and Petropoulos, J. of Phys. D: Appl. Phys., **4**, 181 (1971)

[20] Koplic J., J. of Phys. C **14**, 4821 (1981)

[21] Kikkinides E.S., Tzevelekos K.P., Stubos A.K., Kainourgiakis M.E. and Kanellopoulos N.K. "Application of Effective Medium Approximation for the Determination of the Permeability of Condensable Vapours Through Mesoporous Media." *Chem. Eng. Sci*, **52**(16) 2837 (1997).

[22] Kainourgiakis M.E., Kikkinides E.S., Stubos A.K. and Kanellopoulos N.K. "Adsorption-Desorption Gas Relative Permeability through Mesoporous Media. Network Modeling and Percolation Theory" *Chem. Eng. Sci.,* **53**(13), 2353 (1998).

3.1.1.2.1.2 Gas Relative Permeability

In principle, the network model can be related to the geometry and the topology of pore space, so that flow through the network is equivalent to flow through the porous medium. Direct replication, however, has proven elusive because the pore space in real porous solids is quite complicated. A standard method which is employed to study the effect of structural characteristics on the flow behavior in the porous membrane is the gas relative permeability method, where we block part of the pore space and measure the permeance of a non-adsorbable gas[23,24].

For the case of micro- and mesoporous media, the effect of pore blocking on the overall transport process is achieved by introducing a stationary condensed phase of an adsorbed vapour into the porous material and subsequently measuring the permeability of a second non-adsorbable gas which does not condense in the pores at least under the conditions of the experiment. Several attempts have been made to relate relative permeability curves with microscopic structural parameters of the porous material[25]. The present study focuses on the construction of relative permeability curves for stochastic three dimensional networks with particular emphasis in the neighborhood around the percolation threshold, where previous models have proved to be inadequate. Percolation theory is also applied and compared to the results from the three dimensional networks and EMA models. Bethe trees, which are lattices that do not admit reconnections, are also considered since they can give simplified expressions for several properties of the porous medium, while at the same time retain most features of percolation theory[26].

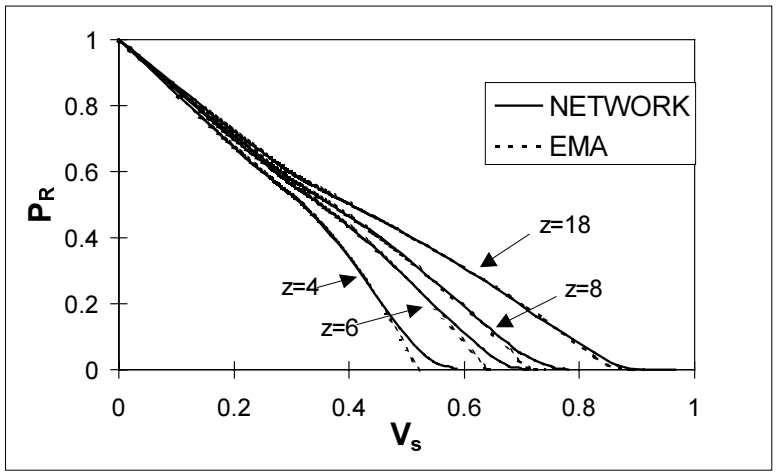

Figure 13. Effect of connectivity on gas relative permeability curves.

During adsorption, pores are blocked by the adsorbed gas randomly. Gas flows through the supercritical pores following Knudsen flow, (assuming long capillaries). In Figure 13, relative permeability curves computed by the network model are plotted for different values of the connectivity, z. EMA results are also shown in this figure, for comparison purposes. It appears that as z increases the P_R curve becomes broader as it approaches the percolation threshold, V_{SC}. In all cases EMA is in very good agreement with the network solution, except in the neighborhood of V_{SC}. In that region, the EMA predicted P_R curve decreases linearly with V_S, while the network solution results in a non-linear behavior and reaches a higher percolation threshold, V_{SC}. This is because V_{SC} predicted by the network model corresponds to the theoretical f_{bc} predicted by percolation theory ($f_{bc} \sim 1.5/z$)[27], while V_{SC} found by EMA corresponds to $f_{bc}=2/z$ [27].

Thus it appears that relative permeability curves follow percolation theory, since they satisfy both the theoretical percolation threshold and the scaling law for three dimensional networks [26,27]. The same conclusion is valid for different pore size distribution functions $f(r)$.

23 Ash, R., Barrer, R.M. and Pope, C.G., Proc. R. Soc. London, Ser. A, 271, 19 (1963)
24 Ash, R. Barrer, R.M. and Sharma, R.J. , J. Membr. Sci. 1, 17 (1976)
25 Petropoulos J.H., Petrou J.K. and Kanellopoulos N.K., Chem. Eng. Sci., 44, 2967 (1989)
26 Sahimi M., Gavalas, G.R. and Tsotsis T.T., Chem. Eng. Sci., 45, 1443 (1990).
27 Shante V.K.S. and Kirkpatrick, S., Adv. Phys., 20, 325 (1971).

When comparing the theoretical results from 3D network modeling, it was found that as the percolation threshold is approached, all relative permeability curves regardless pore connectivity and/or pore size should have a universal behavior:

$$P_R \propto \left(1 - \frac{V_S}{V_{SC}}\right)^t \qquad (1)$$

where t is a universal critical exponent predicted by percolation theory to be around 1.9±0.1.

Observations from three different sets of experiments have been considered including various adsorbates and materials differing in chemical structure, pore connectivity and pore size distribution. In Figure 14 P_R is plotted against 1- V_S / V_{SC}, in a logarithmic plot. Evidently, the behavior of P_R near f_{bc} follows the scaling law of percolation theory regardless the porous medium's topology, which only affects the pre-exponential factors, or equivalently the corresponding ordinates in Figure 14. The slopes of all reduced relative permeability curves in Figure 14 lie close to 2 (from 1.85 to 1.91). It is interesting to point out that in some experiments [23,24] the porous medium is nearly microporous (Carbolac 1 with a pore size distribution from 7 to 15 A) and hence the validity of Kelvin equation for capillary condensation is questionable. Nevertheless, this does not affect the behavior of the reduced relative permeability curves near the percolation threshold. Thus, the above results indicate that the behavior of the reduced gas relative permeability curve in mesoporous media is universal regardless the topology of the porous medium and the nature of the adsorptive gas and obeys the scaling law of percolation theory as expressed by eq. (1).

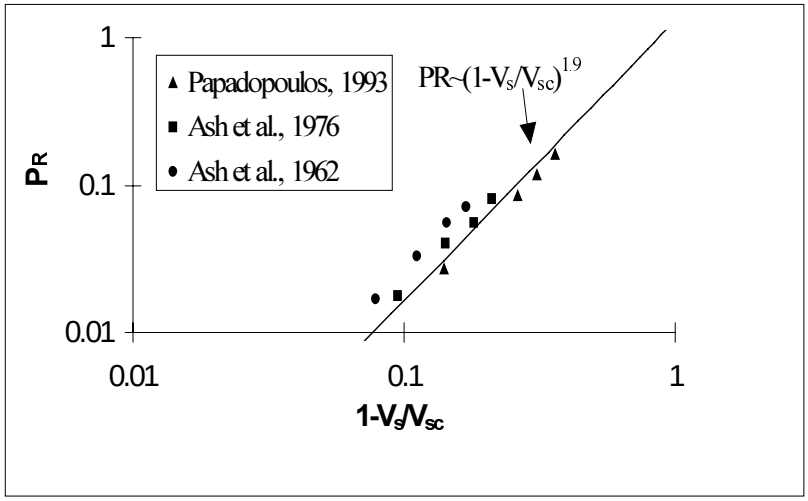

Figure 14. Universal behavior of gas relative permeability near the percolation threshold.

3.1.1.2.2 Condensable Vapour Permeability

The flow of a condensable vapour through a mesoporous membrane is a phenomenon of great complexity. As the membrane is exposed to a certain vapour pressure gradient, adsorption, capillary condensation and surface flow phenomena occur at the same time, during the initial stages of the experiment. As the system reaches a steady state, a film of adsorbate has been formed on the pore walls, while at the same time capillary condensation occurs in the subcritical pores.

It is clear that the three phases of the penetrating fluid coexisting in the porous matrix, contribute independently to the overall permeability.

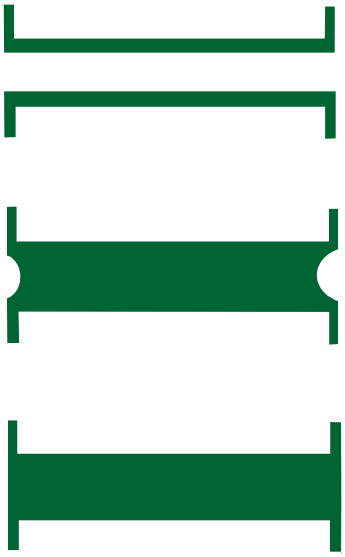

Gas + Surface Flux ($r < r_k$)

$$J_g = \left(\frac{32\cdot\pi\cdot M}{9\,R\cdot T}\right)^{\frac{1}{2}}\cdot(r-t)^3\cdot\frac{\Delta P_g}{l} \qquad J_s = \frac{2\cdot\pi\cdot r\cdot\chi^2\cdot R\cdot T}{P_m\cdot C_R\cdot S^2}\cdot\frac{\Delta P_g}{l}$$

Capillary Enhanced Flux ($r_k \le r < t$)

$$J_c = \frac{\pi\cdot r^4\cdot\rho_l}{8\cdot n_l}\left[1+\frac{(r-t)^2}{r^2}\cdot\frac{\rho_l\cdot R\cdot T}{M\cdot P_m}\right]\cdot\frac{\Delta P_g}{l}$$

Liquid Poiseuille Flux ($r \le t$)

$$J_l = \frac{\pi\cdot r^4\cdot\rho_l}{8\cdot n_l}\cdot\frac{\Delta P_g}{l}$$

Figure 15. Different flow regimes developed inside the individual pores, depending on the specified pressure gradient across the network.

Depending on the specified pressure gradient across the network, different flow regimes may develop inside the individual pores (Figure 15). At low enough mean pressures, the observed mass flux is considered to be made up of non-adsorbed molecules moving in the free pore space, (gas phase component, J_g) and of adsorbed molecules moving along the pore wall surface (surface flow component, J_s). The mechanism of the gas-phase varies from diffusive to viscous depending on the gas concentration (or equivalently pressure). Following multilayer adsorption on the pore wall, capillary condensation occurs at high enough pressures, as indicated by the Kelvin equation.

Equation describing the flow in the capillary enhanced regime, when compared to Poiseuille's law for viscous condensate flow, is characterised by an enhancement factor ($\tilde{n}_l RT/MP_m$), which is physically attributed to capillary pressure gradients[28,29]. Indeed, an additional driving force occurs due to the difference in the curvatures of the menisci that are formed between nodes and bonds filled with condensate. This capillary action is gradually diminishing as the mean pressure increases for a given bond. The reason is that the menisci begin to flatten as the pressure is raised above Kelvin equilibrium conditions. This effect is taken into account by multiplying the enhancement factor with the term $(r-t)^2/r^2$, as suggested by Lee and Hwang[9]. It is clear that the effect of the enhancement factor decreases as t increases, and is totally eliminated at the relative pressure where the condition r=t is fulfilled. At this particular relative pressure the liquid surfaces at the end of the bonds are planar. From this relative pressure on and up to saturation conditions, the flow obeys the liquid Poiseuille formulation.

Presently, two and three-dimensional networks with pore connectivity of z=4, 6 and 8, are considered. The theoretical case study involves the flow of freon 113 on Vycor glass at 314.5K; surface flow has been neglected for the shake of simplicity. The results are presented in Figure 16. It is evident that as the pore connectivity increases the maximum permeability value also increases. In addition, the higher the network connectivity, the lower the relative pressure, at which the capillary enhancement effects start becoming significant. In the same figure (Figure 16) the permeability curve for the case of a three dimensional regular network with z=6 is also shown in comparison with the curves for the two dimensional networks. When looking at the two curves with z=6, it appears that the 3D case shows a considerably lower maximum permeability value compared to the 2D case. This result should be

28 K.H. Lee and S.T. Hwang, J. Colloid. Interf. Sci., 110, 554 (1986).
29 Tzevelekos K.P, Kikkinides E.S., Stubos A.K., Kainourgiakis M.E. and Kanellopoulos N.K. ,Advances in Colloid and Interface Sci., 76-77, 373 (1998).

expected because for the 3D case although the connectivity is 6, there are only 4 bonds in each plane in the direction of flow. Thus the permeability curve for z=6 in three dimensions looks closer to the permeability curve for z=4 in two dimensions.

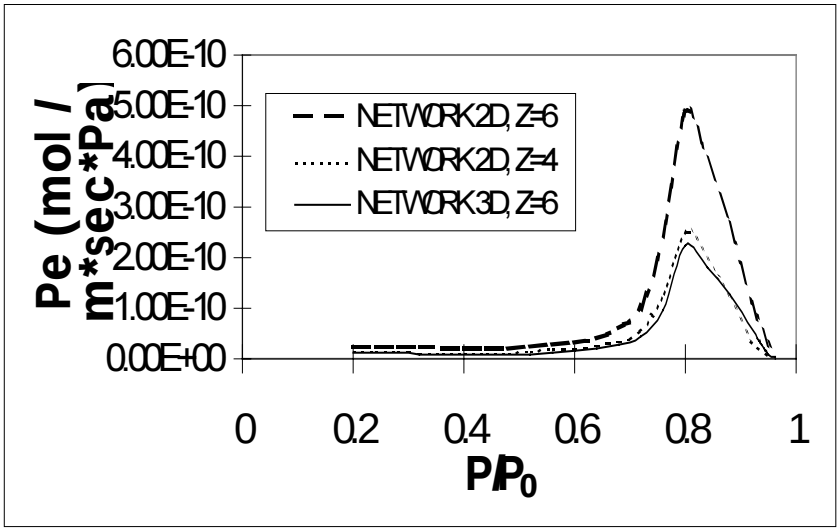

Figure 16. Freon permeability on Vycor glass (Uniform p.s.d. with Rm=30Å and ó=15Å) for various network dimensionalities and connectivities.

In order to visualise the percolating behaviour of the capillary enhanced "super-conducting" pores two 3D snapshots for a 10x10x10 network at P/P_0=0.55 and at P/P_0=0.622 are presented in Figure 17a and Figure 17b. The first snapshot corresponds to a fraction, p, of only ~10% of capillary condensed pores where no percolating cluster is formed across the network. In the second snapshot where ~25% of capillary condensed pores appear, a percolating cluster spans across the network. This result is again in accordance with ordinary percolation theory, according to which the percolation threshold, p_c, for the case of simple cubic lattice (z=6) is ~0.25.[27]

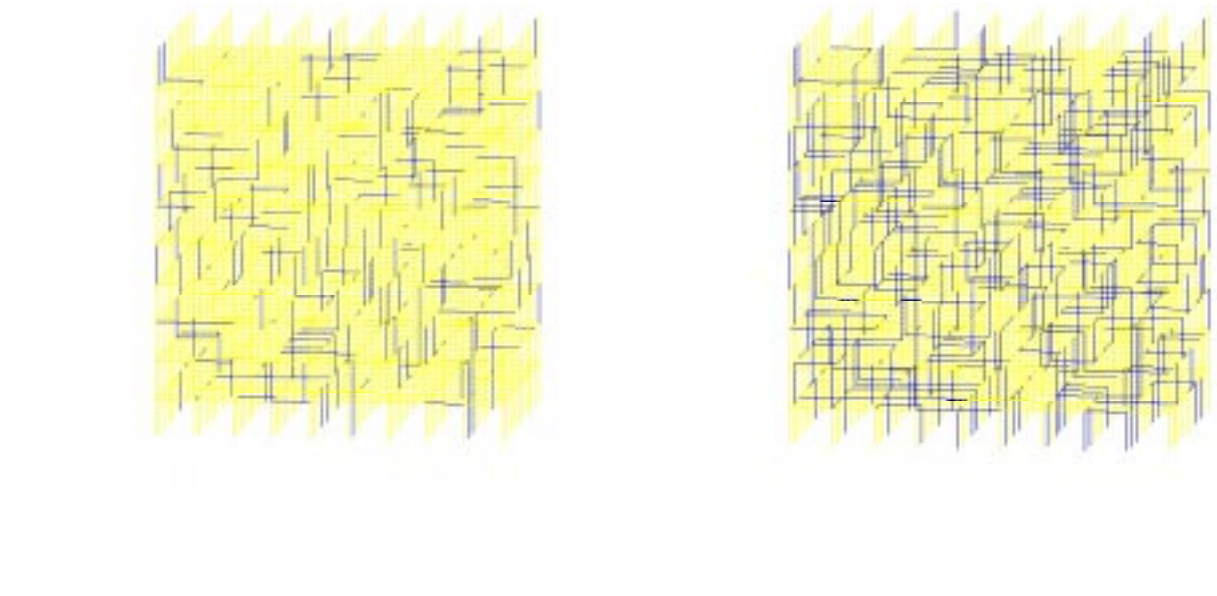

(a) (b)

Figure 17. Network snapshots for regular cubic lattice (z=6) at a) P/Po=0.55 and b)P/Po=0.622. Gray pores follow gas + surface flow, and black pores follow capillary enhanced flow.

Experimental data from the literature[28] concerning freon 113 permeability on a vycor glass membrane were simulated by the 3D network model. An average effective length of each pore was selected in a way that the (non-condensing) helium permeability predicted by the network matches the experimental values, and at the same time gives a porosity and surface area close to the experimental ones for this material.

Subsequently, the pore size distribution obtained from porosymetry and the effective pore length were used for the simulation of the condensable vapour permeability.

The agreement between the experimental points and the theoretical results is excellent, for two different temperatures, as can be observed from Figure 18. This agreement is attributed mainly to the narrow pore size distribution of the vycor membrane, as well as to the shape of the pores for vycor which appear to be well represented by cylinders.

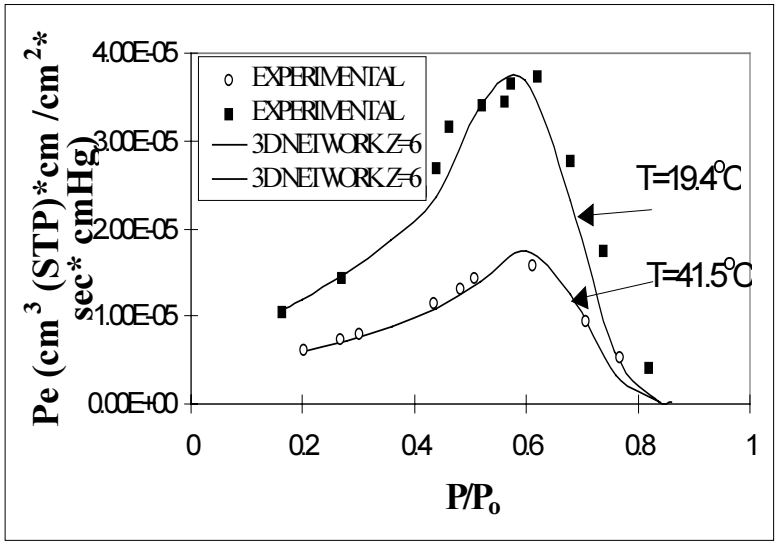

Figure 18. Comparison of network and experimental results[28] of Freon 113 permeability on Vycor glass membrane.

3.1.1.2.2.1 Effect of Pore shape and length

So far we have assumed infinitely long capillaries in our network models. However, this need not necessarily be the case. It is therefore important to see the effect of other pore geometries in the value of the diffusion coefficient, even for the simplest case which corresponds to Knudsen diffusion. Since in the general case the Knudsen diffusion coefficient is given by:

$$D_K = (f_T L)\, u_T/4 \qquad (2)$$

where L is the length of the pore, $u_T=(8RT/\pi M)^{1/2}$, is the mean thermal speed of the molecules, and f_T is the fraction of molecules transmitted across the pore of length L. For large values of L, the product $f_T L$ reaches a constant value of 8/3. Substitution to eq. (2) results in the classic expression for Knudsen diffusivity in an infinitely long tube.

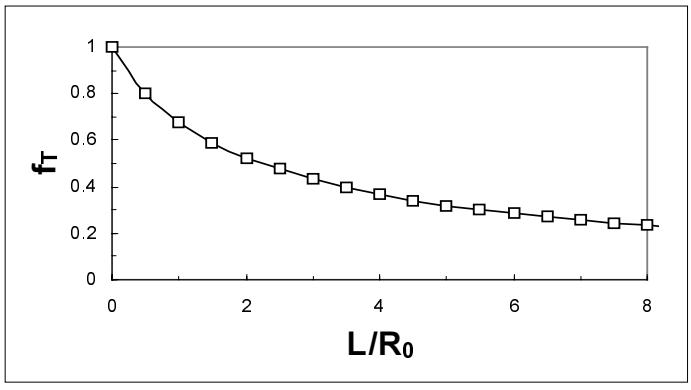

Figure 19: Effect of tube length on the transmission probability

in Knudsen flow

3.1.1.2.2.2 Short tube effects

When varying the length of the pore L to low values then the assumption of infinitely long capillaries may be no longer valid. To study the effect of L on the value of D_K one has to resort to Monte Carlo simulations using either mean square displacement[30] or test particle methods[31]. In this work we have employed the test particle method details of which can be found elsewhere. Results are shown in **Figure** 19 for the value f_T vs L/R_0, the aspect ratio of the cylinder.

30 Burganos V.N. and Shotirchos S.V., Chem. Eng. Sci, 44, 2451 (1989
31 Davis D.H., J. of Applied Physics, 31, 1169 (1960).

From the above figure it appears that as L/R_0 increases f_T drops to zero as expected. However the product $f_T L$ reaches an asymptotic value which corresponds to the classic expression for Knudsen diffusion in an infinitely long tube.

3.1.1.2.2.3 Hyperbolic pore shape

A more realistic pore shape is that of a converging-diverging geometry which is a combination of a short tube connecting to large spherical pores. In such a geometry the same simulation scheme as above can be applied in order to estimate the value of f_T. A typical particle trajectory is shown in Figure 20.

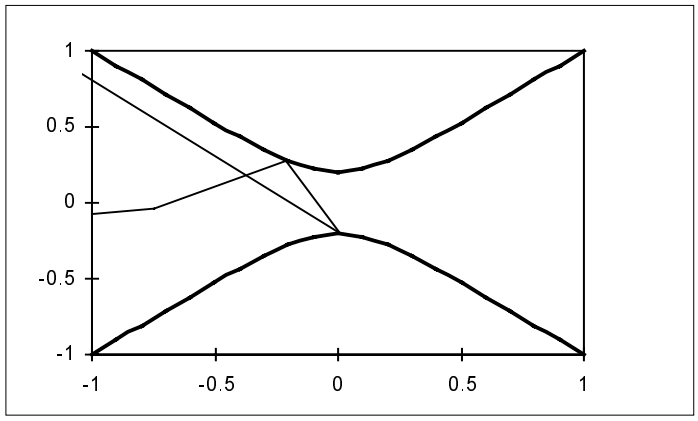

Figure 20: Typical particle trajectory in a pore of hyperboloid shape during Knudsen flow

The result for a hyperbolic type of pore in terms of D_K/D_{K0} (D_{K0} being the Knudsen diffusivity for the case of a cylinder with radius R and length 2R) for different values of throat over pore radius is shown in **Error! Reference source not found.**

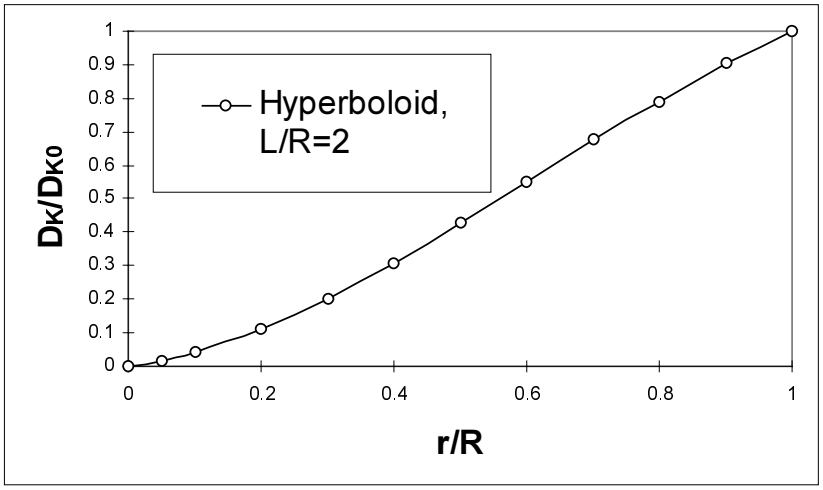

Figure 21 Ratio of diffusivities in hyperboloid and cylindrical pores of the same length and maximum radius size vs minimal to maximal radius ratio.

From the above results it is evident that the radius of the throat can have a severe effect in the value of the diffusivity even for the simplest case of Knudsen diffusion.

The above approach can be fairly easily extended to more complex pore geometries of the chamber and throat type, by adding a sort cylindrical part in the hyperboloid. A typical result form the test molecule method is shown in **Figure 22**, for the shake of completeness.

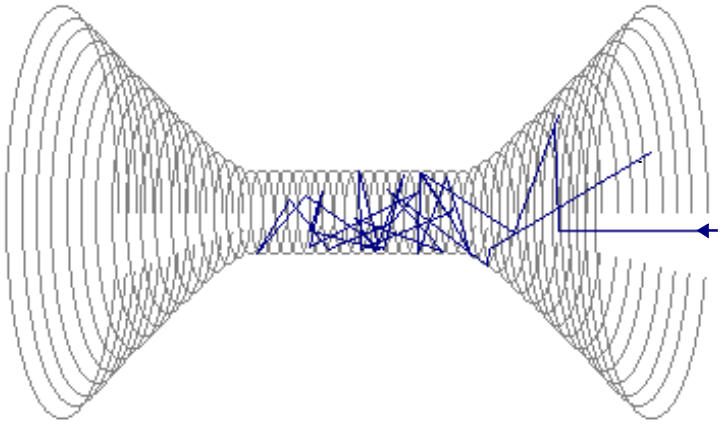

Figure 22: Typical particle trajectory in a chamber-and-throat pore during Knudsen flow

3.1.1.2.2.4 Microporous Materials

The above approach has been successfully applied, so far, to mesoporous materials. For the case of microporous materials a similar analysis can be performed provided that we get information for the individual pore diffusion as a function of the pore radius. Since these results are obtained through computationally expensive molecular dynamics simulations, we can only expect a limited number of diffusivities vs pore radii. Nevertheless, these points can be stored in a data bank and one can generate as many points as he wants through proper interpolation schemes. The accuracy of such an approach obviously depends on the number of diffusivity points that we have available.

3.1.2 Palladium Membrane Model

For the palladium membranes, where the complexity associated with adsorption and transport in pores and pore networks is absent, a detailed model was developed, based on Sieverts law. This is similar to other models presented in the literature as the only variable is the exponent (0.82 in this study). This was subsequently coded by ECN into an Aspen module for use in the flowsheeting studies by Continental Engineering, Siemens and Essen University which also incorporated a non selective parallel pathway to allow for leaks in the system. This has allowed the development, we believe for the first time, of fully optimised flowsheets for a variety of high temperature processes.

For the model which is used to describe the transport through the palladium membranes the flowing assumptions have been used:

- steady state;
- ideal gas law is applicable;
- isothermal process;
- ideal thermal mixing;
- no pressure drop;
- no mass transfer limitations;
- no influence of geometry.

An extensive description of a palladium membrane model has been made[32]. The following general expression, known as Sieverts law, for transport of hydrogen through palladium membranes has been used:

$$J_{H_2} = Q_{H_2}\left(P^n_{f,H_2} - P^n_{p,H_2}\right) \qquad \text{Equation 1}$$

In which: JH_2 = the hydrogen flux through the membrane (mol/m^{2}s)
QH_2 = the hydrogen permeance (mol/m^{2}sPa)
PH_2 = partial hydrogen pressure on feed (f) and permeate (p) side
n = a coefficient whose value is between 0.5 and 1

When the diffusion through the membrane is much slower than the dissociation of hydrogen in the metal structure (in general this is the case when the membrane layer is rather thick), the concentration of hydrogen in the membrane is proportional to the square root of the hydrogen pressure and n = 0.5. If other transport mechanisms are governing the hydrogen transport n > 0.5 and could become 1. In [33, 34] values of 0.78 and 0.58 respectively are given for n. In the model used in this project the value for n can be chosen between 0.5 and 1. In the flowsheeting part (section 4) the value of n will be given based upon experiments using palladium membranes.

The palladium model also accounts for the transport of other components than hydrogen, e.g. through small defects in the membrane or sealing. For that, Poiseuille flow is the main transport mechanism and so for all components other than hydrogen the mechanism for transport is:

$$J_i = Q_i X_{f,i}\left(P^2_{f,i} - P^2_{p,i}\right) \qquad \text{Equation 2}$$

In which: J_i = the flux of component i through the membrane (mol/m^{2}s)
Q_i = the permeance of component i(mol/m^{2}sPa)
$P_{f,i}$, $P_{p,i}$ = partial pressure on feed (f) and permeate (p) side of component i
$X_{f,i}$ = feed concentration of component i

The flow profiles that have been used are ideal mixing on both sides of the membrane which, as shown by calculations, is applicable and counter current flow mode.

The physical problem which now appears is given in Figure 23.

32 M. Bracht, “Palladium membraan model voor ASPEN+ implementatie” (in Dutch: Palladium membrane model for ASPEN+ implementation), report ECN-FB-7.2016-GR2, Jan. 1997.
33 S. Uemiya, N. Sato, H. Ando and E. Kikuchi, “The water gas shift reaction assisted by a palladium membrane reactor”, Ind.Eng.Chem.Res., 1991 (30) 585.
34 J.P. Collins and J.D. Way, “Catalytic decomposition of ammonia in a membrane reactor”, J.Membrane Sci., 1994 (96) 259.

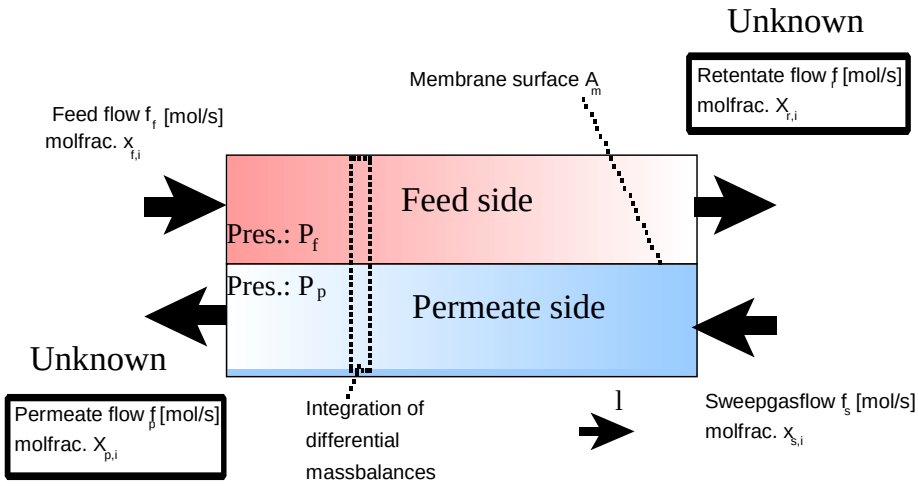

Figure 23 Physical problem of the palladium membrane model

The differential mass balances on both the feed side and permeate side have to be solved in order to calculate the flow on the retentate and permeate side and the concentrations on both sides of the membrane. To solve the differential equations for all the components in the feed and permeate stream is very difficult. Therefore some simplifications have been made which are:

- the leakage of components other than hydrogen through the membrane is negligible;
- the leakage of these components is only through the seals of the membrane and only on the feed entrance side;
- the leakage of hydrogen through the seals is negligible compared to the flow of hydrogen through the membrane.

This leads to the simplified palladium membrane model as shown schematically in Figure 24.

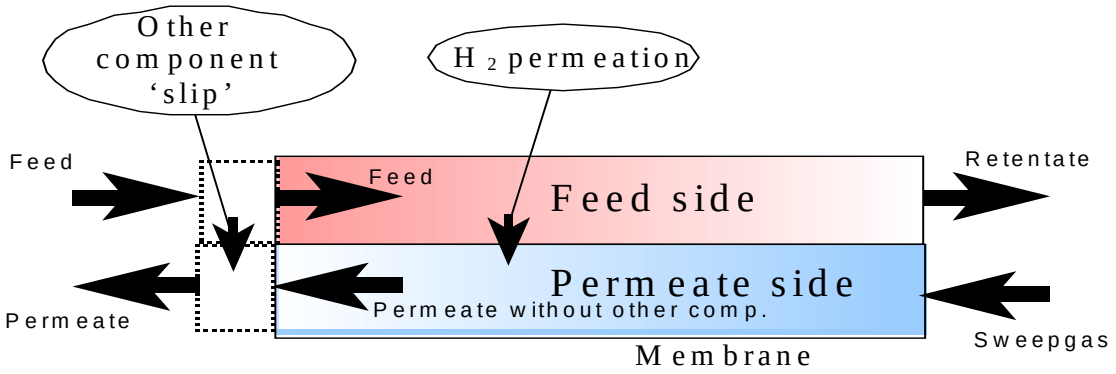

Figure 24 Simplified palladium membrane model

The parameters in this model were then evaluated using the membrane performance data generated by ECN using the Johnson Matthey palladium membranes. It can be seen from **Figure 29** that the experimental data under constant sweep gas flow conditions fits equation 1 very well with an exponent of

0.82. This was true of all data where the feed pressure, feed flow rate and sweep flow were kept constant.

Figure 25 Hydrogen flux vs partial pressure difference with a constant sweep flow

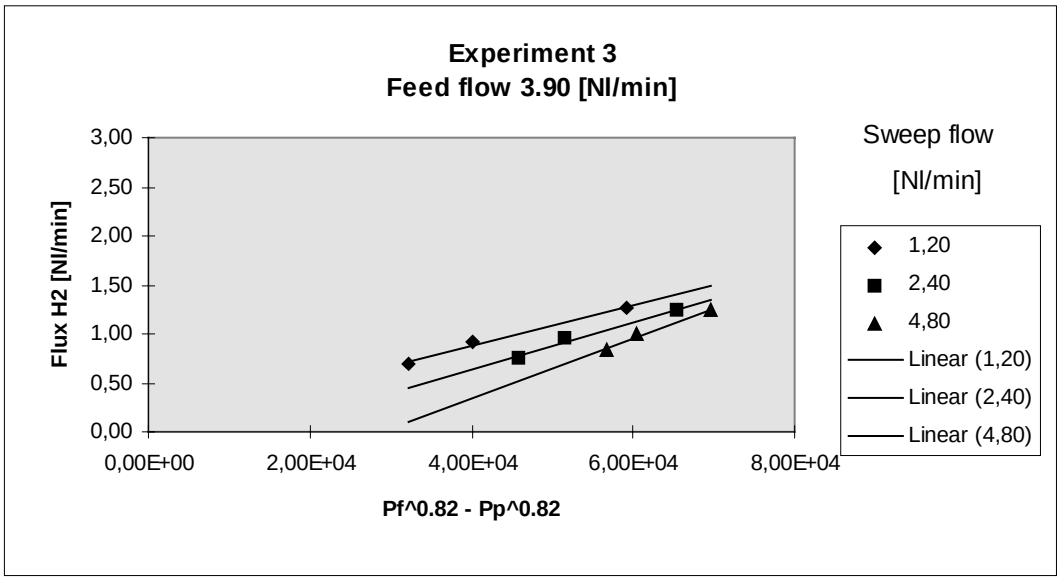

However if any of these parameters were changed (e.g. sweep flow - Figure 26) there was no correlation with equation 1. It seems probable that this is due to the dispersion effects discussed in section 3.1.3 and the effect will only be eliminated when the fluid dynamics dispersion model is incorporated into the data analysis.

Figure 26 Hydrogen flux vs partial pressure difference with variable sweep flows

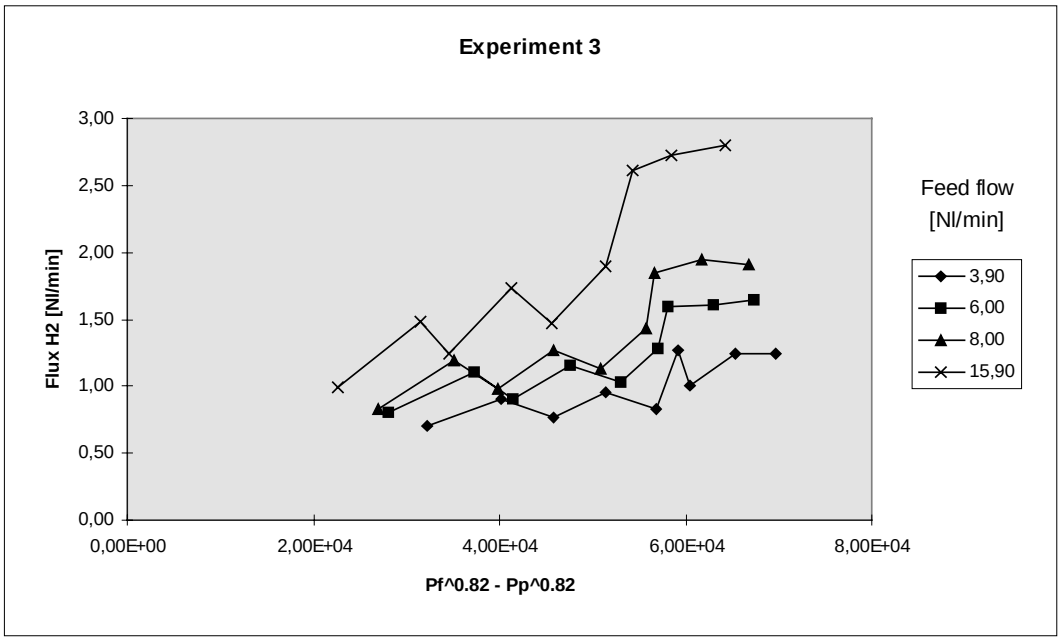

However the underlying model remains valid and this was therefore implemented in the ASPEN+ flowsheeting package by a FORTRAN encoded subroutine which was subsequently used in the flowsheeting studies by the University of Essen and Siemens.

3.1.3 Dispersion Modelling

All of the models have however been based on test data generated using a simple tubular membrane and one of the other questions to be answered by the project was the validity of the data generated in these test programmes. Whilst single component permeation data is not subject to any errors, operation in real mixed feed gases, a major objective of this project, leads to surface polarisation phenomena that can seriously reduce membrane performance. This was evaluated in detail by the National Technical University of Athens using fluid dynamics for the hydrogen recovery applications. These studies demonstrated that the surface polarisation effects, in the laminar flow regimes where all laboratory reactors operate, would give rise to significant concentration gradients. These would result in the observed membrane performance being significantly less than the flux and selectivity that might be available in a full scale membrane system where turbulent flow was present. The net effect is that the studies in this project, and the flowsheets developed using the lab data, will tend to underestimate full scale membrane performance. A more detailed assessment could be carried out using the fluid dynamics calculations to remove the errors from the lab data. The alternative in the future is to use reactor systems, such as the spider reactor developed by ECN in this project, designed to eliminate or substantially reduce these errors. Computational fluid dynamics methods help to:-

a) develop reliable engineering tools for predicting the flow, temperature, etc. fields,
b) reduce the costs of the experimental methodologies used for most of the relevant engineering designs,
c) allow for a better understanding of the physicochemical processes involved, so that more efficient and safer equipment can be designed; and
d) provide a platform for the easy development and testing of new ideas.

NTUA's task was to simulate the performance of systems embodied with ceramic membranes and this task was based on the use of a commercial computational fluid dynamics code (the well known PHOENICS® package). As this code uses the finite-control volume approach for the solution, details on this method will only be presented.

3.1.3.1 COMPUTATIONAL FLUID DYNAMICS (CFD) TECHNIQUES

The fundamental principles of computational fluid dynamics within the context of the "finite control volume approach" are presented. The mathematical problem, the general form of equations, and the numerical procedure are outlined.

3.1.3.1.1 General

PHOENICS® CFD code is a computer code which simulates fluid flow, heat transfer, chemical reaction and related phenomena. The starting point of the analysis is the set of three-dimensional partial differential equations that govern the phenomena of interest. This set consists, in general, of the following equations: the continuity equation, the three momentum equations that govern the conservation of momentum per unit mass in each of three space directions (the Navier Stokes equations); the equations for conservation of energy and species concentrations, etc. The differential equation which expresses the conservation of a quantity Ö, inside a differential volume dV, can be expressed in the following general form[35,36,37,38,39]:

$$\frac{\partial(\tilde{n}\ddot{O})}{\partial t} + div(\tilde{n}\rho\ddot{u}\ddot{O} - \tilde{A}_{\ddot{O}} grad\ddot{O}) = S_{\ddot{O}} \qquad [1]$$

35 Markatos, N. C., Computational fluid flow capabilities and software, Ironmaking and Steelmaking 16, 266-273 (1989).
36 Patankar, S. V., "Numerical Heat Transfer and Fluid Flow", Hemisphere Publishing Corporation, (1980).
37 Markatos, N. C., and A. Moult, The Computation of Steady and Unsteady Turbulent, Chemically-Reacting Flows in Axisymmetrical Domains, Trans. Instn. Chem. Engrs. 57, 156-162 (1979).
38 Markatos, N. C., Mathematical Modelling of Single- and Two-Phase Flow Problems in the Process Industries, Revue de l' Institut Francais du Petrole 48, No 6, 631-661 (1993).

where: t is the time

ñ is the fluid density

Ö is the dependent variable (e.g. velocity, mass fraction of component i, enthalpy)

$\vec{u}$ is the velocity vector

Γ_{Φ} is the effective exchange coefficient of variable Ö. It is equal to $\Gamma_{\Phi}=\Gamma_{\Phi l}+\Gamma_{\Phi t}$, where the $\Gamma_{\Phi l}$ and $\Gamma_{\Phi t}$ refer to laminar and turbulent flow respectively. In the momentum equations this coefficient is equal to the mixture viscosity ì (Pa.s). In the mass fraction equations, this coefficient is calculated from the relationship $\Gamma_{\Phi,i}=\rho D_i$ where D_i, is the dispersion coefficient of component i. In the energy equation, the coefficient is equal to $\Gamma_{\Phi}=\lambda^{eff}/C_p$ (kg $m^{-1}s^{-1}$) where C_p is the mixture specific heat and λ^{eff} is the mixture thermal conductivity.

S_{Φ} is the source term which expresses the consumption or the production of Ö (e.g. pressure gradient for the momentum equations, reaction source for the concentration equations) inside the domain of interest.

The term $\partial\rho\Phi/\partial t$ is the unsteady-state contribution. The term $div(\rho\vec{u}\Phi)$ expresses the transfer of the quantity Ö due to convection with the fluid while the term $div(\Gamma_{\Phi} grad\Phi)$ expresses the transfer of Ö due to diffusion.

3.1.3.1.2 The method of finite control volumes

The method used for the solution of the previous set of partial differential equations is called “method of finite control volumes"[35,36,37,38,39, 40] and is embodied in the PHOENICS® package. In this method, the integration is similar neither to the Taylor series expansion, which is used by the classical finite-difference techniques, nor to the finite-element techniques, although it shares features of both, and it allows for direct physical interpretation of the mathematical manipulations.

The calculation domain is divided to a number of non-overlapping control volumes such that there is one control volume surrounding each grid point (Figure 27). The differential equations are integrated over each control volume. Piecewise profiles expressing the variation of Ö between the grid points are used to evaluate the required integrals.

39 Spalding, D. B., A General Purpose Computer Program for Multi-dimensional One or Two-Phase Flow, Mathematics and Computers in Simulation 13, 267-276 (1981).
40 Anderson, D. A., Tannehill, J. C., and Pletcher, R. H., Computational fluid mechanics and heat transfer, Hemisphere Publishing Corporation, (1984).

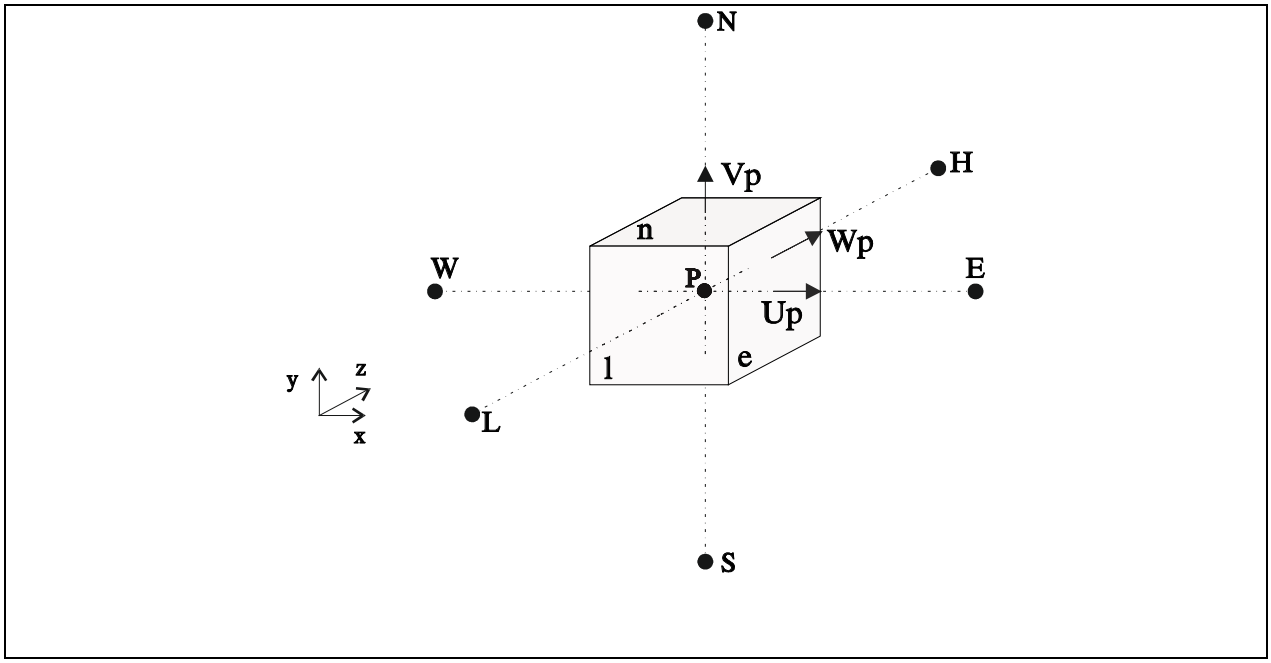

Figure 27: **Typical control volume used in "control volume approach".**

The most attractive feature of the control-volume formulation is that the resulting solution would imply that the integral conservation of quantities such as mass, momentum and energy is exactly satisfied over any group of control volumes and of course, over the whole calculation domain. This characteristic exists for any number of grid points-not just in a limiting sense when the number of grid points becomes large [36]. Thus, even the coarse-grid solution exhibits exact integral balances.

Also, in the control-volume approach, the interpolation formulas or the profiles used to describe the variation of Ö between two grid neighbour points, are regarded as auxiliary relations needed to evaluate the required integrals in the formulation. Once the discretization equations are derived, the profile assumptions can be forgotten. This viewpoint permits complete freedom of choice in employing, if we wish, different profile assumptions for integrating different terms in the differential equation.

In Figure 1, a typical control volume (cell) is presented. The point P which is placed in the centre of this volume, is regarded as the representative of the cell and the fluid property values • are solved and stored for it. It is surrounded by neighbouring nodes which shall be denoted by W(west), E(east), N(north), S(south), H(high) êáé L(low). The cells are "topologically" Cartesian. They can be either strictly Cartesian or polar cylindrical or generally curvilinear (orthogonal or non-orthogonal) but will always have six sides and eight corners in the three dimensional case.

Cells and nodes for velocity components are "staggered" relative to those for all other variables. The values of the velocity components u_P for the finite control volume of nodal point P are calculated and stored for the points that lie on the faces of the control volumes e (u_{Px} Þ u), n (u_{Py} Þ v), h (u_{Pz} Þ w). This is called the "staggered grid approach" and an immediate consequence of it is that the mass flow rates across the control-volume faces can be calculated without any interpolation for the relevant velocity component. Integration of the Eq. [2.1] in a differential control volume dV, results to :

$$\iiint_V \frac{\partial}{\partial t}(\rho\Phi)\,dV + \iiint_V div(\rho u\Phi - \Gamma_\Phi grad\Phi)\,dV = \iiint_V S_\Phi\,dV \qquad [2]$$

If it is assumed that the various quantities are uniformly distributed inside the control volume the Eq. [2] is rearranged to :

$$\frac{\partial}{\partial t}[\rho\Phi]\Delta V + \iiint_V div(\rho u\Phi - \Gamma_\Phi grad\Phi)\,dV = [S_\Phi]\Delta V \qquad [3]$$

where the [ ] refer to the mean value of the quantity inside the control volume. According to the Gauss theorem if ç is the unit vector vertical to surface A surrounding the control volume V:

$$\iiint_V div K\,dV = \iint_A K\,n\,dA \qquad [4]$$

where Ê is a vector quantity.

Eq. [3] through Eq. [4] is transformed to the following form :

$$\frac{\partial}{\partial t}[\rho\Phi]\Delta V + \iint_A (\rho u\Phi - \Gamma_\Phi grad\Phi)\,ç\,dA = [S_\Phi]\Delta V \qquad [5]$$

If Eq. [5] is applied to the control volume of node P in Figure 1, then :

$$\frac{\partial}{\partial t}[\rho\Phi]V_P + g_e - g_w + g_n - g_s + g_h - g_l = [S_P]V_P \qquad [6]$$

where:

$$g_i = \iint_{A_i} (\rho u_i \Phi - \Gamma_\Phi \frac{\partial \Phi}{\partial x})\,dA_i \ldots i = e, w, n, s, h, l \qquad [7]$$

is the flux of Ö through the surface of the control volume.

3.1.3.1.3 Discretization - Linearisation.

If uniform distributions of various quantities inside the control volume are assumed then:

$$[\rho\Phi]V_P = \rho_P \Phi_P V_P \qquad [8]$$

$$[S_\Phi]V_P = S_{\Phi_P} V_P \qquad [9]$$

Also, by assuming uniform distribution on the faces of the control volumes Eq. [7] becomes :

$$g_i = (\rho u)_i A_i \Phi_i - \Gamma_i A_i \left.\frac{\partial \Phi}{\partial x}\right|_i \ldots i = e, w, n, s, h, l \qquad [10]$$

Under steady state conditions, the first term of Eq. [6] is discarded.

The values of the partial derivatives are approximated, using several methods, from the values in the centre of the neighbouring cells, e.g. the partial derivative of Ö at x direction is calculated from :

$$\left.\frac{\partial \Ö}{\partial x}\right|_e = \frac{\Ö_E - \Ö_w}{\ädx_{EW}} \qquad [11]$$

The Pe number is equal to:

$$Pe = \frac{F_i}{D_i} \qquad [12]$$

where $F_i = A_i u_i \ñ_i$ represents the convection contribution to the flow of Ö and $D_i = \frac{(\Ã_\Ö)_i A_i}{\ä_i}$, represents the diffusion contribution to the flow of •, where $\ä_i$ is the distance of node P from the faces i of the cell (i: s, n, e, w, l, h).

Finally, the source term $S_\Ö$, is linearised as:

$$S_\Ö = S_c + S_P \Ö_P \qquad [13]$$

where: $S_c = S^0_\Ö - (\frac{dS_\Ö}{d\Ö})^0 \Ö^0_P$ and $S_P = (\frac{dS_\Ö}{d\Ö})^0$, while the exponent 0 expresses that the value of the quantity is calculated in the previous iteration of the solution procedure.

The Eq. [3] after the discretization of all the terms is transformed to the following algebraical equation:

$$(\á_P - S_P V_P)\Ö_P = \sum_i \á_i \Ö_i + S_c V_P \ldots i = E, W, N, S, H, L . \quad [14]$$

The coefficients $\á_i$ are calculated as :

$$\begin{aligned} \á_i &= D_I + \|-F_I, 0\| \quad i = E, N, H \\ \á_i &= D_I + \|F_I, 0\| \quad i = W, S, L \end{aligned} \qquad [15]$$

while $\á_p$ is equal to:

$$\á_p = \sum_{i=E,W,N,S,H,L} \á_i \qquad [16]$$

3.1.3.1.4 The four basic rules

The system of the partial differential equations has been transformed to a system of algebraical equations and its solution will provide the values of Ö in the grid nodes. The discretization equations should obey four basic rules in order to ensure physical realism and overall balance [36]:

1. **Consistency at control-volume faces.** When a face is common to adjacent control volumes, the flux across it must be represented by the same expression in the discretization equations for the two control volumes.
2. **Positive coefficients.** All coefficients ($•_P$ and neighbours $•_i$) must always be positive.
3. **Negative slope linearisation of the source term.** When the source term is linearised as shown in Eq. [2.13] the coefficient S_P must always be less than or equal to zero.

4. **Sum of the neighbour coefficients.** It is required that $á_p = \sum_{i=E,W,N,S,H,L} á_i$ for situations where the differential equation continues to remain satisfied after a constant is added to the depended variable.

3.1.3.1.5 Boundary and Internal Conditions - Auxiliary Relations

Partial differential equations must satisfy "boundary conditions" of the type : f(•,grad•)=0 at specified points, lines, areas, or volumes [35]. These points, lines, etc., need not be at boundaries, but they can be within the calculation domain, when such additional information is given.

For a boundary cell, the boundary condition is nothing more than a replacement of the unknown • value at the corresponding neighbouring cell by the known value. Therefore, the treatment of boundary cells can be identical to that for any other cell; and the known boundary relations can be expressed again by integration over the cells containing the boundaries. In this manner, the boundary (and internal) conditions simply make contributions to the b and $•_P$ of the finite domain equations (Eq. [13], [14]).

Auxiliary relations must be provided to close the problem, and refer in general, to thermodynamic and transport property relations (the density of the mixture •, expressed as function of pressure, enthalpy, concentration, the viscosity, •, the thermal conductivity •, the diffusion coefficients, etc.) or in interphase transport expressions.

3.1.3.1.6 Numerical Solution

The SIMPLEST algorithm embodied in the PHOENICS® package [35,38,39] is used for the numerical solution of the system of the partial differential equations.

Special relaxation techniques are used in order to facilitate convergence and avoid big changes of the dependent variables between two consequent iterations as the latter could cause divergence.

The realism and the correctness of the obtained solution is assured by following the criteria listed below :

1. The balances of all the equations for all the dependent variables must be satisfied in all the calculation domain.
2. The values of the dependent variables in a certain point of the calculation domain must not change with iterations. This value is called 'spot value' and it is usually a "sensitive" point of the domain.
3. The difference in the values of the dependent variables, between two consequent iterations, must be in the range of the desired accuracy.
4. The obtained solution must be grid independent.

3.1.3.2 APPLICATION OF COMPUTATIONAL FLUID DYNAMICS TECHNIQUES TO THE SIMULATION OF SYSTEMS EMBODIED WITH CERAMIC MEMBRANES.

3.1.3.2.1 General

NTUA has developed mathematical models for the simulation of systems embodied with ceramic membranes using the PHOENICS® CFD environment 41, 42, 43, 44. These models could serve as reliable engineering tools for predicting the distribution of flow, component concentrations and temperature inside these systems while they could help to obtain a better understanding of the physicochemical processes involved, so that more efficient equipment can be designed.

NTUA's task in the project was to modify and adapt its existing algorithms to the size of the experimental setup of ECN used for membrane separation and reaction experiments in order to proceed to the validation of the mathematical models with experimental results in collaboration with colleagues at ECN. As the ceramic membranes used in the experiments were highly selective for hydrogen, non ideal flow effects may play an important role on the separator performance [35]. Thus, two cases were studied in order to investigate which of them fits better the experimental results. In the first case, plug flow conditions on both sides of the separator were assumed (simplified model, S.M.) and in the second case non ideal flow effects were taken into account (dispersion model, D.M.). A brief description of these models and some typical results from their application for the project purposes are presented in the rest of this document.

3.1.3.2.2 The physical problem considered

The most common configuration of a membrane reactor-separator comprises an annulus, the inner cylinder of which supports the membrane. The feed gas enters into the space between the two tubes or inside the membrane tube, while the membrane, allowing the selective passage of certain species (e.g. hydrogen) from the reaction mixture across its structure, is put on the inner cylinder surface. In case of a membrane reactor, the reaction proceeds in the forward direction until equilibrium is reached. An inert gas (sweep gas) is fed either into the inner tube (*separation side*) or to the space between the two tubes respectively, sweeping the permeated gases to the outlet (Figure 28).

41 Koukou, Ì. Ê., N. Papayannakos, and N. C. Markatos, "Dispersion Effects on Membrane Reactor Performance", AIChE Journal, Vol. 46, No. 9, 2607, (1996).
42 Koukou, M. K., G. Chaloulou, N. Papayannakos and N. C. Markatos, "Mathematical Modelling of the Performance of Non-Isothermal Membrane Reactors", International Journal of Heat and Mass Transfer, Vol. 40, 10, 2407-2417, (1997).
43 Bracht, Ì., P. T. Alderliesten, R. Kloster, R. Pruschek, G. Haupt, E. Xue, J. Ross, M. K. Koukou and N. Papayannakos, "Water gas shift membrane reactor for CO2 control in IGCC systems: techno-economic feasibility study", Energy Conversion and Management, Vol. 38, Suppl., S159-S164, (1997).
44 Koukou, M. K., L. Peristeras, N. Papayannakos, N. C. Markatos and P. Alderliesten, "Design of a full scale adiabatic water gas shift membrane reactor", 1st European Congress on Chemical Engineering, ECCE-1, Florence, May 4-7, (1997).

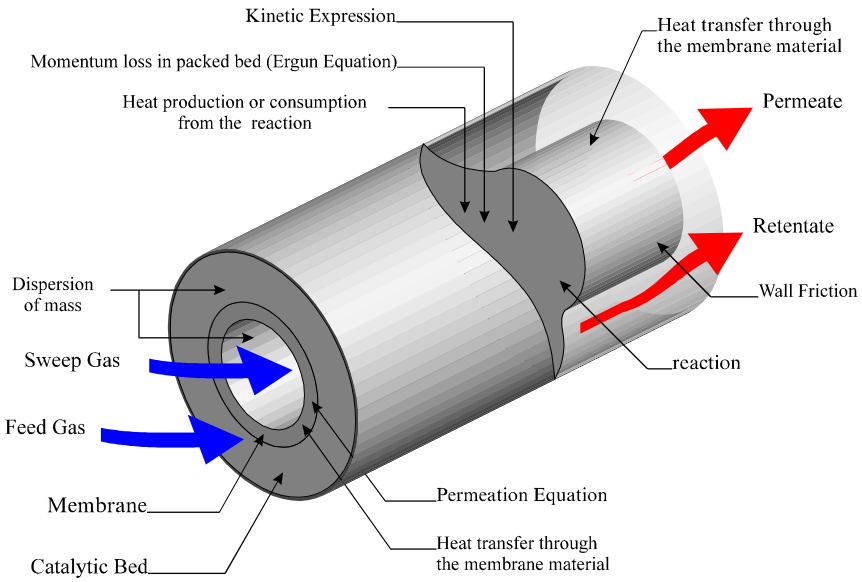

Figure 28: **The physical problem considered in case of a membrane reactor with co-current flow of sweep gas and feed gas.**

3.1.3.2.3 Mathematical formulation

The mathematical analysis is based on a set of elliptic, partial differential equations expressing the conservation of mass, momentum, energy (in the non-isothermal model) and chemical species in steady, two dimensional flow. A polar-cylindrical (r, z) co-ordinate system is used, where its two components r, z are the independent variables of the problem. The models are considered two-dimensional because both transport of mass and energy occurs not only in the direction of the bulk flow, but also in the vertical direction. The main dependent variables are: the pressure P, the radial and axial velocity components v, w, the mass fractions of chemical species c_i and the specific enthalpy h (in the non-isothermal model). The differential equations for all variables are expressed in the general form of Eq. [1].

The solution of the set of partial-differential equations requires appropriate boundary conditions and special internal conditions (e.g. reaction rate, separation-rate equation) describing the physical problem considered.

3.1.3.2.4 Typical Results - Validation of the Models

In this section, typical results from the application of the isothermal model to the simulation of the performance of a membrane separator are presented. The model was modified and adapted to the experimental setup and conditions of the separation experiments carried out at Netherlands Energy Research Foundation, ECN.

Convergence was easily obtained by applying relaxation of the false-time step type in the mass fraction equations, and linear relaxation for the other variables. Up to 2000 (simplified model) and 2500 sweeps (dispersion model) of the computational domain were performed to obtain full convergence. Each sweep took about 1 s. The choice of the computational grid used in the performed runs was related to the physical problem considered. Grid independence runs were carried out and grid independent solutions were assured.

Results obtained both from the simulations and the experimental apparatus for the following three cases and for various pressure conditions, are presented and discussed:

i. The space between the two tubes contains a catalytic bed and no sweep gas is used.
ii. The two tubes are empty and no sweep gas is used.
iii. The two tubes are empty and sweep gas is used in counter-current flow with the feed gas.

It is generally observed that the predictions obtained from the simulations are in a good agreement with the separation experiments carried out at ECN and one crucial remark made is the important influence of dispersion effects on the separation of the gases and especially of hydrogen through the highly selective ceramic membrane.

The results are presented either in terms of hydrogen flow rates at the outlet of the separation side of the system considered or in terms of radial hydrogen partial pressure profiles. In Figure 29and Figure 30 flow rates at the outlet of the separation side of the membrane separator are presented for the cases (i) and (ii). As it is shown in the figures:

- By increasing the pressure difference, the separation rate of hydrogen through the membrane material increase.
- The dispersion model predicts better the experimental results while the simplified model provides unrealistic predictions.

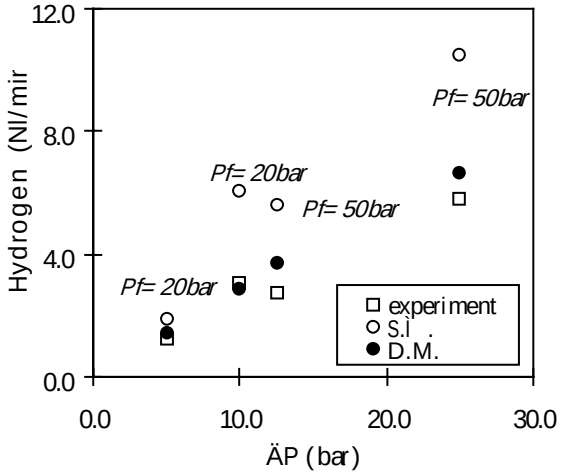

Figure 29: Hydrogen at the outlet of the separation side vs. pressure difference.Q_f= 18.55 Nl/min P_f= Feed Side pressure.Case (i).

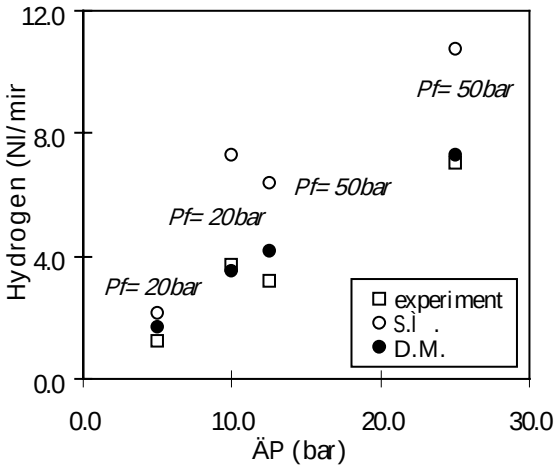

Figure 30: Hydrogen at the outlet of the separation side vs. pressure difference. Q_f=18.6Nl/min,Case (ii).

In Figure 31 and Figure 32 results obtained for the case (iii) and for various inlet sweep gas rates, are presented while it is noticed that:

- By increasing the pressure difference and the inlet sweep gas rate, the separation of hydrogen through the membrane material increase.
- The dispersion model predicts better the amount of hydrogen separated through the membrane especially when high sweep gas rates are applied while the predictions of the simplified model are not realistic.

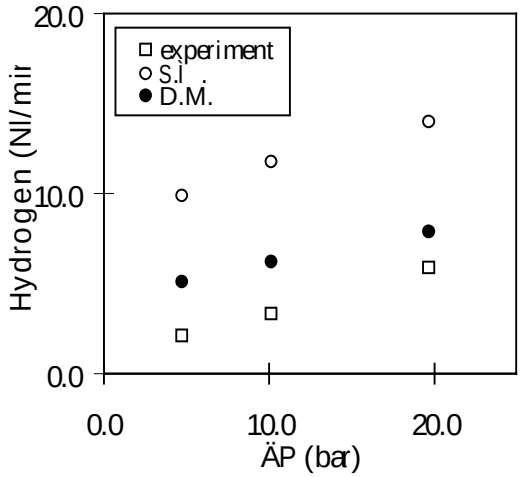

Figure 31: Hydrogen at the outlet of the separation vs.pressure difference.Q_f= 23.8 Nl/min Q_s= 6.7 Nl/min,Case (iii).

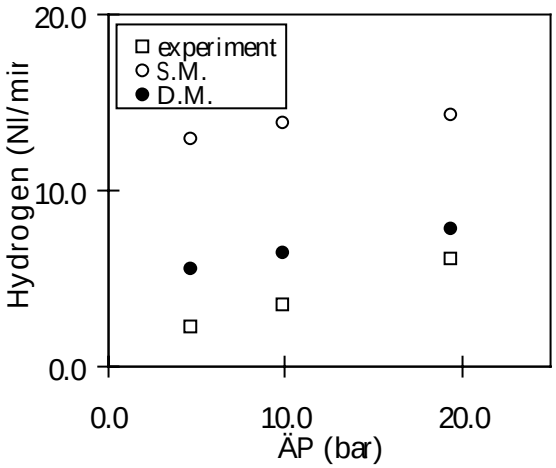

Figure 32: Hydrogen at the outlet of the side separation side vs. pressure difference Q_f=23.8Nl/min,Q_s=13.24Nl/min,Case (iii).

The radial profiles of the various mixture components provide a deeper insight to the previous results. In Figure 33 and Figure 34 typical radial profiles of hydrogen partial pressure are presented, predicted by both models. The simplified model predicts flat radial profiles while the dispersion model predicts radial profiles which are not flat but close to the membrane the hydrogen partial pressure decreases on the feed side and increases on the separation side and thus the pressure difference decreases causing a decrease on the hydrogen separation rates.

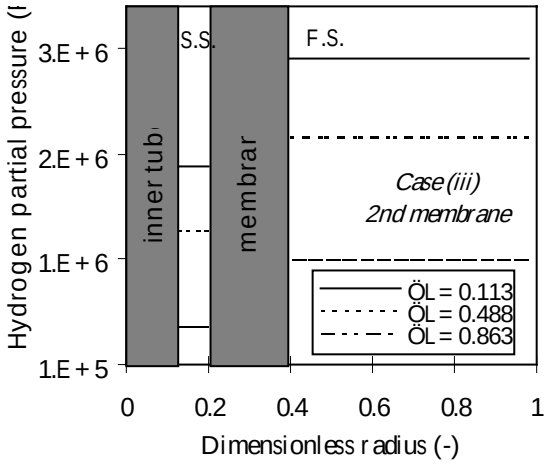

Figure 33: Hydrogen partial pressure radial profile at three axial points in the reactor. P_f=51bar P_s=41bar,Q_f=24Nl/min,Q_s=13.19Nl/min. Simplified model

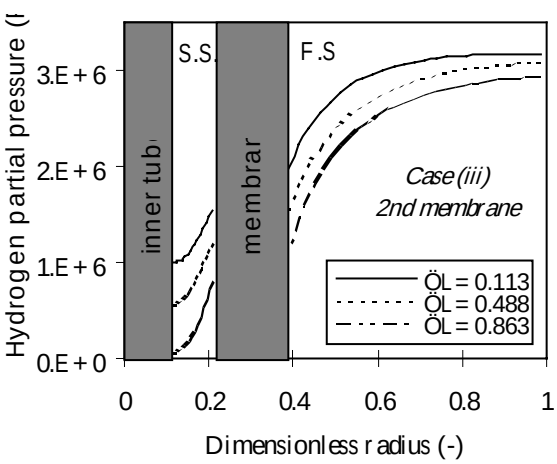

Figure 34:Hydrogen partial pressure radial profile at three axial points in the reactor. P_f=51bar,P_f=41bar,Q_f=24Nl/min, Q_s=13.19Nl/min. Dispersion Model

The predictions obtained from the simulations are in a good agreement with the separation experiments carried out by ECN using its highly selective silica membranes and they point out that the non ideal flow effects have a dramatic influence on the separation of the gases and especially of hydrogen through the highly selective membrane as they decrease the gas permeation rates. Thus, the realistic design of the gas separation systems embodied with membranes could be achieved by using a mathematical model which accounts for the non ideal flow effects. The small deviations appeared between the experimental results and the dispersion model predictions could be attributed to the calculation of the permeability

coefficients used which were calculated by performing permeation experiments using pure gases and thus the possible interactions between the various gases have not been taken into account.

This major point has to be taken into account during the incorporation of the mathematical model in a flowsheeting package. If this model does not take into account the non ideal flow effects, the performance of the separation system will be overestimated and this will lead to unrealistic calculation of mass balances of the whole process in the flowsheeting package. Thus, it is concluded that the simple plug flow model which has already been incorporated in the flowsheeting package, ASPEN®, will need to be replaced by the more complicated non-ideal flow model.

3.1.3.3 NOMENCLATURE

A surface surrounding the control volume V [m^2]
dV differential control volume V
Pe Peclet number [-]
$S_Ö$ source term in the differential equation of Ö inside the control volume expressing the consumption or production of • [$kg/m^3.s$]
t time [s]
$\vec{u}$ is the velocity vector [m/s]
V_p volume of cell P [m^3]

Greek Symbols
$Ã_Ö$ is the effective exchange coefficient of variable Ö [kg/m.s]
ñ is the mixture density [kg/m^3]
Ö is the dependent variable Ö (e.g. velocity, mass fraction of component i, enthalpy)

3.1.4 Finite Element Modelling - Module Design

All of the work in this project has been carried out using tubular membranes, approximately 1cm OD x 30cm long. Ultimately, if these membranes are to find commercial application, it seems probable that more complex multi-tubular monolithic geometries will be required to give improved surface:volume ratios. A further part of the fundamental studies was the development by Democritos of a finite element model to help with the design of optimum geometry monoliths. This has shown that, based on the typical permeabilities of the membrane layer and support structures achieved in this project, that up to a 37 channel monolith should be usable without severe performance degradation. If the development of these more complex structures is part of a future programme this approach, which only requires a direct measurement of the support and membrane layer permeability's, should be part of the scale up process.

To extend the pore level models developed in other tasks of the project to a real system it is necessary to account for support effects and total system geometry. There is evidence in the literature[45] that the membrane performance can be sensitive to whether the feed is on the membrane or support side of these asymmetric systems as well as to the configuration adopted for the design of the monolith structure in practical applications and similar effects were also seen in the earlier Brite Euram project with the carbon membranes.

As part of this project NCSR Democritos therefore adapted and extended properly a preliminary 2-D computer code (initially developed in previous project) simulating the flow field across a multi-channel monolith cross section. For all practical purposes it can be shown that the main conclusions concerning the optimisation of the monolith structural design remain unchanged as the study extends from two to

45 Dolecek P., J. Membrane Sci., 100 (1995) 111-119.

three dimensions. It has therefore been decided to refine the 2-D version of the code and test it against available tubular data to reach appropriate conclusions.

3.1.4.1 Model Description

To study and optimise the design of a multi-channel monolith in terms of size, number and distribution of the feed lines across a typical cross section, the numerical solution of the steady state equations for the flow of an incompressible gas in a two-dimensional porous domain is undertaken first. The model is based upon Darcy's law for single phase flow in a porous medium which is assumed to be homogeneous. The transport of permeate through the substrate and the separation process that takes place inside the thin membrane layer (skin) are decoupled for the purpose of the simulation without any loss of generality. The problem of permeate flow through the substrate is described in general by the continuity equation and Darcy's law. Their combination results in the following partial differential equation:

$$(k / \acute{\imath}) \nabla P^2 + Q = 0 \qquad (1)$$

where P is the gas pressure, k is the porous substrate permeability, í is the permeate gas kinematic viscosity and Q represents a given source function of the spatial co-ordinates. Suitable boundary conditions read:

(a) P = Po on S, where S stands for a section of the boundary with specified pressure (here S denotes the perimeter of the monolith cross section where an external pressure is imposed), or
(b) Given normal derivative of the pressure on S, where S in this case represents the part of the boundary which is characterised by known mass flux (feed lines).

Finite difference discretization on a rectangular grid would be the simplest way to follow for the solution of equation (1) at least as far programming complexity is concerned. However, the required flexibility in geometry in order to account properly for the geometric features of the monolith design dictates the use of the finite element approach. Accordingly, the domain (monolith cross section) is divided in triangular or quandrangular elements and the gas pressure is obtained at each node of the resulting 2-D grid.

3.1.4.2 Numerical Simulations

Evidently, the usefulness and reliability of the simulations to be performed depend on the validity and accuracy of the input parameter values provided for the membrane (skin) and substrate permeabilities, the gas flow rate in each of the feed lines, their geometric characteristics (sizes and distribution pattern).

The first set of predictions obtained using the FEM code refer to ceramic (alumina) monoliths of hexagonal cross section (31 mm width) with 19 feed lines (channels) of 4 mm diameter each. Use is made of experimental data on permeabilities and fluxes for the purpose of comparisons and model validation. In the original version of the code, a simplified approach is taken whereas the feed channels are represented by point like sources of gas (permeate) properly distributed over the cross section of the monolith. This simplification is not considered as having any significant effect on the qualitative conclusions drawn. Nevertheless its validity will be checked later on.

The substrate permeability reported by the monolith manufacturer (3.13×10^{-5} $Nm^3/s/m^2/Pa$) corresponds to a k value (cfr equation (1)) ranging from 1.8×10^{-12} to 4.7×10^{-12} m^2 depending on the absolute feed pressure for the nitrogen gas used in the tests. These permeability values compare well with the ones measured on carbon substrates made from phenolic resin powders (from 1.69×10^{-12} to 5.9×10^{-12} m^2). Employing the above substrate permeability for the hexagonal monolith and the value proposed by the manufacturer for their membrane layer (skin permeability of 8.6×10^{-6} $Nm^3/s/m^2/Pa$) simulations have been performed to obtain predictions for the overall permeability of the system under specific conditions.

3.1.4.3 Results and Discussion

In a first step, we have simulated experimental tests where each individual channel was fed separately and the developed pressure difference and permeate flow rate were measured. The calculated overall permeability (support plus separating skin layer) of 6.4×10^{-6} $Nm^3/s/m^2/Pa$ compares favourably with the value of 6.65×10^{-6} $Nm^3/s/m^2/Pa$ which can be deduced from the experimental data.

Proceeding further, tests where all channels were simultaneously fed have been simulated. In this case, the mean value of the overall permeability is computed as 5.42×10^{-6} $Nm^3/s/m^2/Pa$ while the experimental average permeability is found as 2.8×10^{-6} $Nm^3/s/m^2/Pa$. It is important to note here that the calculations show that the gas pressure in the different feed channels varies from 0.44 to 0.64 bar (i.e. a mean of 0.54 bar $\pm$18.5%) depending on the position of the channel on the monolith cross section. All pressures recorded herein are relative to the externally applied value at the outside surface of the monolith. The maximum pressure is obviously found in the central channel whilst the minimum is related to the peripheral feed lines. This is expected since the flow rate in each channel is kept constant in this version of the model (channels simulated as point like sources of gas). Then, the difference in the distances to be covered by the radially escaping gas (depending on the position of the channel) and the extra resistance to the flow of gas coming from the central channels due to the presence of the peripheral rings of feed lines in the monolith cross section cause the observed pressure variation. During the measurements, similar in size fluctuations of pressure ($\pm$20% around the mean) were detected. The discrepancy between calculated and observed overall permeability is partly due to these pressure fluctuations and the requirement of the present version of the model for fixed gas flow rates at all feed lines. However, it should be stressed that the measured overall permeability value seems rather low as it implies that the pressure drop related to the substrate is almost twice as that caused by the skin layer. The computed value on the other hand indicates a more balanced partition of the two contributions to the total resistance to flow through the system.

In addition to the above, various configurations of the channel distribution pattern across the monolith cross section have been examined with a view to minimising the non-uniformity of pressure and optimising the monolith performance. The results, like the typical pressure contours in Figure 35, suggest that for the considered combination of substrate and skin permeabilities and the given flux characteristics no more than two rings of channels can be allowed (to keep pressure fluctuations at the aforementioned levels).

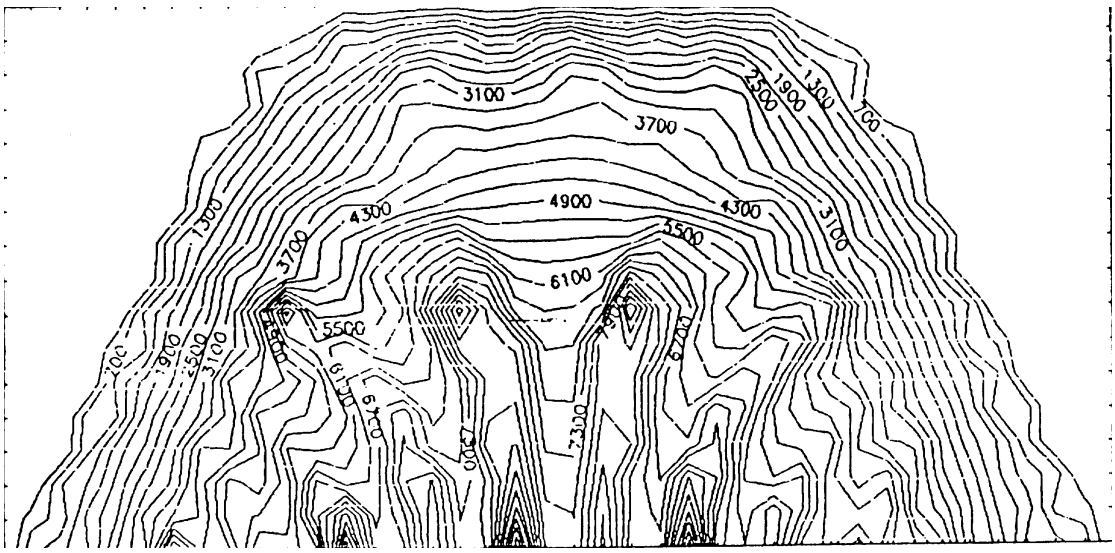

Figure 35 Pressure Contours

The suppression of the central channel or its transformation to permeate collector have also been tested numerically and the simulation shows considerable improvement regarding the issue of pressure non-uniformity. Figure 36 represents the case of the central channel functioning as permeate collector (low pressure at the centre of the monolith).

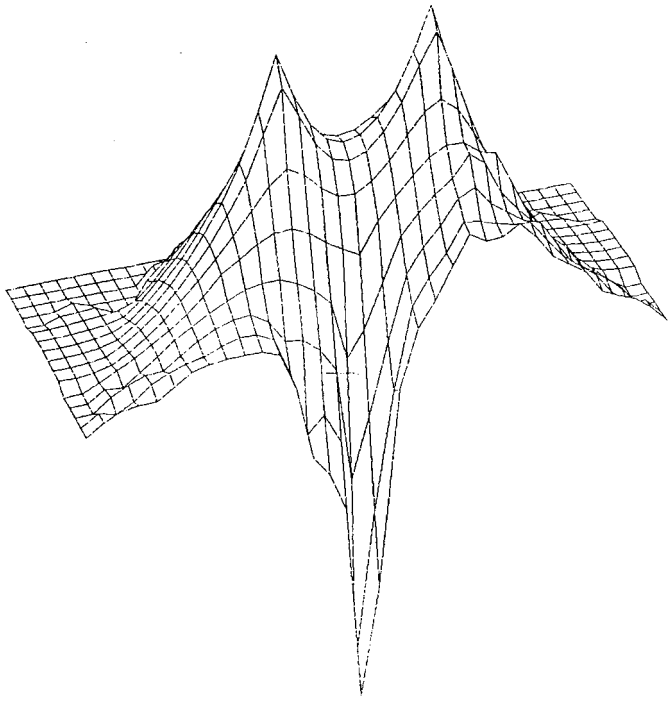

Figure 36 Central Channel - transformation of the central channel to permeate remover

An improved version of the model has been implemented offering a more realistic representation of the monolith configuration. Indeed, the channels can be simulated as circular holes of variable diameter and position across the monolith structure. Furthermore, the need to specify constant channel flow rates is eliminated in this new version. Carbon monoliths of circular cross section have been examined by the extended model. A computer program for the interfacing between the triangular grid generation routines and the main FEM code has been written. The next step involves the application of the model on the new grid and the determination of the effect of variable channel size on the pressure distribution. This has been done for the case of cylindrical carbon monoliths with 50 mm external diameter and 25 channels of 5 mm internal diameter each. The skin to substrate permeability ratio takes now values of the order of 1/40,000 leading to pressure drop for the permeate flow through the substrate which is negligible compared to the overall pressure decline (from channel to monolith exterior, i.e. including the skin). This means that the pressure (or flowrate) fluctuations observed before for the alumina monoliths are now almost completely smoothed out due to the fact that the major resistance to flow is caused by the skin regardless of the position (or size) of the feed line. It is also found that in this case of very low skin to substrate permeability ratio the resulting pressure distribution over the monolith cross section remains qualitatively unchanged if point like or circular channels are employed in the simulations.

The code has finally been used for the case of microporous membranes with ã-alumina and silica top layers and á-alumina substrates (in the form of monoliths). The values of gas (helium) permeability vary widely between skin and substrate as implied by the measurements performed during the project at NCSR Democritos and the relative pore sizes of the several layers. In fact, the difference in permeabilities between substrate and skin is more than three orders of magnitude leading (as before for the carbon monoliths) to the conclusion that the number and distribution of the feed lines should be determined by other than flow related considerations (e.g. mechanical strength). Permeate flow through the substrate is not affected even if large monoliths with several channel rings are used.

In conclusion, the size and distribution pattern across the monolith cross section should be selected based on production considerations (mechanical strength, etc.) if the skin permeability is very much lower than the substrate permeability. On the contrary, if the two permeabilities can be considered as comparable, the permeate flow through the substrate will be affected by the distribution and number of feed lines

(number of channel rings, internal diameter of channels) leading to pressure (or flow rate depending on the practical conditions) fluctuations that should not be neglected during the monolith design stage.

3.1.5 Practical Studies

The practical studies undertaken in the fundamentals part of the project were designed to support the theoretical studies and to provide the essential data for the microporous membrane models. Whilst the primary goals were to supply the diffusion constants and the adsorption isotherms they have also provided some important insights into some of the underlying physical processes.

3.1.5.1 Pulse Field Gradient NMR Studies (PFG NMR)

For the first time, PFG NMR has been successfully applied to the characterisation of microporous ceramic membranes for gas separation processes. Information about both trans-port-relevant structural properties of the membranes and the intrinsic mobility of the guest molecules has been provided under conditions of both single- and multicomponent adsorption.

Novelties in PFG NMR, which could be realised within the present project, are
- the direct measurement of hydrogen diffusion in adsorbate-adsorbent systems,
- single- and two-component diffusion measurements in adsorbate-adsorbent systems using ^{2}H NMR,
- space-resolved diffusion measurements in membranes as a probe for elucidating the extension of the crystalline constituents.

The PFG NMR technique is a unique method for tracing molecular displacements *r* over a space scale of a few micrometers during observation times *t* of milliseconds. The results are generally represented in terms of an effective diffusivity $D = \langle r^2(t) \rangle / 6t$, where $\langle r^2(t) \rangle$ denotes the mean value of the squared distance covered by the molecules during *t*. The effective diffusivity contains twofold information, viz. about the mobility of the molecules contributing to the observed NMR signal and about the transport-relevant structural properties of the membranes. Correspondingly, the PFG NMR studies were intended to unveil the diffusional behaviour of guest molecules and the structural peculiarities of the actual membrane material, relevant for the project. Moreover, systematic studies of the dependence of the diffusivity on process-relevant parameters like temperature, concentration and composition were thought to provide experimental background for the NEMD studies.

The PFG NMR measurements planned within the project necessitated a number of preliminary experiments as well as a further improvement of the experimental procedures. These activities were in particular become necessary for

(i) the investigation of novel carbon membranes as a consequence of the reduced transverse nuclear magnetic relaxation times of the guest molecules due to para-magnetic centres in the carbon,
(ii) the measurement of hydrogen diffusion, where the conventional way of PFG NMR sample preparation had to be modified owing to the relatively low adsorption affinity of hydrogen and
(iii) two-component diffusion studies, where for the first time by using both ^{1}H and ^{2}H PFG NMR the observation of the mobility of either component has become possible.

A major experimental problem in both this and the gravimetric studies was the provision of adsorbates representative of the actual zeolite layer. In the case of the carbon, silicalite and silica membrane it was not possible to remove the membrane layer from the tubular substrates in sufficient quantity to use this directly and it was therefore necessary to produce free standing material to simulate the membrane layer. As a result there is no certainty that the material examined is actually identical to the real membrane layer. In the case of the silicalite the key uncertainties are the crystallite size and degree of the aluminium substitution. For the carbon a method was developed for preparing thin carbon films of similar geometry to the membrane layer (~10microns thick) but as the carbonisation conditions were very different this could have lead to some changes. A cross check on this was performed by using an

alternative granular form of the carbon. As this gave similar properties to the thin films it can be assumed that the pore properties are relatively independent of the preparative procedure[46]. Only in the case of the zeolite A membranes, where one form is prepared on a porous metal substrate, was it possible to use the actual membrane material[47]. This also then allowed a direct comparison between the small particles present in the membrane and larger, free standing crystals.

Figure 37 provides a comparison between the diffusivities of hydrogen in different zeolitic host systems. The diffusivities increase in the sequence chabazite, NaA and NaX, which may be rationalised by the pore diameters increasing in the same sequence. Completely unexpectedly, the hydrogen diffusivities in ZSM-5 are below these values. According to the pore apertures (10-membered rings, to be compared with 8-membered rings for A and chabazite and 12-membered rings for X) hydrogen diffusion in ZSM-5 should assume a medium position. From quasi-elastic neutron scattering, however, one may deduce that a substantial fraction of hydrogen molecules are within the pentasil chains, where their mobility is clearly much smaller than in the main channel system of ZSM-5. During the measuring time of PFG NMR these "trapped" hydrogen molecules exchange with those in the channel system, obviously leading to the observed decreased mean diffusivity. This may have significant implications for the use of silicalite as the membrane materials in separations involving hydrogen. The inverse temperature dependence for the silicalite that arises as a result of this phenomena needs also to be taken into account when using hydrogen as an “inert” probe molecule when characterising the different membranes.

The impact of Si:Al ratio was also examined (Figure 38). Whilst the overall magnitude of the effect is relatively small it does appear that at very low Al contents the diffusivity is reduced. The temperature dependence is however independent of the aluminium loading.

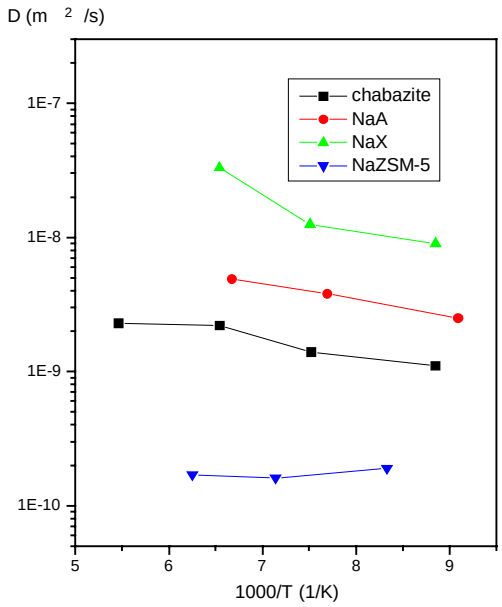

Temperature dependence of hydrogen diffusivities in different zeolites.

Figure 37

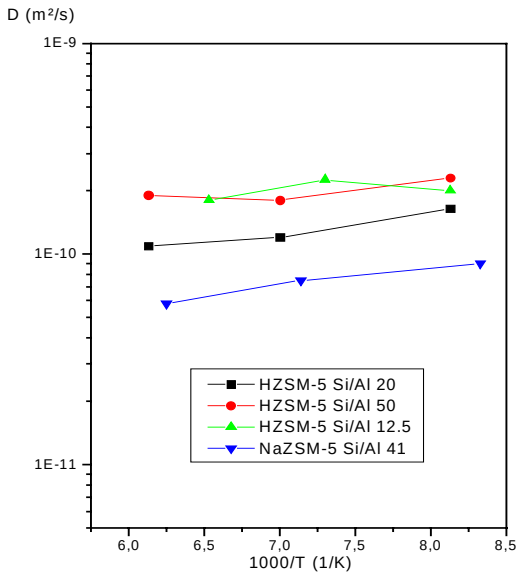

Temperature dependence of hydrogen diffusivities at different ZSM-5 zeolites at loading of 1.5 molecules/ch.i.

Figure 38

46 W. Heink, J. Kärger, S. Tennison: Pulsed Field Gradient NMR Diffusion Studies with Carbon Molecular Sieves, Carbon, to be submitted

47 W. Heink, J. Kärger, T. Naylor, U. Winkler: PFG NMR Study of the Transport Properties of A-Type Zeolite Membranes, J. Chem. Soc., Chem. Comm., to be submitted

Figure 39 provides a comparison of the hydrogen diffusivity in a carbon molecular sieve membrane with those for other adsorbates. Comparison with the zeolite data in Figure 37 shows that carbon has a diffusivity intermediate between the silicalite and the NaA. Figure 39 also shows the expected decline in the diffusivity with molecular weight across the series methane-ethane-propane although the similarity of the ethane and propane is perhaps surprising. The diffusivity of ammonia is also much than lower than expected on a size/molecular weight basis and implies a string interaction of the ammonia with the acid sites on the carbon surface. Comparison of Figure 39 and Figure 40 also shows that the ammonia diffusivity is much lower in the carbon than in the silicalite. This clearly has implications for the use of the materials in membranes for ammonia recovery.

This demonstrates one of the underlying the effects in diffusion in pores - that if the molecules are able to interact strongly with the surface it can severely reduce the diffusivity. The interaction also changes the concentration dependence of the diffusvity. When molecules interact with surface sites the diffusivity is expected to increase with pore concentration as the sites become saturated. Conversely if the there is little interaction with the surface molecule-molecule interaction increase with pore concentration leading to a reduction in diffusivity. The increase with loading is shown very clearly for silicalite and ammonia (Figure 40).

This data also shows a marked difference between the quasi elastic neutron scattering and PGGNMR data. In this instance the difference can be attributed to the time scales of the two measuring techniques. This is much shorter in the case of the QENS and the technique does not therefore see all of the molecules - particularly the more slowly moving ones. If the effect of the trapped molecules is allowed for the agreement is better.

A detailed examination of the effects of loading for methane, ethane and propane in the carbon membrane materials also shows an unusual response characteristic. It can be seen from Figure 41 and Figure 42 that whilst the methane diffusivity increases with concentration, suggesting a strong interaction with the surface, the ethane and propane diffusivities decrease indicating that the molecule-molecule interaction is stronger than the molecule -surface interaction. Clearly if it was required to develop a micropore membrane model for the transport of a mixture of these gases, the concentration dependence of the diffusivity would become extremely complex.

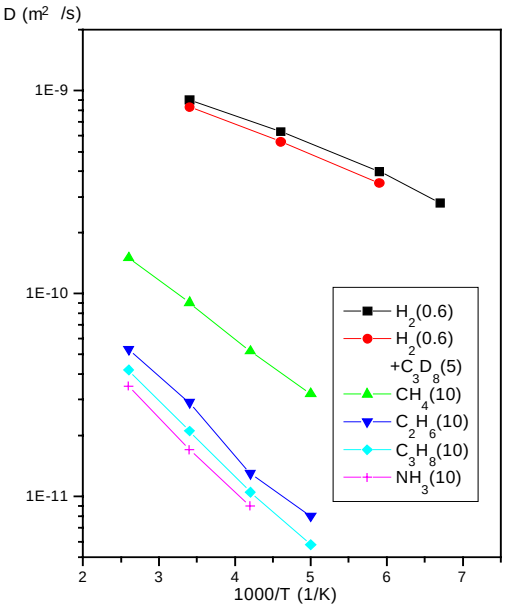

Comparison of the diffusivities of the different molecules considered in this study in carbon molecular sieves. Loadings in mass %, particle size 30 µm.

Figure 39

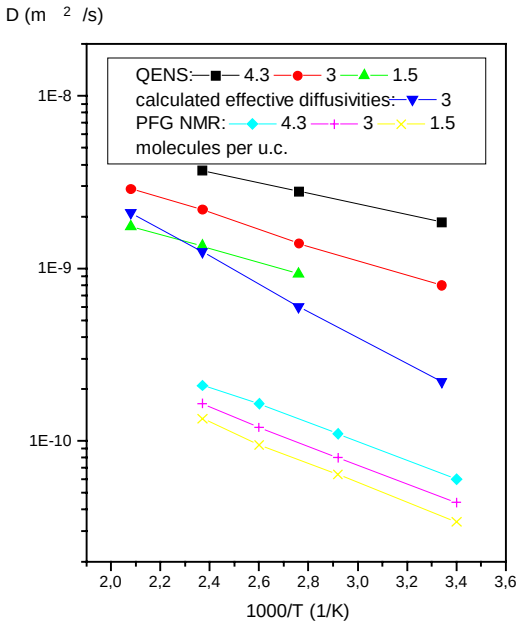

Ammonia diffusivities in silicalite obtained by QENS and PFG NMR for different quantities of molecules per u.c.

Figure 40

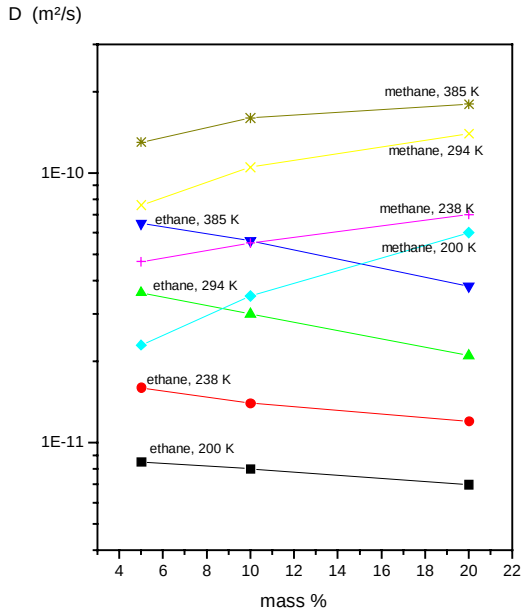

Diffusivities of methane and ethane in carbon molecular sieve particles (15 µm) as a function of the loading for different temperatures.

Figure 41

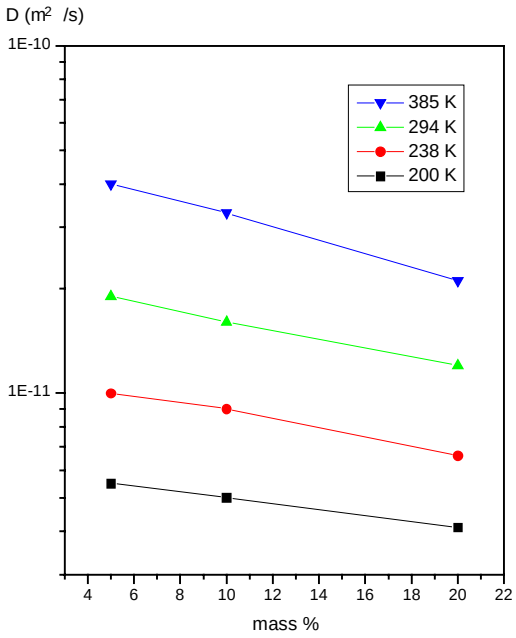

Diffusivity of propane in carbon molecular sieve particles (15 µm) as a function of the loading for different temperatures.

Figure 42

In all PFG NMR studies, interestingly enough, the hydrogen diffusivities were found to be only slightly affected by the presence of co-adsorbed molecules. One has to conclude, therefore, that the hydrogen molecules prefer diffusion paths which are different from those preferred by propane. As an example, Figure 39 has shown that the diffusivities of hydrogen in carbon molecular sieves in the presence and in the absence of propane are essentially identical. The same situation is reflected by Figure 43, showing the deuterium diffusivities in NaX without and with co-adsorbed propane. It is interesting to note that the ratio between the diffusivities of hydrogen and deuterium at single-component adsorption coincides with the reciprocal value of the square root of their mass ratio. Such a behaviour should exactly result under the condition of gas phase or Knudsen diffusion. Similar experiments with ZSM-5 failed, probably as a consequence of the H-D exchange between hydrogen and deuterated propane.

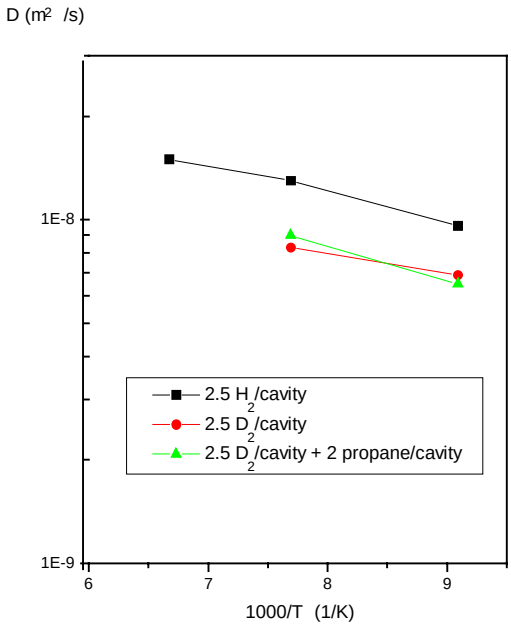

Diffusivities of deuterium with and without co-adsorbed propane in NaX. For comparison: pure hydrogen diffusivity.

Figure 43

This is not the case however with larger molecules. Figure 44 shows the diffusivity of ammonia in silicalite without and with co-adsorbed methane, while Figure 45 shows the reverse, viz. methane mobility without and with co-adsorbed ammonia. The representations clearly reflect the higher mobility of the non polar

methane molecule, both under single-component and two-component adsorption. Not unexpectedly, the presence of the less mobile ammonia reduces the methane mobility. It is interesting to note, that - also vice versa - the more mobile methane molecules effect a reduction of the ammonia mobility.

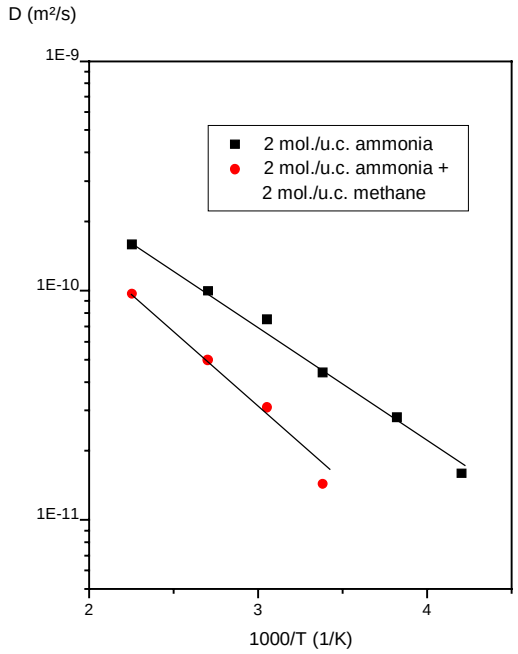

Ammonia diffusivities in silicalite, co-adsorbed (deuterated) methane.

Figure 44

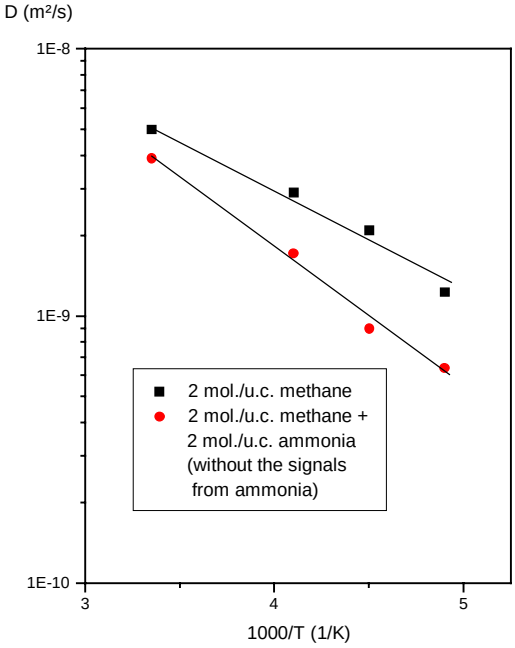

Methane diffusivity in silicalite, co-adsorbed ammonia.

Figure 45

This result shows again the complexity of the transport properties of these small pore domains whereby hydrogen is unaffected by co-adsorbed molecules whilst the larger molecules show strong interaction effects. This will present a considerable problem for incorporation into a comprehensive micropore membrane model. The results have also demonstrated that the PFGNMR technique is very well adapted to the study of the transport properties of these materials and can provide critical insights into the physics of the transport processes.

3.1.5.2 Quasi Elastic Neutron Scattering (QENS)

The translational and rotational dynamics of molecules adsorbed in microporous materials can be characterised by quasi-elastic neutron scattering (QENS).

This neutron technique is called quasi-elastic because the spectra are centred around zero energy transfer and small energy transfers are implied, typically ± 2 meV. If motions of the molecules are much slower than the time scale of the experiment, the spectra will only consist of an elastic peak associated with neutrons scattered without energy transfer. A broadening of the spectra will be observed if the molecules diffuse over a time scale ranging from 10^{-8} to 10^{-12} s.

Neutrons are scattered by the whole sample and therefore the adsorbent should scatter less than the adsorbate. Since the hydrogen atom has the largest incoherent scattering cross section, the largest signal will be obtained with hydrogenated molecules. However, the scattering from deuterated molecules can be measured.

3.1.5.2.1 Mobility of H_2 in the MFI structure : ZSM-5 and silicalite

The porosity of MFI is known to consist of two types of intersecting channels made by 10-membered oxygen rings. The free diameter of both channels is of ≈ 5.5 Å. However, QENS shows that a significant proportion of hydrogen (molecular) is trapped in this structure, on the time scale of the experiments (10^{-10}-10^{-12} s). The measurements were performed at the Institut Laue-Langevin in Grenoble, in the temperature range 90 - 200 K, using the IN6 and IN5 spectrometers. The proportion of trapped molecules varies with the temperature and loading. The trapping was found to be more effective in silicalite than in ZSM-5. A large increase of diffusivity with increasing loading was observed, which shows the existence of higher energy sites. The mean diffusivity of hydrogen in this structure is at least one order of magnitude smaller when compared with all other zeolites. This has been confirmed by PFG NMR measurements[48].

It is suggested that hydrogen is trapped in between the channels, inside the pentasil chains. The pores of these cavities are limited by 6-membered oxygen rings. Theoretical calculations are in progress to quantify the potential wells inside the chains.

3.1.5.2.2 Mobility of ammonia in silicalite

The diffusivity of ammonia in silicalite has been measured by QENS, using the IN5 spectrometer at the Institut Laue-Langevin[49]. The experiments were performed at different loadings and in the temperature range 300 - 480 K. The mobility increases with increasing loading. This is due to a larger interaction of the first molecules with silanol groups. During the time scale of the QENS experiment, two different ammonia species are measured : there are mobile molecules diffusing by jumps along the channels (mean jump length 3 - 5 Å), and immobile molecules, those interacting with silanol groups, whose proportion varies with temperature and loading. The residence time for molecules in interaction with silanol groups was estimated to be of the order of 1 ns. On the much longer time scale of the PFG NMR experiments, only one type of molecule is observed, having an effective diffusivity lower by one order of magnitude with respect to the mobile molecules measured by QENS.

3.1.5.3 Gravimetric Adsorption Studies

Work in the Department of Materials Science and Engineering, University of Bath, on the JOULE ceramic membrane project involved the measurement and analysis of adsorption isotherms for various gas adsorbates on different powdered ceramic adsorbents over ranges of pressures and temperatures. The aim of this work was to provide fundamental kinetic and equilibrium adsorption data to input into flowsheets for selected gas separation processes using ceramic membranes. The main materials examined are summarised in along with their surface area characteristics. As shown in Table 3 the pores of the ECN silica were to small to permit low temperature nitrogen adsorption.

The data was collected using a Hiden IGA which can measure adsorption isotherms gravimetrically for total pressures in the range 0-8 bar and temperatures in the range 25-460 °C. Samples are contained in a small, stainless-steel cone (volume ~ 0.3 cm^3) hung within a chamber heated by an external, annular furnace. The sample container is connected via an articulated gold chain to a horizontal beam balance. Temperature is controlled via a feedback loop between the furnace and a thermocouple adjacent to the sample container. Pressure is controlled by servo-valves (admitting and exhausting gas to the sample chamber) in a feedback loop with pressure transducers. Experimental control and data acquisition (sample weight, temperature and pressure) is via a PC connected to the balance, thermocouple and pressure transducers. The adsorbate gases and temperatures listed in Table 4. were selected to suit the separation processes of interest in the project. This measurement programme shows that even where isotherm temperatures are below the critical temperatures of adsorbates, saturated vapour pressures are in all cases above the maximum operating pressure of the IGA, so that no condensation should occur.

48 12th IZC, Baltimore, 1998, N.-K. Bär, H. Jobic and J. Kärger.

49 H. Jobic, W. Heink, J. Kärger, A. Tuel and M. Bée., Microporous and Mesoporous Materials, submitted in May 1998

However, measurement pressures for *n*- and *i*-butane are reduced to 3.6 and 6.8 bar respectively to avoid condensation in the balance head which is maintained at 35 °C to protect the beam mechanism.

Table 3 Characteristics of Ceramic Powders.

Sample	**SEM**	**N_2 adsorption @ 77 K**
silicalite	spherical particles ~ 2 μm diameter	BET* surface area = 425 m^2 g^{-1} DR** micropore volume = 0.20 cm^3 g^{-1} average DR micropore width = 0.57 nm
carbon	slab-shaped flakes ~ 25 μm thick	BET surface area = 691 m^2 g^{-1} DR micropore volume = 0.27 cm^3 g^{-1} average DR micropore width = 0.65 nm
silica	slab-shaped crystals ~ 50 μm thick	no measurable adsorption

* Brunauer-Emmett-Teller ** Dubinin-Radushkevich

Table 4. Isotherm Measurement Programme.

Adsorbate	**Nominal isotherm temperature / °C**						
	25	100	150	200	300	400	500
methane, CH_4	T_c = -82 °C						
ethane, C_2H_6	p^0 ≈ 40 bar	T_c = 32 °C					
propane, C_3H_8	p^0 = 9.39 bar	T_c = 97 °C					
carbon dioxide, CO_2	p^0 ≈ 60 bar	T_c = 31 °C					
n-butane, *n*-C_4H_{10}	p^0 ≈ 3.6 bar at 35 °C			T_c = 152 °C			
i-butane, *i*-C_4H_{10}	p^0 = 6.8 bar at 35 °C			T_c = 135 °C			
nitrogen, N_2	T_c = -147 °C						
ammonia, NH_3	p^0 = 10.03 bar	p^0 = 62.5 bar	T_c = 133 °C				

Key

	sub-critical (p^0 = vapour pressure)	Data from the CRC Handbook of Chemistry and Physics (75th Edn., 1994)
	super-critical (T_c = critical temperature)	
	not measured	

Typical equilibrium isotherms for carbon dioxide adsorption on silicalite and different temperatures are shown in Figure 46. Note that the amounts adsorbed in these isotherms are in mmol *excess* (i. e., the total amount less the amount that would have been in the pore volume if no adsorption had occurred) per unit de-gassed sample weight. All the isotherms are type I, showing a more-or-less steep rise in amount adsorbed until a flat plateau is reached. At higher temperatures less is adsorbed, as expected, and the isotherms approach linearity over the pressures accessible experimentally. Adsorption of different gases on different solids showed similar behaviour.

Various equations have been used by other workers to fit equilibrium isotherms of light alkanes and other simple gases on silicalites and zeolites[51,52,53,54] including the Dubinin-Radushkevich, Langmuir, Freundlich and Ruthven equations, and various Langmuirian forms such as the Tóth, Mathews-Weber, Jaroniec and Langmuir-Freundlich isotherms. The last of these has proven to give the best fit to adsorption data obtained so far at Bath.

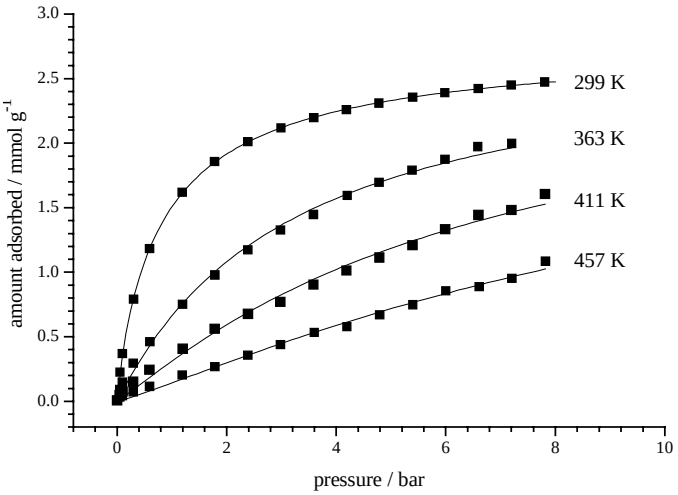

Figure 46. **Example Equilibrium Isotherms (CO_2 on silicalite; curves are best fits using equation [3]).**[50]

The Langmuir-Freundlich (LF) isotherm may be written as

$$n = a\frac{bp^c}{1+bp^c} \qquad [3]$$

where n is amount adsorbed and p is pressure and a is the adsorption capacity (the maximum amount adsorbed in the limit $p \to \infty$), b is an energy parameter (units of inverse pressure) and c is a dimensionless exponent. The quantities n and p are the LF variables, and a, b and c are the LF parameters. The energy parameter is given by an Arhenius equation

$$b = b_0 \exp\left(\frac{E}{RT}\right) \qquad [4]$$

where b_0 is a pre-exponential factor, E is an adsorption energy and R is the gas constant. For $c = 1$, the LF equation reduces to the Langmuir equation, and in the limit $p \to 0$ it reduces to the Freundlich equation, $n = abp^c$. The energy parameter is a pseudo-Henry's Law constant, though it should be noted that only for $c = 1$ does the low pressure limit of the LF equation reduce to Henry's Law. The curves in .Figure 46 confirm the LF equation is a good fit to all the adsorption data for CO_2 on silicalite; this conclusion applies to all other equilibrium data obtained at Bath. It proved impossible to use simpler isotherms forms such as the Langmuir equation and this therefore has implications for the membrane models used to data and the future development of more comprehensive models. It also shows tends to show that there is no real reason to resort to the complexity of the two site Langmuir model developed at IFP to described adsorption in silicalite. A summary of the LF parameters for the various adsorbents and adsorbates is given in Table 5(silicalite), Table 7 (carbon) and Table 6 (silica).

50 Choudhary, V R and Maydevi, S (1996). Adsorption of methane, ethane, ethylene and carbon dioxide on silicalite-I. Zeolites 17, 501-507

51 Abdul-Rehman, H B, Hasanain, M A and Loughlin, K F (1990). Quaternary, ternary and pure component sorption on zeolites. Ind. Eng. Chem. Res. 29, 1525-1535.

52 Choudhary, V R and Maydevi, S (1996). Adsorption of methane, ethane, ethylene and carbon dioxide on silicalite-I. Zeolites 17, 501-507

53 Hampson, J A and Rees, L V C (1993). Adsorption of ethane and propane in silicalite and zeolite NaY. J Chem. Soc., Faraday Trans. I 89, 3169-3176.

54 Dunne, J A, et al. (1996). Calorimetric heats of adsorption and adsorption isotherms (of different gases on different zeolites). Langmuir 12, 5888-5895; 12, 5896-5904; 13, 4333-4341.

Expansion of these parameters for silicalite and carbon gives the results shown in Figure 47 and Figure 48 for all of the adsorbates tested. This demonstrates the relative similarity of the adsorption extents on these two materials.

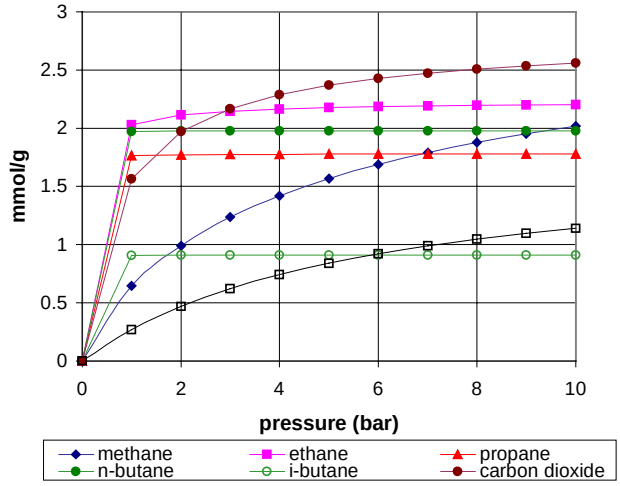

Figure 47 Adsorption on Silicalite at 25C

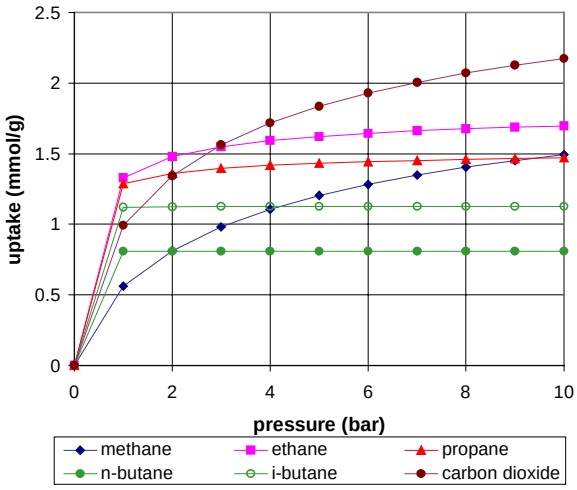

Figure 48 Adsorption on Carbon at 25C

Table 5. Best Fit Equilibrium Adsorption Parameters for Silicalite.

	Langmuir-Freundlich Parameters $n = a\,bp^c / (1 + bp^c)$; n / mmol g^{-1}, p / bar				
		$b = b_0 \exp(E / RT)$		$c = \alpha + \beta T$	
adsorbate	a / mmol g^{-1}	ln (b_0 / bar^{-1})	E / kJ mol^{-1}	α / -	β / T^{-1}
methane	3.22	-7.26	14.5	0.29	0.0018
ethane	2.24	-9.37	28.7	-0.21	0.0034
propane	1.78	-11.43	39.8	0.57	0.0018
n-butane	1.98	-10.41	39.6	1.92	-0.0021
i-butane	0.91	-9.70	39.5	1.82	-0.0018
carbon dioxide	2.82	-7.36	18.7	0.42	0.0016
nitrogen	1.77	-5.65	9.7	1.66	-0.0022

Table 6. Best Fit Equilibrium Adsorption Parameters for Silica.

	Langmuir-Freundlich Parameters $n = a\,bp^c / (1 + bp^c)$; n / mmol g^{-1}, p / bar				
		$b = b_0 \exp(E / RT)$		$c = \alpha + \beta T$	
adsorbate	a / mmol g^{-1}	ln (b_0 / bar^{-1})	E / kJ mol^{-1}	α / -	β / T^{-1}
carbon dioxide	2.37	-11.21	26.1	0.077	0.0028

Table 7 Best Fit Equilibrium Adsorption Parameters for Carbon.

	Langmuir-Freundlich Parameters $n = a\,bp^c / (1 + bp^c)$; n / mmol g^{-1}, p / bar				
		$b = b_0 \exp(E / RT)$		$c = \alpha + \beta T$	
adsorbate	a / mmol g^{-1}	ln (b_0 / bar^{-1})	E / kJ mol^{-1}	α / -	β / T^{-1}
methane	2.27	-8.41	18.0	0.47	0.0010
ethane	1.85	-7.57	21.0	0.01	0.0021
propane	1.57	-5.21	16.6	-0.38	0.0030
n-butane	0.81	-8.40	38.7	3.01	-0.0030
i-butane	1.13	-7.68	31.0	0.33	0.0007
carbon dioxide	3.08	-10.47	24.0	-0.37	0.0036

The parameters can also be used to look at the temperature dependence of the adsorption. Figure 49 demonstrates that even for propane there is a substantial weight uptake at 400C and 10 bar that would impact substantially on the pore transport properties. It should not therefore be assumed that adsorption approaches zero at high temperatures, particularly for higher molecular weight molecules.

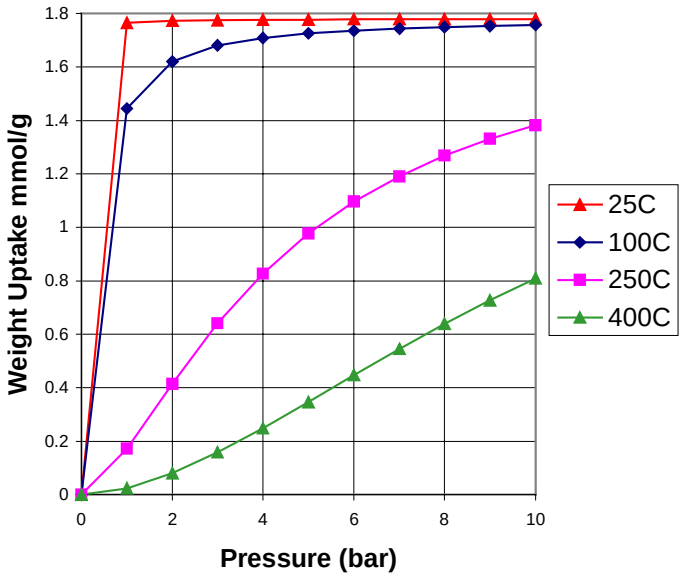

Figure 49 Propane Adsorption on Silicalite as a function of temperature

As the primary reason for determining the single component isotherms was to model multicomponent adsorption in the membrane models a preliminary evaluation was made by the BG Technology centre of the multicomponent adsorption isotherms using the extended Langmuir Freundlich model based on the excess adsorption isotherms given above. Further work is required to test the difference between the excess and total isotherms as earlier simulation work has shown that this makes a subsatntial difference to the calculated mixed adsorbed phases when using ideal adsorption theory[1].

3.1.5.3.1 Fundamentals - Conclusions

In summary there is a considerable amount of work still required to provide a comprehensive understanding of the adsorption and transport properties of micropore membranes. An understanding that will be crucial to the future development of microporous membrane based processes. This will need to encompass further work in the area of micropore adsorption and transport as well as pore network effects. The larger scale phenomena involved in the design of monoliths and the control of surface polarisation phenomena are now reasonably well understood and could be implemented in future development projects. In the case of the palladium membranes the model is fully developed and operational. The only uncertainty hinges around surface polarisation and its effects on the observed behaviour which may impact both on the efficiency of the membranes and their response to hydrogen

partial pressure. Some further validation data is also required under the more severe steam reforming conditions which were not readily accessible during this project.

3.2 Membrane Production and Testing

The membrane testing programme had several objectives. In the first instance it was there to provide the operating data that would support the flowsheet development studies. As such it was crucial that the membranes were tested on real gas mixtures under realistic operating conditions. The programme was also designed to allow a wider range of membranes to be tested under identical conditions to provide for the first time a genuine comparative test. A central requirement of the test programmes was that all of the membranes should be available in tubular form so that these comparative tests were not compromised by changes in geometry and whilst the project was not aimed at membrane development there was scope for some modification and improvement of the various membranes during the project. The test programme also provided for a direct comparative evaluation of the membranes using single component gases to be able to provide some simple ranking free from the problems of evaluating mixed gas behaviour.

3.2.1 Membrane Production

The membranes used in the project were all selected because the were available in tubular form with proven capabilities. In the event, for a variety of reasons, problems were experienced with some of the membranes although this has not impacted on the overall conclusions from the study. The membranes available to the project were, and shown in approximate size order based on their performance characteristics-

Microporous		
Silica	ECN	
Zeolite A	Smart Chemical Co.Ltd	(0.4nm)
Silica Alumina	British gas	
Carbon	MAST Carbon Ltd	
Silicalite	CNRS Lyon	(0.55nm)
Non porous		
Palladium	Johnson Matthey	
	Salford University	

It was planned at the start of the project that the silica, zeolite A, silica alumina, silicalite and Salford palladium membranes would all be produced on the ECN alumina substrate tube. Despite the high quality of these tubes this ultimately caused a lot of problems for a variety of reasons and all except the BG silica alumina and the Salford palladium membranes reverted to their original tubular supports. Despite some slight changes in geometry as a result of this the comparative testing was not compromised.

3.2.1.1 Microporous Membranes

3.2.1.1.1 ECN Silica Membranes

The ECN silica membranes comprise a multilayer structure with the supporting layers made from alumina and the separating layer from sol-gel silica. The support system for the silica membrane consists of 4 layers and is made in the following way. The α-alumina macroporous support tubes which are used as structural carrier for the actual membrane are made by ceramic paste extrusion followed by a sintering procedure. The diameter of the support tube is ID/OD = 8/14 mm and they can be manufactured in a length up to 1 m. Before the final membrane layers can be applied to this tube two intermediate layers are applied to the support. These layers reduce the surface roughness and pore size in order to obtain a nearly defect free support system for the gas separation membrane layers. Such an intermediate layer is coated onto the support tube by means of a film coat technique using an α-alumina colloidal suspension. After drying a sintering step is involved ensuring consolidation. The so called Knudsen membrane layer is

applied onto the second intermediate layer by slip coating of a boehmite sol. After drying and during a heat treatment this boehmite transforms to gamma-alumina which forms the Knudsen diffusion gas separation membrane layer. All layers are applied on the outside of the tube. Characteristics of the support system are given in Table 8.

Table 8 General characteristics of ECN membrane support system

	Layer of ECN support system			
	1	2	3	4
Material	α-Al_2O_3	α-Al_2O_3	α-Al_2O_3	γ-Al_2O_3
Thickness	3 mm	30 - 50 µm	30 - 50 µm	2 - 4 µm
Porosity	35 %	35 %	35 %	55 - 60 %
Pore diameter	5 µm	0.28 µm	0.16 µm	4 nm

The silica membrane layer is made by means of sol-gel processing. A silicon alkoxide is hydrolysed from which a polymeric inorganic silica sol is obtained. This sol is coated onto the support followed by drying and calcination. The final structure of the membrane can be seen in Figure 50. The thickness of the silica membrane measured with SEM is in the range 100-200 nm. Unsupported silica layers have been characterised in a Coulter Omnisorb 460 with N_2 physisorption using the Horvath-Kawazoe equation. Normally a maximum in the pore size distribution is always observed near 0.7 nm pore diameter. Unsupported silica membranes for the adsorption and diffusion studies have been made by pouring silica sol in a hour glass and drying it. It is commonly acknowledged that pore structure developed by this route is probably different to the pore structure of a silica membrane which is coated on a porous support. This is probably due to the different drying rate. From gas permeancy measurements using molecules with different sizes the pore size has been estimated to be about 0.4 nm. As the silica membrane layers can be coated onto support tubes already 1m in length, no limitations are foreseen in scaling up the production. The reproducibility is currently being examined. The silica membrane layers are currently calcined at 400°C which limits the operating temperature to a maximum off 350°C. The material is also susceptible to deterioration when exposed to water vapour at temperatures above 300°C. ECN have supplied the silica membranes to Bath, British Gas and IFP for the membrane testing programmes and the substrate tubes to British Gas, IRC :Lyon, Smart Chemical Company and Salford University for use as supports in the preparation of the silica-alumina, silicalite, zeolite A and palladium membranes.

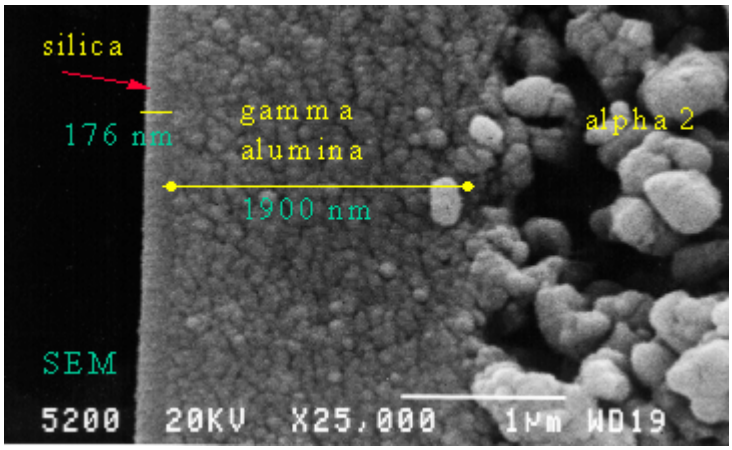

Figure 50 micro pore silica layer on ECN membrane tube

3.2.1.1.2 Smart Chemical Company Zeolite A membranes

Although SCC already produce zeolite A membranes commercially on stainless steel supports it was decided that to enhance comparability of the different systems SCC would attempt to produce their membrane using the ECN substrate tubes. Since it was already known that zeolite membrane growth occurs best on alpha alumina rather than on gamma alumina, due to the partial dissolution of gamma alumina in highly alkaline zeolite growth solutions, only alpha alumina samples were obtained from

ECN. Analysis of the growth on these tubes by X-ray diffraction and scanning electron microscopy indicated that zeolite X had formed instead of zeolite A. Despite variations in the growth conditions used, such as increased or decreased growth times and higher or lower growth temperatures, or even variations in the composition of the growth solution, no sample exhibiting clean, highly twinned zeolite A crystals were obtained. Further development of the zeolite growth technique allowed the production of what appeared to be a good membrane layer but separation tests still revealed this to be highly defective (Figure 60). At his stage production reverted to the standard porous stainless steel substrates. The surprising variability of the zeolite growth on the ECN ceramics contrasts with the experience of SCC with notionally similar ceramics from other suppliers. This indicates that there is probably some difference in the fine detail of the composition of the ECN ceramics.

Figure 51 Zeolite A Growth on ECN Alpha Alumina Substrates

The unsupported "membrane" samples for the adsorption and diffusion studies were prepared by a "solution" technique in which the NaA zeolite membrane nucleated and grew on a surface. After growth, the supernatant liquid was carefully poured away and the remaining zeolite film carefully and thoroughly washed with doubly distilled, deionised water until neutral, (pH 7). Subsequently, the fragments of zeolite membrane were removed from the surface by careful agitation and small (circa. 0.25cm^2 samples) carefully transferred to a beaker containing calcium nitrate (0.1 molar). The fragments were left to stand at 20^{o}C for 3 days to allow ion exchange. The samples were then drained, well rinsed and left to dry in air for 24 hours prior to dispatch. Typically, samples of around 1-2 grams could be prepared at a time.

Figure 52 Membrane Production Route

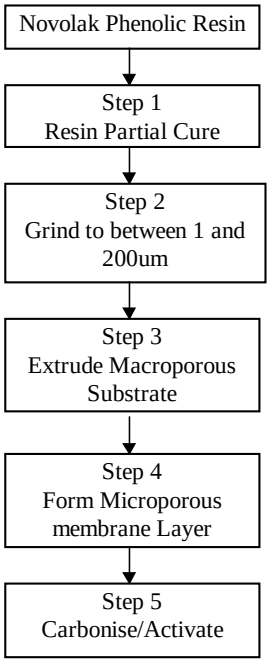

3.2.1.1.3 MAST Carbon Ltd Carbon Membranes

The microporous carbon membranes were originally developed[55] at the BP Research centre for applications in natural gas processing and high temperature hydrogen/hydrocarbon separation. Further development of the membranes subsequently took place under a BRITE-EURAM project aimed at developing both the applications and the membrane production technology[56]. The technology is now been further developed by MAST International Ltd where improvements to the production route have been introduced. The production route to the MAST membranes is summarised in Figure 52 and is radically different to conventional oxide based microporous membranes and other carbon membrane systems. The entire process, up to the firing stage, is based on conventional polymer processing and is therefore both low temperature and relatively low cost. The key to the membrane production process lies in the production of the macroporous polymer substrate (step 3). And the subsequent formation of the bi-layer,

55 European Patent 0 474 424 A2 filed 28/8/91
56 BRITE EURAM project BREU-CT92-0568

membrane - support, structure (step 4). In the final carbonisation (step 5), both the support and the separating layer undergo essentially the same degree of shrinkage eliminating any tendency to differential shrinkage and crack formation and permitting the formation of defect free microporous layers in a single firing step. The route, via the polymer coating step (step 4), which is essentially paint technology, has the additional benefit that the 10μm separating layer can be produced on a large pore support (macropores up to around 10μm) eliminating the necessity for the graded support structure that is always used in oxide ceramic membrane production. The elimination of the multiple firing stages implicit in the production of the graded oxide supports should give the carbon systems a major price advantage.

The structure of the membrane produced via this route is shown in Figure 53. The particulate substrate and the 10um separating layer are clearly visible. The critical part of the production process is in the resin precure for the support production as it is essential that the degree of cure is sufficient that the particles maintain their form during the carbonisation step, as is apparent from the figure, but not so high that sintering cannot take place. The limit on thickness of the membrane layer that can be produced has not been established but it seems likely that it will of the same order of magnitude as the pores in the substrate. This is directly related to the size of the powder used in the substrate production and is approximately 20% of the particle diameter.

Figure 53 : Membrane Structure

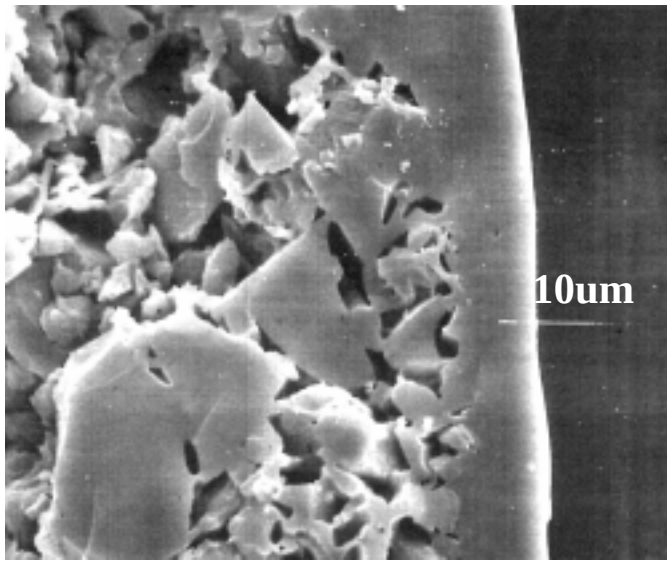

Two main routes have been examined for the production of the microporous separating layer involving either multiple thin resin coats with a cure step after each coat or one single thicker coat. Typical performance characteristics for the carbonised single coat membrane in a helium leak test is shown in Figure 54. Surprisingly the result shows a minimum in the Knudsen flux which is theoretically associated only with long straight pores - not the kind of pore structure that would normally be associated with glassy carbon structures.

The pore size distribution of the membrane layer is shown in Figure 55 and typically has slit widths of around 0.8nm. Theoretical studies have shown that this is approximately optimal for separation via the "adsorption" mechanism[57] (Figure 55).

57 R F Cracknell, D Nicholson and N Quirke, Molecular Simulation, 13, 161 (1994)

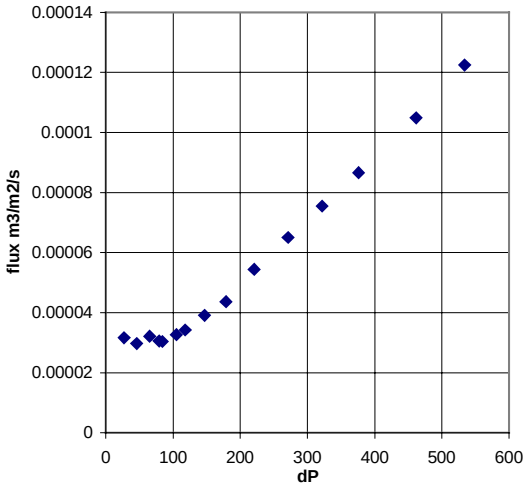

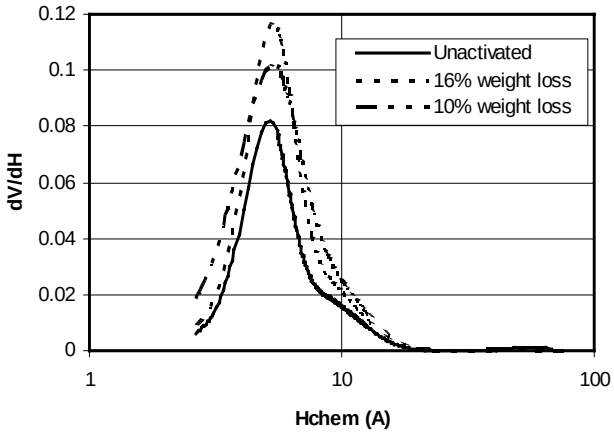

Figure 54 Knudsen Plot for Single Thick Coat Membrane

Figure 55 Micropore Structure of Carbon membranes

The membranes are highly resistant to chemical attack. The main limitation to the use of the carbon membranes is that they oxidise. Gas phase oxidation will normally be limited to oxygen, steam or carbon dioxide although other gases, such as NO2, can also attack the structure. The carbon is also subject to attack by oxidising chemicals such as nitric acid although it is resistant to both strong alkalis and simple acids. The rate of oxidation is in the order :-

Oxygen > steam > carbon dioxide

With oxygen attacking the membranes at temperatures as low as 250-300C whilst steam attack commences at about 700C and carbon dioxide at ~800C.

The samples for the adsorption and diffusion studies were prepared by dip coating the resol precursor, used in the production of the actual membrane layer, onto polished stainless steel plates. After drying and curing these were then carbonised under the usual conditions. This caused the polymer layer to shrink and peel of from the steel substrate producing thin, ~10 micron, flakes of glass carbon. Approximately 200mg of the carbon flakes could be produced using ~20 5cmx 2cm plates. Earlier studies demonstrated that the adsorption and transport properties of the flakes were very similar to those of the actual membrane layer.

3.2.1.1.4 IRC Lyon, Silicalite Membranes

The pore size of the MFI zeolites (ZSM-5, silicalite-1) is about 0.55 nm and beside molecular sieving, selective adsorption plays a major role in separation mechanisms with MFI membranes. However, the performance of the separation is drastically affected by the presence of defects in the zeolite layer (any passing-through pathway not controlled by a zeolite pore can be considered as a defect).

In most of the zeolite membranes described in the literature, a continuous zeolite layer is supported on top of a porous ceramic support. When compared to bulky, self-supported zeolite membranes, supported materials present a higher permeance, given their much lower thickness, and better mechanical properties. However, it is still always necessary to build a continuous zeolite layer to avoid defects, which represents a challenge when important membrane surfaces are required.

At IRC, a different concept has been used and the zeolite membrane consists of a composite material obtained by a pore-plugging method[58], the zeolite being synthesised by a hydrothermal step in the pores of α-alumina macroporous tubular support. This in-situ synthesis results in a separative zeolite phase

located in (and not on top of) the host ceramic material[59]. This composite membrane may provide a series of potential advantages when compared to conventional supported systems: In principle, it seems easier to prepare a large area of zeolite membrane by pore plugging than by building a continuous defect-free supported layer. In the composite material, the maximum size of a defect will be that of the pore, when much larger defects may occur in the supported membrane. When used, and especially during thermal cycling or under mechanical effort, long-range stresses could appear in the supported films, which could lead to a detrimental, irreversible formation of cracks. This not the case in the composite material, where discrete zeolite aggregates are distributed within the host porous framework. The separative material is here protected by the alumina matrix. This could be important when some abrasion may occur during specific applications, as when combining the membrane with catalyst pellets.

A detailed description of the hydrothermal synthesis has been published[58]. Briefly, the support (Membralox T1-70, purchased from SCT-US Filter), which consisted of a macroporous multilayered α-alumina tube, was placed in a teflon-lined stainless steel autoclave containing a clear solution prepared using tetrapropyl ammonium hydroxide (TPAOH) (1M solution from Aldrich) and silica (Aerosil Degussa 380). Synthesis was carried out at 443 K for 72 hours. At the end of the synthesis, the tube was removed from the autoclave and dried at 373 K for 12 hours. At this stage, the template molecule (TPAOH) was present in the zeolite pores and, in absence of defects, the tube is gas-tight. This was observed in almost all cases (> 95%) after only one hydrothermal step. The template was removed after 20 h calcination at 773 K (heating ramp, 1 $K.min^{-1}$) under a stream of 5% O_2 in N_2.

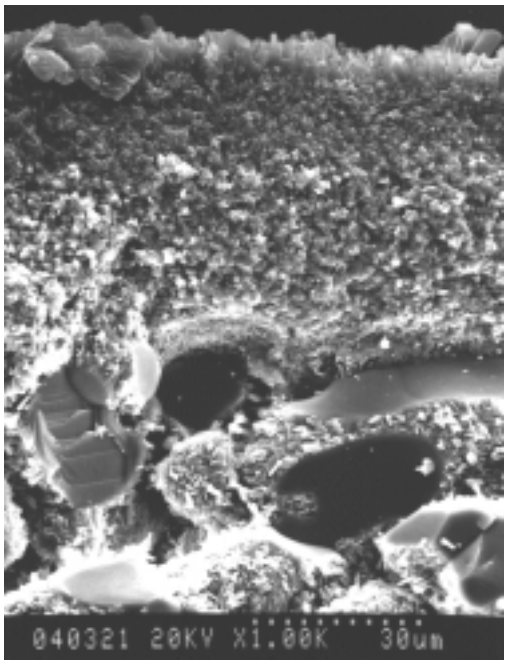

Figure 56. SEM photograph of the composite zeolite-alumina membrane cross-section.

Figure 56 shows a SEM micrograph of a cross-section of the tube after zeolite synthesis. Small zeolite crystals, with the typical MFI shape can be observed on the large α-alumina particles of the external layer (with the largest pore size). However it is more difficult to discriminate between zeolite and alumina in the two other layers.

SEM-EDX analyses have shown that, in these two layers, the ratio Si/Al fits the value corresponding to the filling up of the pores by zeolite[59]. Finally, on top of the final layer, large, non-connected zeolite crystals can be observed. These two observations, presence of non connected crystals on top, filling up of the intermediate layers, suggests that the zeolite separative layer is confined in the porous framework, in agreement with the pore-plugging method.

3.2.1.1.5 BG GRC Silica-Alumina Membranes

Previous work at BG Technology had led to the development of membranes based on an alumino-silicate separating layer prepared by sol-gel methods. This membrane was initially prepared on the inner surface of a porous alumina tube, supplied by Fairey Ceramics (UK). The quality of the porous support tube was rather variable and this led to a requirement for multiple cycles of sol-gel deposition and firing to produce the finished membrane.

On switching to the ECN support tubes several difficulties immediately became apparent in preparing the alumino-silicate membrane on the 4 nm -Al_2O_3 support surface . Previous membranes had been made by

58 J. Ramsay, A. G. Fendler, A. Julbe and J.-A. Dalmon, French Patent #055652, (1994)
59 A. Giroir-Fendler, J. Peureux, H.Mozzanega and J.-A. Dalmon, Stud. in Surf. Sci. Catal., 101 (1996) 127

sol-gel deposition on the inner surface of a support tube whereas the prepared surface of the ECN support was the outer tube surface. This meant that the coating, drying and subsequent handling of the membrane tube became more difficult, particularly as there was the possibility of damage to the coating whilst drying.

In addition, the entire drying regime was altered by the reduced surface porosity of the support tube compared to the previous substrate. The highly polished finish of the Al_2O_3 top layer of the ECN support also proved problematical in that the alumino-silicate membrane layer did not adhere well to the surface. This was shown by spallation of the membrane coating either before or after firing. As the project brief did not extend to making major alterations to the membrane formulation or preparation techniques, it was decide to address these matters by varying the sol concentration (and thus its viscosity) and the sol-substrate contact time. Further variations were also made in the drying regime and in the firing regime.

Once a coherent coating was achieved it was further found that the tubes prepared in this way had a high permeability, indicative of a defective coating. Therefore, it was decided to coat each tube twice, in order to obtain a reasonable permeation rate. This was similar to the situation in the original BG membrane preparation where multiple cycles of coating and firing were required to achieve a separating layer. This had been attributed to the coarseness of the original supporting layer, and it had been hoped that the new substrate tubes would permit the application of the membrane layer in a single coating-firing cycle. It may therefore be that multiple coating cycles are necessary to minimise the effects of microscopic cracks in the membrane layer, even on the new substrate. Membranes were therefore prepared using two cycles of coating and firing, using a reduced viscosity sol, and with an extended heat treatment time at a low heating rate, and passed on into the membrane testing programme.

Unfortunately subsequent testing demonstrated that whilst these membranes were greatly improved over the single coat systems they still showed evidence for some defects in the hydrogen permeation testing (see section 3.2.2). As the option to return to the original support was not available as Fairey had ceased production work will continue using he ECN support tubes after the current project ends.

3.2.1.2 Salford University Palladium membranes(Johnson Matthey Palladium Membranes

Two types of ceramic supported palladium membranes were used in this project. Johnson Matthey supplied membranes on a commercial basis to the project along with the special module for their use. These systems were however limited to 400C and 25Bar.

In parallel Salford University prepared and tested membranes both via a magnetron sputtering approach and electroless plating although the MS route was abandoned early in the project. Although the surfaces of supports with complex geometries can be coated with a uniform layer of metal film using the conventional electroless plating technique, the metallic film is just formed via the free deposition and growth of the reduced metallic particles on the pre-deposited palladium nuclei during the electroless plating process. Therefore, it is very difficult to maintain the deposited metallic film dense or crack-free. Electroless plating combined with an osmosis technique was employed to make Pd-based composite membrane at Salford University. Dense or crack-free Pd films were successfully made by this technique.

Four kinds of supports, e.g. porous stainless steel (SS), γ-Al_2O_3, α-Al_2O_3, Vycor glass (VG), were used as supports for the preparation of Pd composite membranes by electroless plating combined with osmosis. The palladium was coated on the outside surfaces for all these tubular supports:-

1. Vycor glass
2. γ-alumina coated supports
3. α-alumina tubes
4. porous stainless steel

it was found that neither Vycor glass nor γ-alumina supports produced adherent deposits of Pd when tested in hydrogen atmospheres and further trials with these two materials were abandoned. The work then concentrated on the ECN α-alumina tubes and porous stainless steel.

Dense or crack-free Pd composite membrane was successfully made when α-Al_2O_3 was used as support. No palladium peeling off of the deposit was observed even after several temperature cycles. The composite membrane possessed appropriate hydrogen permeability and a high hydrogen selectivity. Since the average pore size of the top layer of α-Al_2O_3 support is about 0.2 μm, which is larger than the size of palladium particles deposited from the plating solution, the palladium particles were able to form and grow on the inside wall of the α-Al_2O_3 pores. These particles coalesce with the palladium film on the surface of the support to "anchor" or fix the palladium film with the support. So the adhesion of Pd film with α-Al_2O_3 support was increased considerably. For γ-Al_2O_3, due to the small pore size of top layer (about 4 nm), no "anchoring" can occur, so the adhesion of deposited film with the γ-Al_2O_3 support was not strong enough to avoid peeling.

Although the same pre-treatment and activation procedure was used for the SS support as that for other kinds of supports, the Pd deposition rate was much slower on the surface of the SS support. This means that for palladium deposition the surface properties of the SS support were significantly different. After sufficient plating time, however, a palladium layer with an appropriate thickness was still obtained. The Pd/SS composite membrane showed equivalent permselective characteristics for hydrogen as the Pd/α-Al_2O_3 composite membrane. The fact that the SS support has a similar pore size as the α-Al_2O_3 support emphasised the role of "anchoring".

Because some impurities, especially organic ones in electroless plating solution can be co-deposited with the palladium particles on either of the supports, the decomposition of these impurities at high temperatures leads to the formation of pinholes or cracks. These pinholes or cracks can be repaired by the combination of electroless plating with osmosis. Driven by the osmotic pressure, the water in the plating solution near the pinholes or cracks in the Pd film permeated from the plating solution to the NaCl solution. This increases the concentration of $Pd(NH_3)_4^{2+}$ in the area near the pinholes and simultaneously, the flow of water can improve the transfer of $Pd(NH_3)_4^{2+}$ from the bulk solution to the pinhole area. Both can lead to a faster palladium deposition rate in the pinhole, compared to other areas. Therefore, this technique of electroless plating combined with osmosis enable pinholes or cracks to be repaired without causing a significant increase in the thickness of the palladium film. The repairs were carried out for both Pd/SS and Pd/α-Al_2O_3 composite membranes.

Figure 57 shows the nitrogen permeation flux of Pd/SS composite membrane as a function of permeating temperature before and after repair. It is seen that before repairing the nitrogen leak of the Pd/SS tube was large, indicating the presence of pinholes. After repairing, the nitrogen leak decreased significantly. Figure 58 shows the hydrogen permeation flux of the composite membrane before and after repairing. Although the hydrogen permeation flux decreased significantly after repairing, the reduction in hydrogen permeation flux was much smaller than that of the nitrogen permeation flux. Therefore, although the reduction of nitrogen permeation flux resulted partly from the increase of Pd film thickness caused by repairing, it was mainly a result of the disappearance of pinholes. This is confirmed by Figure 59, which shows the hydrogen/nitrogen permeation flux ratio. If the thickness of the Pd film had only increased and pinholes or cracks remained, no improvement in the hydrogen/nitrogen permeation flux ratio would be expected. However, the much higher hydrogen/nitrogen permeation ratio achieved by repairing demonstrates that the Pd/SS composite membrane were almost dense or crack-free.

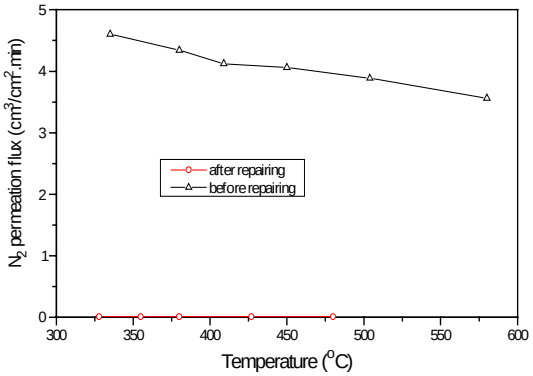

Figure 57 Nitrogen permeation flux of Pd/SS composite membrane as a function of permeating temperature

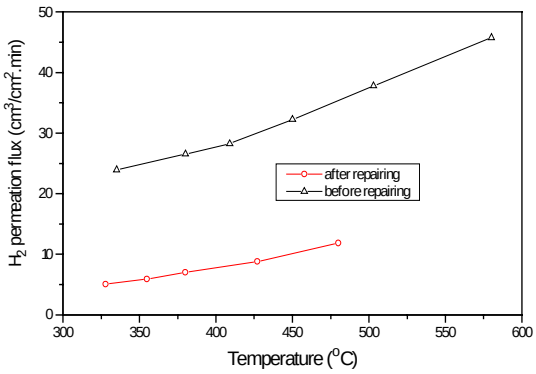

Figure 58 Hydrogen permeation flux of Pd/SS composite membrane as a function of permeating temperature

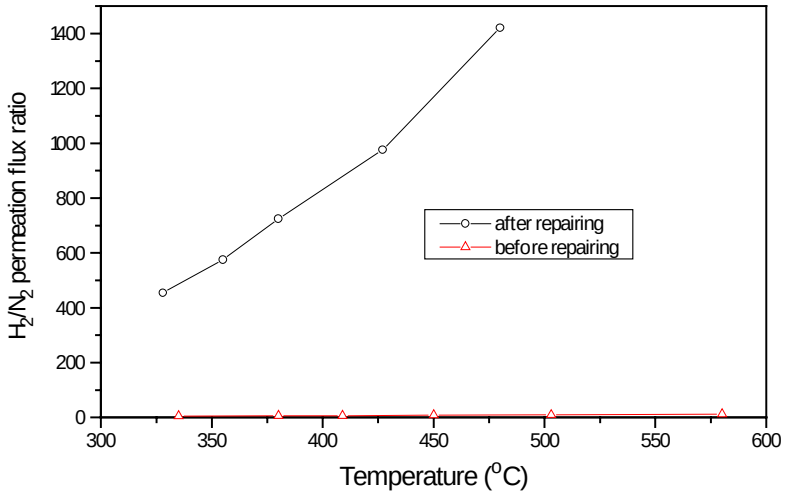

Figure 59 H_2/N_2 permeation flux ratio of Pd/SS composite membrane as a function of permeating temperature

3.2.2 Comparative Testing

Gas permeation measurements have been performed at 100, 200 and 300°C using H_2, He, CH_4 and CO_2. The following sequence of measurement has been used for all membranes:

1. heating of membrane and module with 60 °C/h to 300 °C under He atmosphere;
2. permeability measurement of He, H_2, CH_4, CO_2, and again He;
3. cooling with 60 °C/hr to 200 °C under He;
4. permeability measurement of He, H_2, CH_4, CO_2, and again He;
5. cooling with 60 °C/hr to 100 °C under He;
6. permeability measurement of He, H_2, CH_4, CO_2, and again He;
7. cooling to room temperature under He.

The results of these tests at 100C and 300C are shown in **Table 9** and **Table 10** respectively. In these results the gradient of the hydrogen permeability provides an indication of the degree of perfection of the membranes as the gradient should be zero if there were no defects (pure Knudsen diffusion). It can be seen that the carbon and silicalite gave the best results with the silica close behind whilst the BG silica alumina showed evidence for defects. The poor performance of the BG membrane was in line with the problems experienced by BG in the production process. The permselectivity provides an indication of the relative fluxes of the different pure components, and therefore information on the pore structure of the membranes, but should not be taken as indicating selectivity in a multicomponent environment which will tend to be very different.

Table 9 Comparative testing results of permeation measurements at 100^{o}C

Membrane	H_2 permeability (10^{-6} mol/m^{2}sPa)	Permselectivity at P_{av} = 0 bar			
		H_2/CH_4	H_2/CO_2	CO_2/CH_4	H_2/He
Silicalite; IRC	$0.084*P_{av} + 1.569$	1.7	2.3	0.74	1.5
Silicalite: IRC	$0.002*P_{av} + 0.119$	1.0	1.1	0.91	1.7
Silica: ECN	$-0.008*P_{av} + 0.839$	139	2.8	50	1.0
Silica-alumina: Brit.Gas	$0.149*P_{av} + 2.597$	2.4	3.2	0.75	4.4
Carbon: MAST	$0.003*P_{av} + 0.101$	6.1	1.0	6.1	3.4

Table 10 Comparative testing results of permeation measurements at 300^{o}C

Membrane	H_2 permeability (10^{-6} mol/m^{2}sPa)	Permselectivity at P_{av} = 0 bar			
		H_2/CH_4	H_2/CO_2	CO_2/CH_4	H_2/He
Silicalite: IRC	$0.15*P_{av} + 1.377$	2.2	2.4	0.92	1.0
Silicalite: IRC	$0.004*P_{av} + 0.113$	2.4	3.5	0.69	1.4
Silica: ECN	$0.013*P_{av} + 1.355$	139	10.9	12.8	0.9
Silica-alumina: Brit.Gas	$0.104*P_{av} + 2.008$	2.4	4.4	0.55	1.2
Carbon: MAST	$0.002*P_{av} + 0.063$	7.8	4.4	1.8	2.0

The performance characteristics of the membranes can be more clearly seen from the relative temperature dependencies of the permeability. These are shown at 0Bar and 8Bar average pressures respectively in Figure 60 calculated from the data in **Table 9**, **Table 10** and the additional data at 200C.

This clearly demonstrates the difference in pore size between the carbon and the silica as activated diffusion requires the pore size to be relatively close to the molecular size. It is however surprising that the data apparently shows the carbon to have a larger pore size than the silicalite given the transition to activated diffusion exhibited by the silicalite. The transition away from Knudsen diffusion reflects the increased density in the pores. It should also be noted that, based on these different responses the silica membrane will be most effective at high temperature whilst the carbon should be most effective at low temperature although this will also be effected by the molecular concentration in the pores which will additionally depend both on the pressure and the adsorbing gas.

Figure 60 Permeability as a function of Temperature at Pav = 0 Bar and 8 Bar respectively

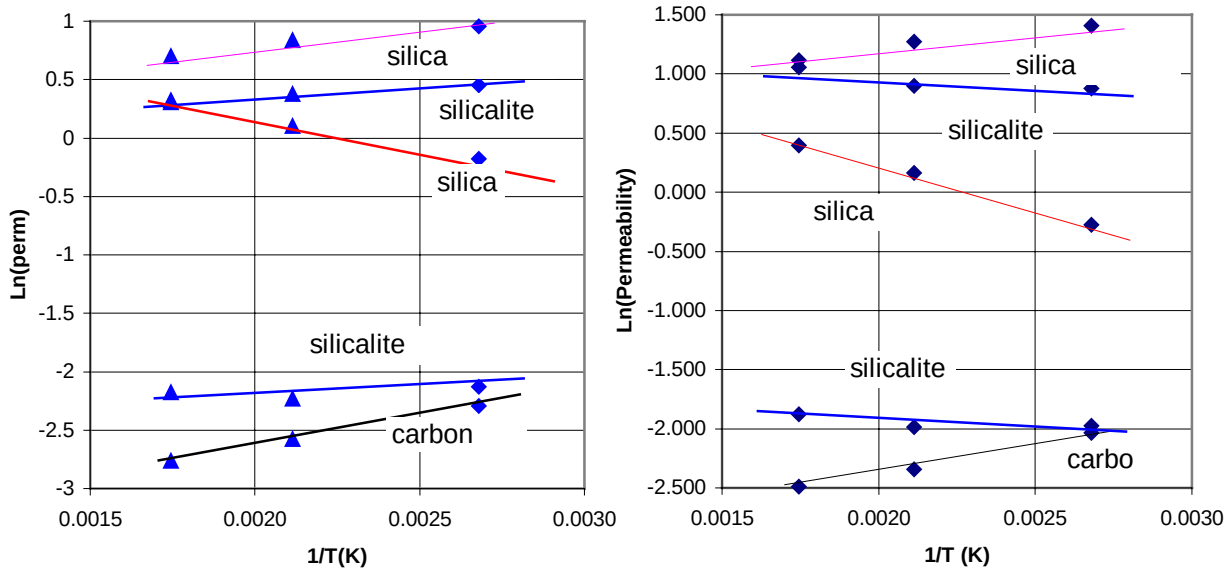

The permeability's of the membranes is also broadly in line with the relative thickness' of the membrane layers although this is complicated by the different pressure responses of the membranes(Table 11). The ECN silica is the thinnest, at around 800nm, whilst the carbon membrane is the thickest at 10um. Direct measurement of the silicalite membrane thickness is not possible but estimates, based on membrane performance, suggest an active layer thickness of around 3um.

Table 11 Calcaulated permeabilities as a function average presure(Bar) and temperature

		Permeability at Pav (Bar) (x10^-6) mol/m2/sec/Pa					
	Temp(C)	0	2	4	6	8	10
Silicalite; IRC	100	1.57	1.74	1.91	2.07	2.24	2.41
Silicalite: IRC		0.12	0.12	0.13	0.13	0.14	0.14
Silica: ECN		0.84	0.82	0.81	0.79	0.78	0.76
Silica-alumina: Brit.Gas		2.60	2.90	3.19	3.49	3.79	4.09
Carbon: MAST		0.10	0.11	0.11	0.12	0.13	0.13
200C							
Silicalite: IRC	200	1.46	1.66	1.86	2.06	2.26	2.46
Silicalite: IRC		0.11	0.11	0.12	0.13	0.13	0.14
Silica: ECN		1.11	1.12	1.14	1.15	1.16	1.18
Silica-alumina: Brit.Gas		2.31	2.56	2.81	3.07	3.32	3.58
Carbon: MAST		0.08	0.08	0.08	0.09	0.09	0.10
300C							
Silicalite: IRC	300	1.38	1.68	1.98	2.28	2.58	2.88
Silicalite: IRC		0.11	0.12	0.13	0.14	0.15	0.15
Silica: ECN		1.36	1.38	1.41	1.43	1.46	1.49
Silica-alumina: Brit.Gas		2.01	2.22	2.42	2.63	2.84	3.05
Carbon: MAST		0.06	0.07	0.07	0.08	0.08	0.08

Overall the results suggest that there is scope for reducing the membrane layer thickness in both the carbon and silicalite membranes so as to improve the flux and membrane utilisation. Whether this is practical without destroying the excellent selectivities is questionable.

In the case of the palladium membranes the hydrogen permeance is given by Sieverts law:-

$$J_{H_2} = Q_{H_2}(P^n_{f,H_2} - P^n_{p,H_2})$$ **Equation 3**

In which: JH_2 = the hydrogen flux through the membrane (mol/m^{2}s)
QH_2 = the hydrogen permeance (mol/m^{2}sPa)
PH_2 = partial hydrogen pressure on feed (f) and permeate (p) side
n = a coefficient whose value is between 0.5 and 1

and, for the JM membranes evaluated in this study, Q = 1.358 * 10^{-5} mol/m^2/s/Pa$^{0.82}$ which gives:-

Table 12 Calculated values for Q and n

T (^{o}C)	Pf (bara)	dP (bara)	Ff (Nl/min)	Fs (Nl/min)	Q (mol/m^{2}sPa$^{0.82}$)	n	A_{mem} (cm^2)
600	40	22	15	1.2	5.34 * 10^{-6}	0.82	140
600	40	22	8	1.2	3.58 * 10^{-6}	0.82	140
600	40	22	6	1.2	3.35 * 10^{-6}	0.82	140
600	40	22	4	1.2	4.30 * 10^{-6}	0.82	140

These hydrogen fluxes are significantly higher at these temperatures than the estimated flux of the ECN silica membranes at a similar temperature.

To summarise, in the permselectivity data in Table 10 and Table 12 the ECN silica membrane stands out. However, as will be shown in the mixed gas behaviour, this reflects the highly microporous nature of the membrane and its molecular sieving capability which results in very poor selectivities in mixed gas feeds where one of the components is strongly adsorbing. These results, taken together with the mixed gas data, demonstrate very clearly the critical requirement to test microporous membranes in real mixed feeds. The results also show that the silica, silicalite and carbon membranes all have excellent structural characteristics that would merit further development if the correct applications can be found.

3.2.3 Dispersion Phenomena

A further element that has been extensively examined is the effect of surface polarisation on the membrane performance as a function of the various flow rates in conjunction with the theoretical fluid dynamic studies at NTUA. The key issue is that when membranes are tested with single pure gases the flux characteristics are absolute and subject to no experimental uncertainties. As soon as a second gas is introduced a radial concentration gradient is established at both the feed and permeate sides of the membrane that reduces the effective driving force at the membrane surface. This is shown schematically in Figure 61. The experimental consequence is that the experimental membrane performance underestimates the true membrane performance in the absence of these polarisation effects. This diminution is more severe under laboratory conditions, as compared to commercial operation, as lower linear velocity, and therefore less turbulent, gas flows are generally used.

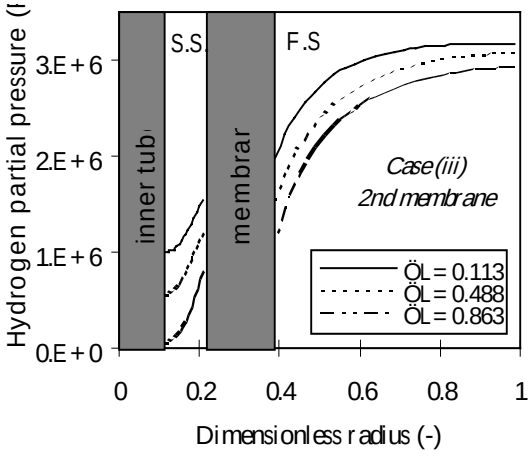

Figure 61: Hydrogen partial pressure radial profile at three axial points in the separator. Dispersion model. P_f=51bar, P_s=41bar, Q_f=24Nl/min, Q_s=13.19Nl/min

To test these effects Several high temperature and high pressure experiments were performed using the dense Johnson Matthey module and the ECN silica membrane. The aim of these experiments was to verify and validate the computational fluid dynamics models which describes the dispersion effects. Permeation measurements with H_2, CH_4, CO_2 and N_2 and separation measurements were performed using a feed mixture of H_2/CH_4 and N_2 as sweep gas at approximately 400°C. An overview of the process conditions for the palladium membranes is given in Table 13.

Table 13 Overview of process conditions used in validation experiments

Pf (bara)	dP (bar)	Ff (Nl/min)	Fs (Nl/min)
25	20, 10, 5, 2.5	25, 15, 5	15, 7.5
12.5	10, 5, 2.5	25, 15, 5	15, 7.5
6.3	5, 2.5	25, 15, 5	15, 7.5

The values of gas permeabilities used in the simulations were obtained from pure gas permeation experiments and are presented in Table 14. It is worthwhile to notice that although J-M membranes are normally permeable only to hydrogen, the calculated permeabilities of methane and nitrogen are not zero probably because of possible small leakages through the membrane material.

Table 14: Permeability values for the J-M membranes calculated from the permeation experiments.

Component	Permeability coefficients ($mol.m^{-2}.s^{-1}.Pa^{-0.82}$)
H_2	1.35E-6
CH_4	1.35E-9
N_2	1.35E-9

The equation used to describe the permeation of the component i through the J-M selective membrane in all the separation experiments was proposed by ECN partners as :

$$Q_i = \alpha_i \left(P_i^{F\,0.82} - P_i^{S\,0.82} \right)$$

where: Q_i represents the separation rate of component i ($mol.m^{-2}s^{-1}$), á$_i$ the permeability coefficient of component i ($mol.m^{-2}.s^{-1}.Pa^{-0.82}$), P_i^F the partial pressure of component i on the feed side (Pa) and P_i^S the partial pressure of component i on the separation side (Pa). The performance of the tubular membranes in a mixed gas environment can then be estimated using the fluid dynamics approach in the presence and absence of dispersion effects. A typical result is shown in **Figure 62**. It can be seen that the estimated performance in the absence of dispersion effects grossly overestimates the observed performance whilst the inclusion of dispersion provides considerably better, although still not perfect, agreement. The reason for the observed discrepancy has not been identified but could for instance result from inaccuracies in single component performance. Further work will be required to resolve this.

However the real issue is that when evaluating mixed gas membrane performance in the laboratory the observed results will always be low as a result of these dispersion effects by an amount that will vary with the test conditions and the membrane performance. As the kinetic models for flowsheet evaluation are then developed using the observed data this will always tend to lead to an underestimate of the performance that might be expected in a full size unit where higher linear velocity gas flows will tend to be used. A possible way around this was evaluated using a novel differential reactor assembly developed by ECN (

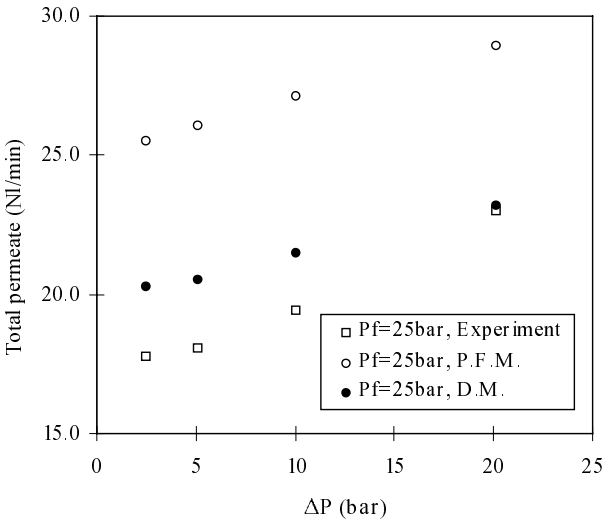

Figure 62: Hydrogen permeate flow at the separation outlet vs. pressure difference.
Inlet feed rate=24.7Nl/min

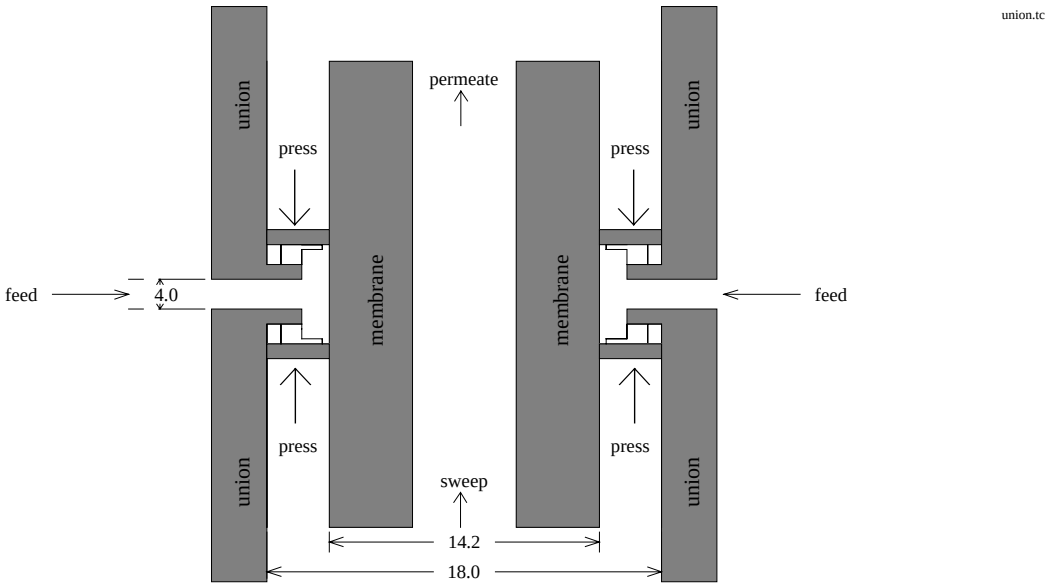

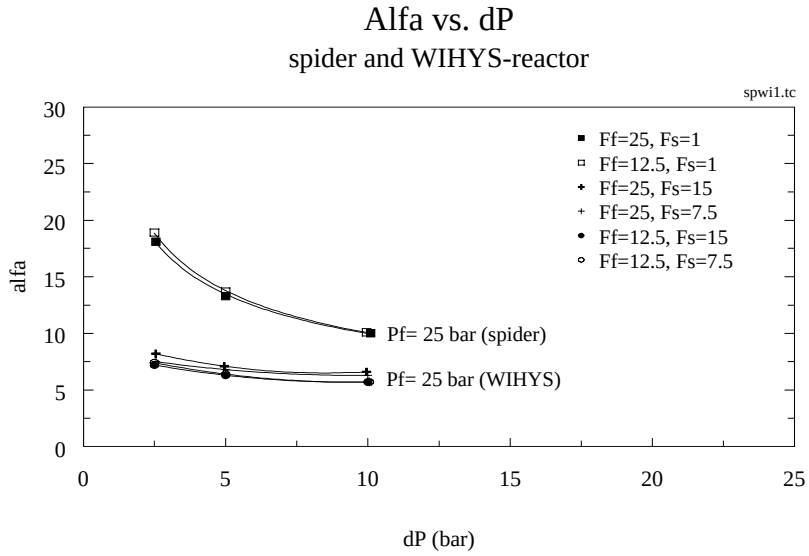

) which sought to minimise dispersion effects. Typical results obtained using a conventional tubular reactor and the spider reactor are shown in (Figure 64) for a microporous silica membrane. It can be seen that when the dispersion effects are reduced the membrane selectivity increases significantly as predicted by the fluid dynamic calculations.

Figure 63 Schematic of differential separator or spider

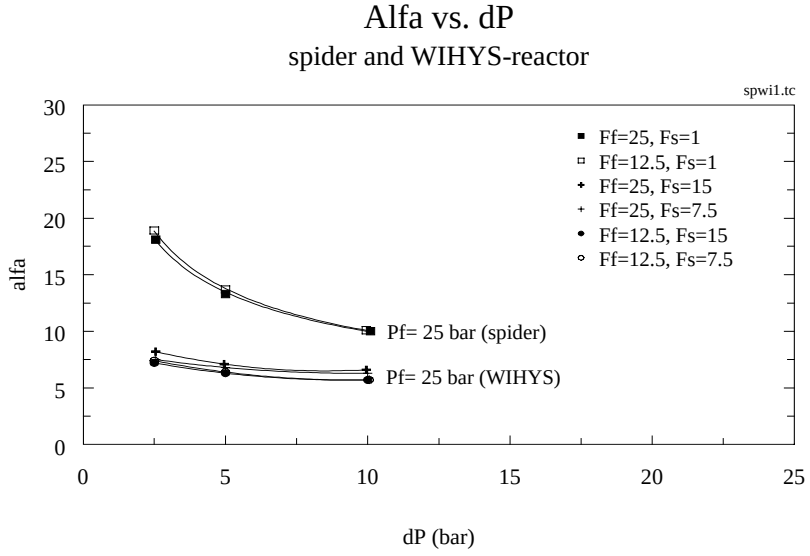

Figure 64 Separation factor (alpha) vs. pressure difference at a feed pressure of 25 bar for the membrane reactor module (WIHYS) and differential separator (spider), Nov. 1996

3.2.4 Membrane Process Testing

The membrane process testing programme was concentrated in 4 main locations:-

- Bath University was responsible for low temperature testing for the FCC offgas and ammonia recovery applications although other gas mixtures were also tested to help classify the membranes
- British Gas were responsible for the high pressure low temperature evaluation of the microporous membranes for natural gas processing (CO_2/methane)

- ECN and Salford were responsible for testing the palladium membranes in the water gas shift/steam reforming reactions with Salford having higher temperature and ECN high pressure capabilities.
- IFP were responsible for high temperature/low pressure hydrogen recovery testing

In addition Democritos was tasked with carrying out some environmental testing but this was curtailed when it became apparent that there little chance of achieving any reasonable permeation of the larger hydrocarbon molecules that were involved (e.g. xylene). In all cases the tests were carried out in tubular reactors and the results are therefore subject to the dispersion phenomena described above.

3.2.4.1 Low Temperature

Low temperature processes in microporous membranes are characterised by an unusual separation mechanism which is dominated by the adsorption properties of the feed molecules. This is most clearly demonstrated by mixtures of hydrogen and hydrocarbons. In this instance the hydrocarbons adsorb into micropores where they are transported as a relatively dense phase, effectively inhibiting hydrogen adsorption and transport. This is a general effect which simply reflects the mixed phase composition in the micropores, which can be estimated from for instance ideal adsorption solution theory, if the single component isotherms are known. It can also be estimated with some precision from equilibrium molecular dynamics. To a first approximation the selectivity behaviour can also be judged from the critical temperatures of the various molecules - the larger the difference in the Tc's the greater the potential selectivity. The "adsorption" selectivity, which in general will reflect the upper limit on the attainable membrane selectivity, can be substantially modified in the actual membranes by transport limitations. Whilst it is the larger molecules that tend to adsorb more strongly, they will also tend to have lower diffusion constants. This leads to a "volcano" type response where the optimum flux, reflecting a balance between adsorption and transport, will occur at some intermediate molecular weight in for instance the permeation of the homologous series - methane-ethane-propane-butane. The position of this optimum will be a function of the pore size of the membrane - the smaller the pore size the lower the optimum molecular weight. However under any combination of conditions it is unlikely that this optimum will be at larger molecules than C3 or C4. In the extreme case of very small pores even relatively small molecules can adsorb so strongly that they effectively inhibit all permeation. All of these properties have been demonstrated in the process tests carried out. These have shown that the pores in the silica and zeolite A membranes are too small to allow effective operation in these low temperatures environments, the carbon pores are to small for some of the applications but quite good for CO_2 applications whilst the silicalite appears to have an optimum pore size for these type of applications.

3.2.4.1.1 FCC Offgas

This application relates to the recovery of valuable paraffins and olefins from fluid cat cracker offgas but is specific to locations where FCC and ethylene steam cracking (ESC) facilities are located close together. ESC (shown schematically in Figure 65) is a process that consumes large amounts of energy in converting ethane and propane, normally nowadays from natural gas feedstocks, to ethylene and propylene by high temperature steam cracking. FCC processes are used to thermally crack heavier oils to light distillate fractions and in the process create significant amounts of C1-C3 paraffins and olefins which then is sent straight to the refinery fuel main where it is burnt. The basis of the proposed process is to recover these C2/C3 olefins and pass these to the ESC product recovery section thereby displacing a significant part of the feed to ESC resulting in a reduction in the ESC furnace gas consumption. Additional energy savings also arise from a reduced load on the cryogenic separation systems (demethaniser) as the amount of methane and hydrogen carried through the process will also be significantly reduced.

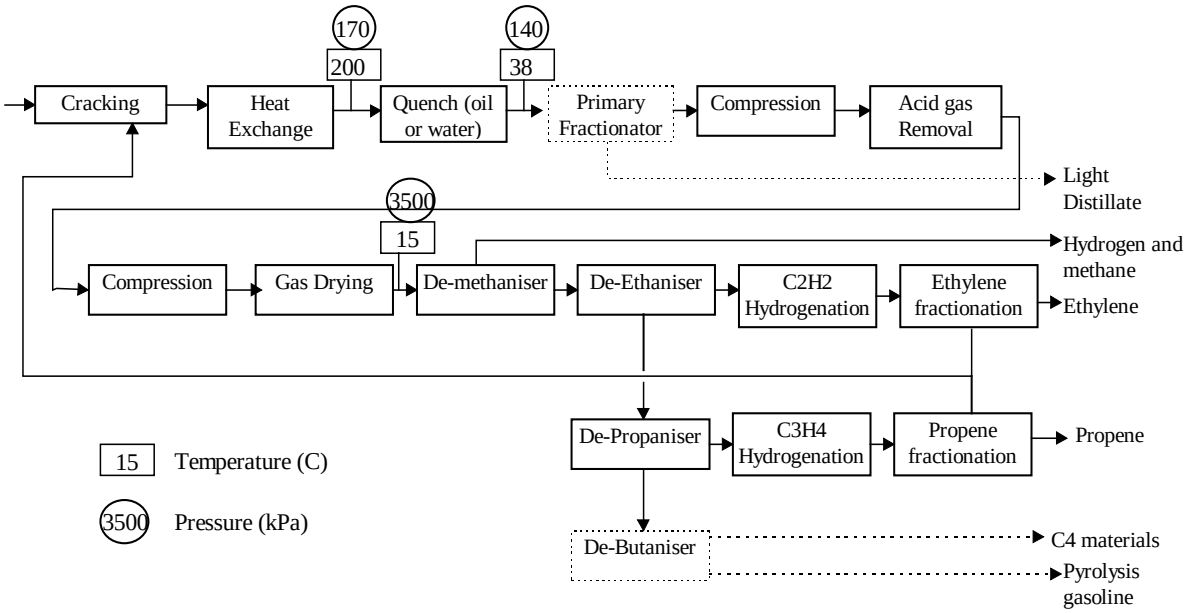

Figure 65:Simplified process flow diagram for ethylene production via gas or liquid cracking

The actual demands on the membrane for this process are relatively low as high efficiencies are not required. Any hydrogen and methane slippage through the membrane simply displaces hydrogen and methane that would have arrived in the separation units via the cracking furnace in the first instance. Such slippage simply reduces the energy savings that might be achieved. In considering this process the ideal separation is for the hydrogen and methane to remain in the feed gas at feed pressure where they will then pass direct to the refinery fuel main. Only the C2 and C3 components will permeate and require perhaps minor recompression to the primary fractionate pressure of 1.4 bar.

Only the IRC silicalite membrane achieved good selectivities in this process. Typical results for a full simulated FCC offgas are shown in Table 15[60]. In this instance the α's are the selectivities based on the full mixed gas tests and analyses. It can be seen that in line with the process requirements, and as expected from multicomponent adsorption behaviour, the selectivity for H_2:C_1 is quite poor (~2-6), is higher for H_2:C_2 (8-20) and much higher for H_2:C_3 (17-41).

60 Deliverable 4.4 - Part 1 Report on detailed FCC Offgas process evaluation studies using membrane flowsheeting module and membrane performance data from this project, R Klosters, Essen University, S.Tennison, Bath University, joule/bath /misc/010/98

Table 15 Typical Separation performance for FCC off gas using IRC Silicalite membranes

T (^{0}C)	F p	P p	Feed flow	Perm flow	Purge flow	H_2 %	C1 %	C2 %	C3 %	α C3/H_2	α C2/H_2	α C1/H_2
20	835	104	150	10.6	18.7	1.3	10	14	8.9	34	13	4
	851	318	120	7.2	14	2.2	10.5	13.5	8.1	18	8	2
	660	228	120	7.8	14	1.6	9	13	6	19	10	3
	361	105	120	6.3	14	1.1	10.5	16	8.5	39	18	5
40	458	106	130	12.2	21	1.1	12	16	9	**41**	18	**5**
	471	105	130	13.7	21	1.1	11.5	17.5	8	36	**20**	5
	756	106	160	20.5	21	1.5	16	17	8.5	29	14	5
	756	222	130	12.6	28	1.6	11	12.6	6.6	21	10	3
	868	315	130	13	21	2.2	13.6	14.8	7.5	17	8	3
60	471	106	150	18.2	37.3	1.4	14	12	5.2	19	11	5
	832	106	180	32.2	23.3	2.6	24	20	7.5	14	10	5
	830	240	160	24.3	23.3	3.3	21	18	7.6	12	7	3
	830	344	150	19	23.3	5.5	18.5	16.8	6.8	6	4	2

Feed composition: 25% H_2, 20% C_2H_6, 5% C_3H_8, 50% CH_4**;** Counter current flow mode; Retentate flow rate: 100-120 ml/min; Purge gas: Nitrogen

A detailed evaluation of the overall silicalite test data carried out by Essen is shown in Figure 66 and shows clearly the enhanced separation that is obtained for the C_2 and C_3 components. None of the other membranes tested showed any significant selectivity in this separation. The poor results achieved with the MAST carbon membrane , which reflected severe pore blocking by propane, were in marked contrast to literature data from Air Products[61,62] on a different carbon membrane where similar, but somewhat inferior, selectivities were obtained with similar feed compositions(Table 16). This may however suggest that the performance of the MAST membrane could also be improved by a similar oxidative treatment to that used by Air Products.

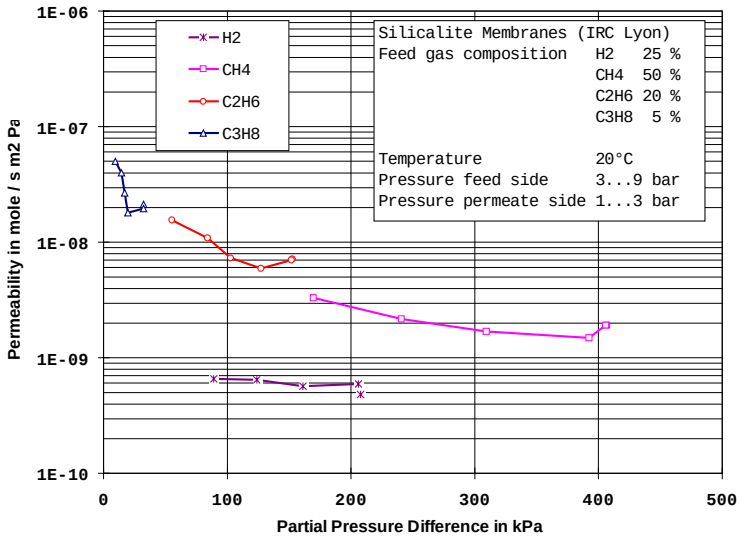

Figure 66 Summary of Bath data on FCC Offgas separation

61 Carbon membranes, US Patent 903430,Jun 24th, 1992.

62 Composite porous carbonaceous membranes, US Patent 5507860, April 16th 1996.

Table 16 Comparison of AP Carbon and Lyon Silicalite Membranes

	Air Products		Lyon/Bath	
	Permeance	Selectivity	Permeance	Selectivity
	m3/m2/s/Pa	Pi/Ph	m3/m2/s/Pa	Pi/Ph
hydrogen	7.45E-12		2.86E-11	
methane	4.85E-11	6.51	1.44E-10	5.03
ethylene	9.46E-11			
ethane	9.07E-11	12.18	6.69E-10	23.39
propylene	3.29E-10			
propane	2.80E-10	37.64	2.16E-09	75.52

3.2.4.1.2 Ammonia Recovery

This application relates to the recovery of ammonia product in ammonia synthesis loops. As in the other low temperature separations using the microporous membranes, this separation relies on the ammonia adsorbing in the pore structure and effectively blocking the pores to hydrogen and nitrogen permeation.

The key requirement is for the ammonia to permeate whilst leaving the hydrogen/nitrogen syngas at loop pressure. There is also a requirement to minimise any slippage of the H_2/N_2 to the permeate side of the membrane. The other constraint on the membranes is the operating pressure as the loop typically operates at up to 140bar whilst the ammonia permeate is initially at ~12bar giving a dP across the membrane of 128bar. Whilst this provides a substantial driving force for membrane operation it also places a major mechanical constraint on the materials of construction.

It is also apparent that laboratory evaluation of the membranes under real process conditions was not feasible due to the cost involved in building a test unit capable of running at both the high pressures and ammonia concentrations. The tests were therefore carried out at Bath using the maximum available pressure and ammonia concentrations. Due to the small size of the ammonia molecule it was anticipated that most of the membranes available would give some selectivity for this separation. This proved to be the case although the selectivities for the silica membrane (**Table 17**) and the zeolite A membranes (Table 18) were insufficient to warrant further evaluation.

Table 17 Permeate side composition (ECN silica membrane; feed mixture: 30% NH_3, 40% H_2, 30% N_2)

	mean pressure 160 kPa	mean pressure 330 kPa	Selectivity over N_2
NH_3	50%	55%	3
H_2	23%	24%	1.5
N_2	27%	21%	---

Table 18 Ammonia Separation Using Zeolite A Membranes

T (^{0}C)	F p	P p	Feed Flow	Permeate	Purge	H_2 %	N_2 %	NH_3 %	α NH_3/H_2	α NH_3/N_2
30	318	102	122	36.1	0	24.1	29	46.9	1.95	2.1
	425	104	122	48.6	25	15	19	31	2.1	2.2
40	226	105	139	32	31	12	14	24	2.0	2.3

A poor performance in the carbon membrane, could be attributed to a surprisingly low diffusivity of ammonia in carbon (Figure 67)which may be due to strong adsorption at acid sites within the carbon pores.

As in the FCC off gas separation the silicalite membrane was the only system to give a selectivity that merited detailed examination and flowsheeting[63]. Typical results are shown in Table 19. It can be seen that a maximum selectivity of 15 for NH_3:H_2 and 24 for NH_3:N_2 was achieved. In the absence of the detailed micropore membrane model it was not possible to extract the precise dependence of the performance on the operating conditions. However some of the performance trends could be extracted when certain operating variables were kept constant. A key result for selectivity as a function of ammonia partial pressure difference is shown in Figure 68. This result appears to be a reflection of a general effect in microporous membranes whereby the optimum selectivity is achieved at the lowest partial pressures.

Extrapolation of these results to the real process operating conditions is clearly subject to considerable risk but is the only approach available at this time.

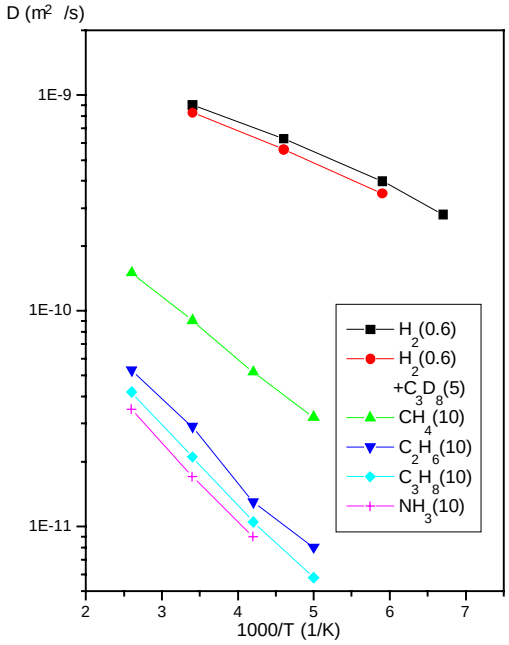

Comparison of the diffusivities of the different molecules considered in this study in carbon molecular sieves. Loadings in mass %, particle size 30 µm.

Figure 67

Table 19 Separation performance for ammonia synthesis product gas

Feed composition: 56% H_2, 31.5% N_2, and 12.5% NH_3

T (^{0}C)	F p	P p	Feed flow	Pflow	purge	H2 %	N2 %	NH3 %	α NH3/H2	α NH3/N2
25	614	104	133	23.6	0	34.5	23	42	5.42	4.60
***	646	112	136	24	33	16.4		25.6	6.95	
***	1592	1134	121	9	13.2	30		12	1.78	
	1305	658	134	12	0	52	29	18.1	1.55	1.57
***	1299	665	135	13	14	15.4		18	5.20	
	1605	670	140	18	0	52.8	29.5	17.7	1.49	1.51
	610	105	123	23	0	42.8	26	31.2	3.25	3.02
30	1110	452	123	12.4	15.9	16	10	18	5.01	4.54
	1108	463	132	11.7	15.9	14.2	9	19.3	6.05	5.40
	1205	600	116	6.4	13	12	7.7	13.3	4.93	4.35
	668	104	125	14.6	13.9	16	3.5	32.5	9.04	23.40
	724	105	136	15.6	28	7.3	2.7	25.4	15.49	23.71
40	624	105	146	36.2	0	38.8	24.66	36.5	4.19	3.73
	620	112	149	38.6	39.7	11.3	16.2	21.6	8.51	3.36
	817	406		40	40	15	16.8	18.3	5.43	2.75

*** purge gas N2, otherwise He, counter-current flow mode.

63 Deliverable 16 - Task 4-4 Detailed Process Evaluation Studies - Ammonia Synthesis Process, a)Improved Hydrogen Production Processes b) Ammonia recovery in Syn-loops, Continental Engineering, R. Birksteiner, joule/bath /misc/016/98

Figure 68 ***The selectivity vs partial pressure of NH_3.***

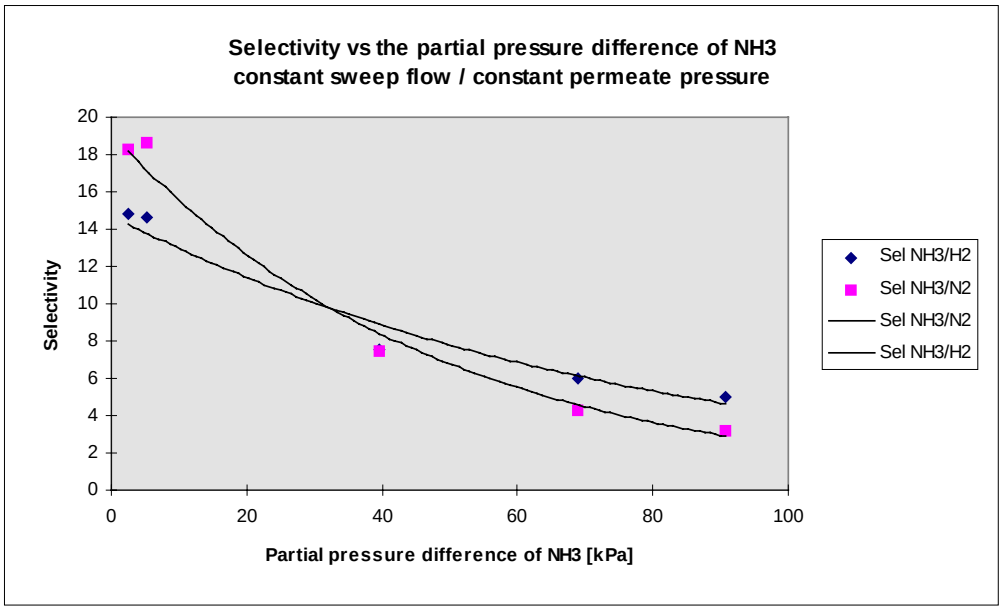

3.2.4.1.3 Natural gas processing

The final low temperature process evaluated was the removal of carbon dioxide from natural gas. This is a key separation as the as-produced natural gas can contain up to around 60% volume of CO_2 depending upon the location of the gas field. The operation is similar to that in the ammonia separation where it is now the CO2 that is the adsorbing gas and methane the non adsorbing. The other key feature is the minimisation of hydrocarbon loss to the permeate stream along with the carbon dioxide which is quite high in polymer based membranes and limits their use in the high CO_2 environments. To minimise slippage in these operating environments it is then necessary to run polymer membranes in cascade mode with interstage recompression which increases both the capital and operating costs.

Estimated performance requirements for the ceramic membranes if they are to achieve the target residual CO2 contents, the low HC losses and run in single stage mode are summarised in Table 19 which then corresponds to the target selectivities which range from 63 to 183 depending on the operating environment

Table 20 Target Selectivities for Ceramic Membrane

Case	Product CO2 (%)	Slippage (%)	Target selectivity
1	2	3	89
2	2	3	183
3	20	3	63

As in the case of the ammonia recovery application it was anticipated that several of the membranes could give usable performance given the small cross sections of the two key molecules. Initial single component tests at British Gas gave using the ECN membrane (Table 21) gave very different results to those achieved by ECN during the quality control testing, albeit at very different temperatures (see Table 9). In the BG tests the single gas permeation actually favoured the methane by a substantial margin whereas in the ECN tests the permselectivity was 50 and 12.8 respectively in favour of CO_2 at 100 and 300C. Whilst the temperature trend in the ECN data partly accounts for the differences in the CO_2 permeability's, the substantial difference in the CO_2:methane permselectivity cannot be explained.

Table 21 Single Gas Permeances on ECN silica membrane determined by B Gas

Gas	**Feed P** *kPa*	**Perm P** *kPa*	**Diff. P** *kPa*	**mean P** *kPa*	**P/l*1E6** *mol/m2.s.Pa*
N2	446	101	345	274	0.03
CO2	446	101	345	274	0.09
CH4	446	101	345	274	0.25

Preliminary test results from Bath using the silicalite membrane and mixed gas feeds are shown in Table 22 and demonstrate that the selectivities are well below those required for the high CO_2 gas fields that the feed composition simulates. The observed results are also obtained using a purge on the permeate side that is unlikely to be possible in practice.

Table 22 Separation performance for CO_2 /CH_4 (35/65 v/v)

T(^{0}C)	F p	P p	purge	permeate	CO_2 %	CH_4 %	α (CO_2/CH_4)
20	325	105	14	15	34	19	3.3
20	520	105	14	18	36	25	2.7
20	410	104	28	18	38	10	7
50	466	104	0	29	55	45	2.2
50	489	104	28	32	51	10	9.5
50	756	106	28	48	55	9	11
50	753	172	28	41	54	9	11

Max. separation factor: 11

The evidence of the studies to date appears to demonstrate that the available membranes do not meet the demanding targets established by BG for commercial viability. There is however some uncertainty around the ECN silica as, although both the BG and Bath tests showed poor selectivity in the mixed gas environments, the single gas tests did not agree with those carried out at ECN. This may reflect for instance inadequate pre-treatment to remove adsorbed water. However if this is the case the operation of the membrane in field could also be compromised as all produced gases contain varying amounts of water. Some further work will however be required to confirm this situation. In the case of the carbon and zeolite membranes the observed performance is in reasonable agreement with the observed adsorption (Figure 69) and calculated multicomponent adsorption behaviour which showed that both membranes should exhibit similar performance with relatively low selectivities.

Figure 69 Adsorption Isotherms on Carbon and Silicalite

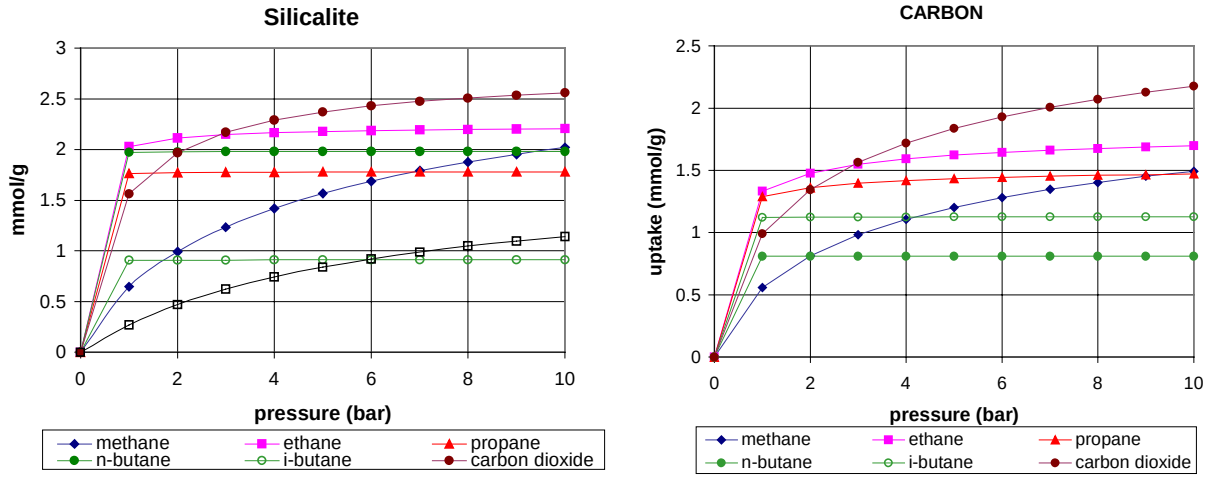

The outstanding question is whether any other ceramic membrane is likely to meet the targets which would require a significant increase in the adsorption selectivity for carbon dioxide. This could be achieved through the use of membranes with surface basic sites although this would also probably then reduce the transport through the membrane. Nonetheless there would appear to be scope for an initial study based simply on adsorption behaviour rather than the preparation of the membranes themselves.

3.2.4.2 High Temperature

The high temperature testing fell into two main categories:-

1. the removal of hydrogen from steam reforming and water gas shift processes in ammonia, methanol and IGCC flowsheets. This places severe constraints on the membrane as a god selectivity between small molecules - hydrogen vs. CO and CO_2 is required
2. the removal of hydrogen in petrochemical processes such as butane dehydrogenation where molecular size is not a constraint but inhibition due to adsorption of the hydrocarbon can cause problems.

3.2.4.2.1 Steam Reforming/Water Gas Shift

A simple evaluation of the requirements of the steam reforming and water gas shift flow sheets demonstrated that microporous membranes would not be able to meet the very high hydrogen recoveries and the high product hydrogen purity (low CO_2/methane slippage) that would be required. Testing for these applications was therefore limited to the palladium membranes. Two membrane types were available to the project:-

1. Johnson Matthey - JM supplied Ag/Pd alloy membranes supported on alumina in purpose built modules ready for mounting in the test facilities. Whilst these were supplied under commercial terms JM have indicated that they do expect to commercialise these membranes for large scale applications.
2. Salford University - SU have been preparing Pd membranes via magnetron sputtering and electroless plating using a variety of supports (ceramic, porous metal etc). As the initial tests with the sputtered membranes were not very successful they mainly concentrated on the electroless plated membranes. They also developed a novel technique for sealing defects in the membranes during the course of this project.

A key issue in the testing of the JM palladium membrane was the way in which the membrane had to be treated during heating and cooling. Johnson Matthey had stated that heating and cooling should be done in an inert atmosphere. However, following the rapid failure of the first membrane it was found that it was also important to flush the membrane for several hours with an inert gas after having performed hydrogen permeation measurements before heating or cooling. This could be a major issue in real process operation.

A direct comparison of the different membranes(**Table 23**) shows that significantly higher fluxes were available from the later Salford membranes although the majority of the process testing was limited to the JM membranes.

Table 23 Comparison of hydrogen fluxes for dense supported Pd membranes

(Feed Pressure, 3 bars; ΔP = 2 Bars, Temp. 380°C**)**

Membrane	Feed Flow Rate Nl/min	H_2 Flux mol/m^2s	cm^3/cm^2.min
Johnson -Matthey	1	0.037	5
	5	0.074	10
Pd/Stainless Steel	1	0.096	13
	5	0.096	13
Pd/α-Al_2O_3	1	0.208	28

The test programmes on the Pd membranes were carried out both at ECN and Salford. In these tests ECN concentrated on the high pressure testing but was limited to 400C (the maximum allowed temperature for the JM module) whilst Salford could operate to higher temperatures but were limited to lower pressures.

Table 24 Effect of N_2, CO and H_2O Addition on Hydrogen Permeation – Pd/ss Membrane

(T - 380°C, ΔP = 2 bars, Concentration of additive: 10%)

Total feed flow (Nl/min)	H_2 Flux (mol/m^2.s)		
	N_2	CO	H_2O
2.0	0.082	0.077	0.062
1.0	0.063	0.058	0.052

One of the main uncertainties that has come out of this test programme has been the influence of components other than hydrogen in the feed on the hydrogen permeation as there has been some disagreement between ECN and Salford as to the magnitude of the effect.. Typical results from Salford are shown in Table 15. In these tests the steam and CO were substituted by nitrogen to remove any effects due to hydrogen dilution. It can be seen that in the presence of 10% of added CO the hydrogen flux is reduced by a relatively small amount whilst steam has a more pronounced effect.

In similar tests at ECN, where the nitrogen was progressively substituted by CO, steam and mixtures but under more severe test conditions (200C, 25bar feed pressure) this marked reduction in hydrogen permeation (H_2 Fp) with steam addition was not observed. However it can be seen that there is some evidence that the selectivity, α, does change - it does not reduce when CO is added, but drops considerably when steam is added and shows no further reduction in the presence of steam and CO. This appears to be due to an increase in the methane slippage rather than a reduction in the hydrogen permeation.

Table 25 Results of ECN steam reformer experiments at 400C

Pf (bara)	dP (bara)	Ff (Nl/min)	Fs (Nl/min)	H_2 Fp (Nl/min)	H_2 recovery (%)	H_2-conc. feed (%)	H_2-conc. perm. (%) [64]	CH_4 slip flow (%)	α
gas mixture 1: $H_2/CH_4/CO_2/N_2$, concentration: 37/13/12/38									
24.75	21.9	3.9	4.8	1.27	85	37.7	99.7	0.56	549
24.75	21.9	8.1	1.2	2.02	66	37.7	99.7	0.28	549
gas mixture 2: $H_2/CH_4/CO_2/CO/N_2$ concentration: 37/13/6/6/38									
24.9	21.95	4.1	4.8	1.28	85	37.2	99.7	0.67	561
24.75	21.8	8.0	1.2	2.03	69	37.2	99.8	0.33	842
gas mixture 3: $H_2/CH_4/CO_2/N_2/H_2O$ concentration: 38/13/12/1/36									
25.15	22.1	4.1	4.8	1.40	90	37.7	99.4	0.80	274
24.95	21.9	7.9	1.2	2.24	74	37.5	99.7	0.37	554
gas mixture 4: $H_2/CH_4/CO_2/CO/N_2/H_2O$ concentration: 38/13/6/6/1/36									
25.15	22.15	4.0	4.8	1.40	92	37.7	99.4	1.15	274
25.5	22.3	8.0	1.2	2.37	76	37.7	99.7	0.50	549

In this table:-

Pf = feed pressure
dP = pressure difference over membrane
Ff = feed flow
Fs = sweep flow
CH_4 slip flow = CH_4 perm. flow/ CH_4 feed flow, and
dP H_2 = hydrogen (partial) pressure difference over membrane = average hydrogen pressure on feed side - hydrogen pressure on permeate outlet

64 The H2-concentration in the permeate is corrected for the amount of N2 as sweepgas.

H_2 Ff	=	hydrogen feed flow
H_2 Fp	=	hydrogen flow leaving as permeate = hydrogen flow through membrane
H_2 conc. perm.	=	hydrogen concentration in permeate (but neglecting sweep gas)
H_2 conc. ret.	=	hydrogen concentration in retentate
H_2 recovery	=	H_2 Fp / H_2 Ff , and

$$\alpha = \frac{y}{1-y} * \frac{1-x}{x}$$

in which: y = hydrogen concentration in permeate (neglecting sweep gas) (=H_2 conc. perm.)
x = hydrogen concentration in the feed

The reasons for the difference between the two sets of data has not been established and will require further evaluation.

In the actual test programmes for the water gas shift and steam reforming applications the two key requirements were the membrane selectivity and the hydrogen recovery. In theory the selectivity of a perfect palladium membrane is infinite whilst in practice defects in the Pd layer and at the membrane seals allows some of the feed gases to pass to the permeate side of the membrane. The hydrogen recovery is however a function of the operating conditions and the reactor design and is severely influenced by the presence or absence of a sweep gas on the permeate side. In the tests carried out the conditions reflected the gas compositions that would be expected in the IGCC flow sheets being developed by Siemens/Essen. A typical feed gas composition for the water gas shift process is shown in table 18. Preliminary flow sheet studies had also shown that the use of the membrane was only likely to be viable if hydrogen recoveries of higher than ~80% could be achieved.

Table 26 Water gas shift conditions

Temperature:	400	°C
Pressure:	23	bar
Pressure difference:	10	bar (aim)
Flow:	1.7048	kmol/s
H_2O	23.03	mol%
N_2	2.49	mol%
H_2	42.10	mol%
CO	7.26	mol%
CO_2	24.67	mol%
Ar	0.44	mol%
CH_4	0.01	mol%

A reduced summary of the test results obtained by ECN using the JM silver/palladium membrane are given in **Table 27**.

Table 27 Results of Pd membrane measurements using IGCC gas mixture after CO-shift

Pf (bara)	dP (bara)	Ff (Nl/min)	Fs (Nl/min)	dP H_2 (bara)	H_2 Ff (Nl/min)	H_2 Fp (Nl/min)	H_2 conc. ret. (%)	H_2 conc. perm. (%)	H_2 recovery (%)	α
23.2	15.2	12	0	1.47	4.96	1.07	36.9	94.5	21.6	25
23.2	19.35	12	0	4.41	4.96	2.37	28.5	94.9	47.8	27
23.0	22.0	12	0	6.14	4.96	3.15	20.8	95.7	63.5	32
23.25	10.4	12	0.15	0.92	4.98	0.35	40.0	97.9	6.9	65
23.35	15.6	12	0.4	2.85	4.98	1.45	33.3	98.8	29.2	118
23.5	15.4	24	0.6	3.42	9.90	2.01	38.7	99.2	20.3	181
23.1	19.2	12	0.7	4.97	4.98	2.47	27.1	99.2	49.6	178
23.4	19.45	24	1	5.44	9.90	3.43	30.7	99.4	34.6	224
23.3	22.3	12	0.9	6.40	4.98	3.29	20.4	99.2	66.1	169
23.45	22.3	24	1.3	7.16	9.90	4.32	27.1	99.5	43.6	259
23.2	10.4	6	0.5	1.87	2.46	0.55	29.2	98.6	22.4	89
23.3	10.45	12	0.5	1.73	4.92	.067	32.5	98.9	13.5	101
23.35	15.45	6	0.5	2.93	2.46	1.20	21.4	98.8	48.9	104
23.5	15.5	12	0.5	2.98	4.92	1.55	26.5	99.1	31.6	126
23.6	19.7	12	0.5	4.80	4.92	2.47	37.0	98.6	50.3	158

Although these cover a wide range of conditions in terms of trans membrane pressure drop (dP), feed flow (Ff) and sweep flow (Fs) certain general observations can be drawn. By increasing the driving force for separation (a higher feed flow, a higher dP or more sweep gas) the hydrogen flow through the membrane increases however the target hydrogen recovery of 80% was not be obtained under any of the process conditions examined. It can also be seen that the selectivity of the membrane, (α), reached a maximum of 259, equivalent to product hydrogen purity, having removed the sweep gas contribution, of 99.5%. Whilst the dispersion effects discussed in the previous section would have reduced the observed hydrogen recovery it seems unlikely that a set of operating conditions could be found where the target 80% recovery could be achieved.

The steam reforming test conditions were considerably more severe than those required for water gas shift and were beyond the maximum recommended operating conditions for the JM module. Typical process conditions are summarised in Figure 70

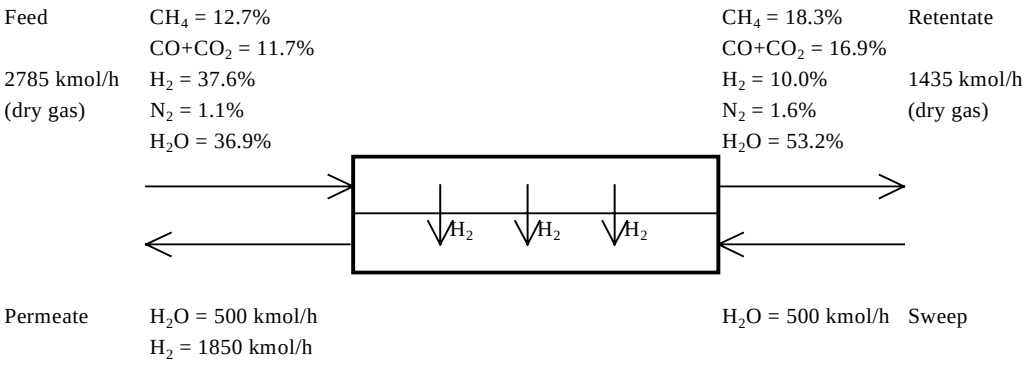

Figure 70 Membrane process conditions for steam reformer testing

From the process point of view the hydrogen recovery should be at least 80% and a methane slip flow with a maximum of 1 % is allowed. Due to the maximum operating temperature and pressure of the module testing was been limited to 400°C and 25 bar feed pressure in stead of 600°C and 40 bar. A set of typical results using a full simulated feed gas is given in **Table 28**. It can b seen from these results that using the high dP conditions combined with a low feed flow and a relatively low sweep flow it was possible to reach both the hydrogen recovery and methane slip targets

Table 28 Results of steam reformer experiments

gas mixture 4: $H_2/CH_4/CO_2/CO/N_2/H_2O$

concentration: 38/13/6/6/1/36

Pf (bara)	dP (bara)	Ff (Nl/min)	Fs (Nl/min)	H_2 Fp (Nl/min)	H_2 recovery (%)	H_2-conc. feed (%)	H_2-conc. perm. (%) [4]	CH_4 slip flow (%)	α
25.5	22.3	8.0	1.2	2.37	76	37.7	99.7	0.50	549
24.95	21.95	8.0	2.4	2.20	71	37.7	99.7	0.46	549
24.9	21.9	8.0	4.8	2.16	70	37.7	99.8	0.38	825
25.15	22.15	4.0	1.2	1.47	96	37.7	99.2	1.37	205
25.25	22.25	4.0	2.4	1.40	92	37.7	99.4	1.06	274
24.3	21.3	4.0	4.8	1.34	88	37.7	99.6	.92	411

These results have then been extrapolated to full steam reforming conditions of 40bar feed, 18 bar permeate and 600C using the pressure and temperature trends derived from the complete data set (**Table 29**).

Table 29 Recalculated results at P_f = 40 bar and T = 600°C

gas mixture: $H_2/CH_4/CO_2/CO/N_2/H_2O$
concentration: 38/13/6/6/1/36

Pf (bara)	dP (bara)	Ff (Nl/min)	Fs (Nl/min)	H_2 Fp (Nl/min)	H_2 recovery (%)	H_2-conc. feed (%)	H_2-conc. perm. (%)	CH_4 slip flow (%)	α
40	22	15	1.2	3.03	29	38	99.9	0.23	1005
40	22	8	1.2	1.91	63	38	99.7	0.47	549
40	22	6	1.2	1.59	73	38	99.6	0.8	418
40	22	4	1.2	1.27	83	38	99.5	1.13	288

It can b seen that by increasing the amount of feed flow (or the ratio of feed flow vs. membrane area) the hydrogen flow through the membrane increases due to a higher driving force for hydrogen transport as more hydrogen is available for permeating through the same membrane area. However, the hydrogen recovery decreases. Furthermore the methane loss to the permeate decreases when increasing the feed flow. It can be concluded that a H_2 recovery of 80% can be obtained without loosing more than 1% of the CH_4 present in the feed stream although this requires a sweep flow that is about 25% of the feed flow.

The performance with time of the membrane used in these studies is shown in Figure 71. After approximately 36 weeks on stream, and despite extreme care with the operating conditions, the membrane performance suddenly deteriorated and post analysis showed some delamination of the Pd layer. There is also evidence for a continuous loss in selectivity with time over the test period. Whilst this represents good performance for such a membrane in the laboratory it would still represent an unacceptably short life under process conditions and an improvement in stability would be a key requirement for any further development programme.

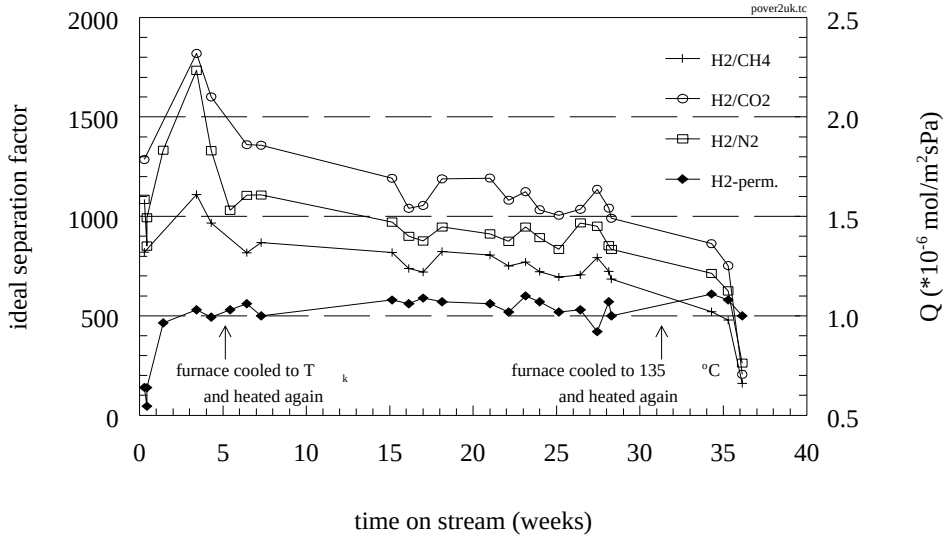

Figure 71 Pd membrane performance at 400°C vs. time on stream

3.2.4.2.2 Butane Dehydrogenation

The other high temperature process investigated was the removal of hydrogen from hydrocarbon streams. The process targeted was butane dehydrogenation where the equilibrium yield of the butene can be increased by removing the product hydrogen during the course of the reaction. In contrast to the low temperature processes investigated in this project the requirement here is to allow the hydrogen to permeate whilst retaining the hydrocarbon components. This then is essentially a molecular sieving process based on the size of the molecules as pure Knudsen diffusion in larger pores would not give the required selectivity (H2:C4 = ~5.2)

The test programme was carried out by IFP and the most comprehensive results have been obtained with the IRC silicalite membranes. The ECN silica membrane gave poor results whilst tests on the MAST Carbon system could not be completed before the IFP laboratory was closed for refurbishment. The results with the IRC silicalite membrane provide a graphic illustration of both the complexity of the transport processes in the microporous membranes and of the necessity for carrying out the tests using real mixed gas feeds. The pure hydrogen flux is shown in Figure 72 as a function of temperature and dP across the membrane and shows the same decrease in flux with temperature as found in the ECN comparative test programme. The hydrocarbons fluxes for n-butane and I-butane are shown in Figure 73 and Figure 74 respectively and demonstrate the greater complexity of the response for adsorbing species and the impact of relatively slight structural changes.

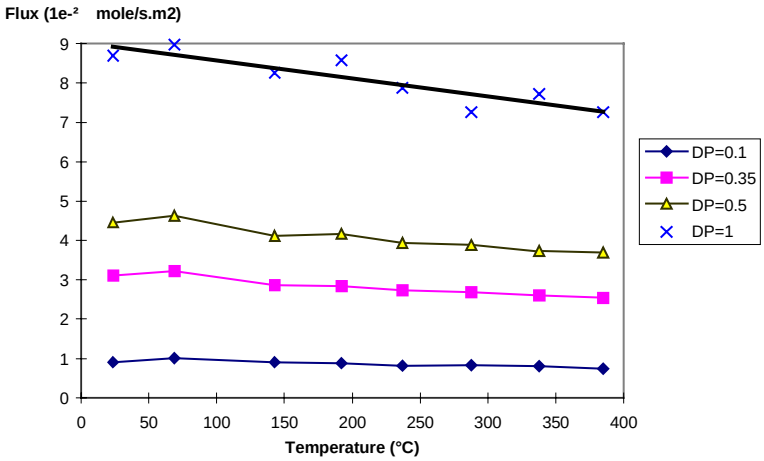

Figure 72 Hydrogen Flux as a function of Temperature

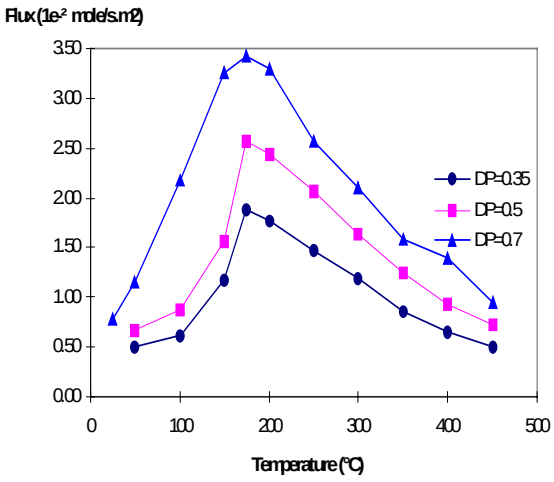

Figure 73 nC4 Flux as a Function of Temperature

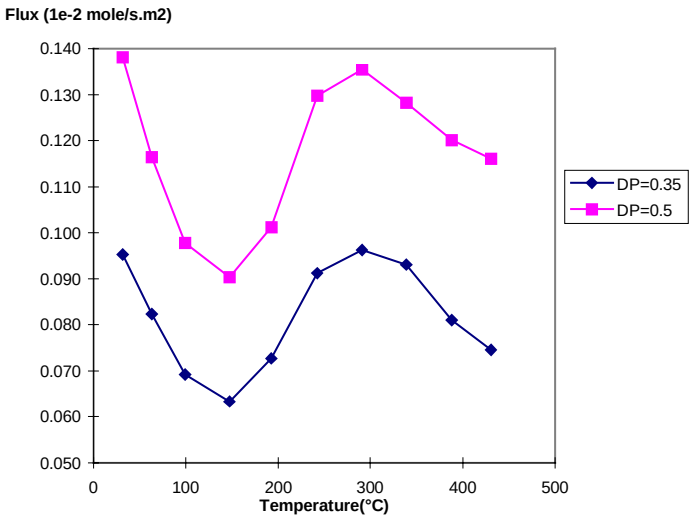

Figure 74 iC4 Flux as a Function of Temperature

The “volcano” type response in Figure 73 can be explained by a balance between activated diffusion at the lower temperature, which gives rise to the increasing flux, followed by a rapid decrease in adsorbate concentration at the higher temperatures which reduces the driving force for diffusion. The complex

response in Figure 74, and in particular the initial decrease in flux, for the i-butane cannot be easily explained.

However, leaving aside these complexities, a comparison of the hydrogen fluxes in Figure 72 with the hydrocarbon fluxes in Figure 73 and Figure 74 would suggest a selectivity to hydrogen at the higher operating temperatures of in excess of ~20-40. The actual results, achieved using a mixed H_2:iC_4 feed are shown in Figure 75 and demonstrate the pronounced effect of adsorbed hydrocarbon on the hydrogen transport. It can be seen that at low temperatures the selectivity to H_2 is ~1 showing that pores have filled with the iC_4 which has essentially stopped the H_2 flow. At higher temperatures, as the iC_4 concentration in the pores drops, the H_2 flux increases rapidly but even then the selectivity to H_2 does not exceed 6 at the highest H_2 feed concentration and at highest hydrocarbon concentration the selectivity does not exceed 2 even at the maximum test temperature.

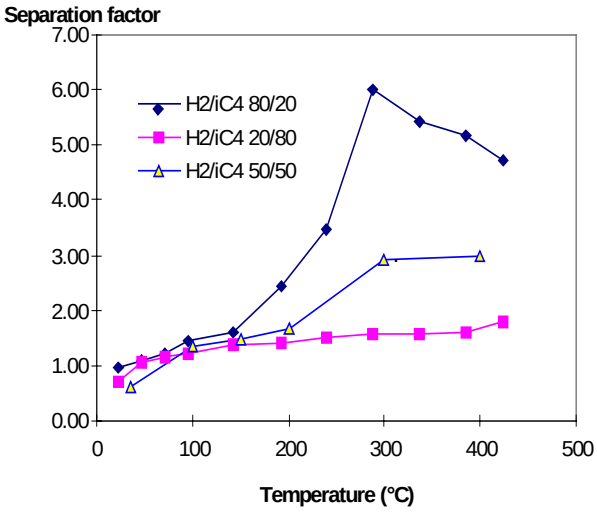

Figure 75 Separation Factor as a Function of Temperature

This effect would be expected to become even more severe for smaller pore systems where the hydrocarbon adsorption would be stronger and the diffusivity of the hydrocarbon would also be reduced due to steric effects. The potential situation with the carbons is complex as whilst the general separation trends suggest that they have smaller pores than the silicalite, the pure hydrogen permeability's reported in section 3.2.2 suggest that the carbon has larger pores than the silicalite. Earlier testing with a mixed hydrogen-butane feed tends to support this as mixed feed selectivities of between 15 and ~100 were observed depending on the feed pressure (Figure 76). Whilst pore size may account for some of the difference a further factor is the hydrogen diffusivity in the membranes.

Figure 76 Butane Hydrogen Separation

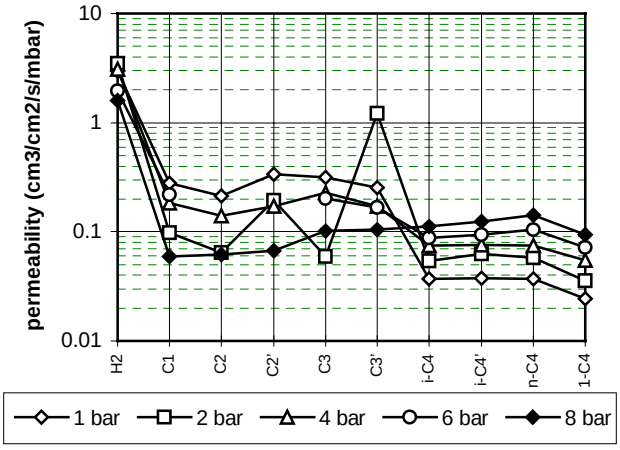

The PFGNMR studies at Leipzig have demonstrated that the carbon and silicalite exhibit very different characteristics. Whilst the intrinsic low temperature hydrogen diffusivities of the two materials are relatively similar the silicalite shows a unique characteristic whereby the hydrogen is trapped in the pentacil cages reducing the diffusivity as the temperature increases (Figure 77). The net effect is that at 600C diffusivity in the carbon should be at least an order of magnitude greater.

Figure 77 Diffusivity in carbon and zeolites

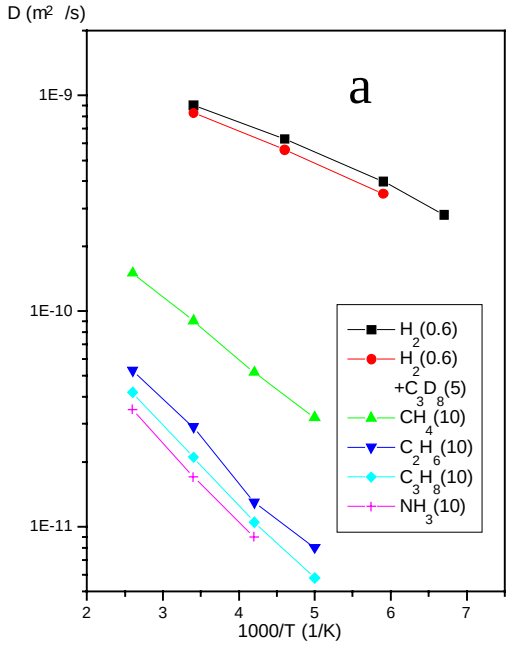

Comparison of the diffusivities of the different molecules considered in this study in carbon molecular sieves. Loadings in mass %, particle size 30 µm.

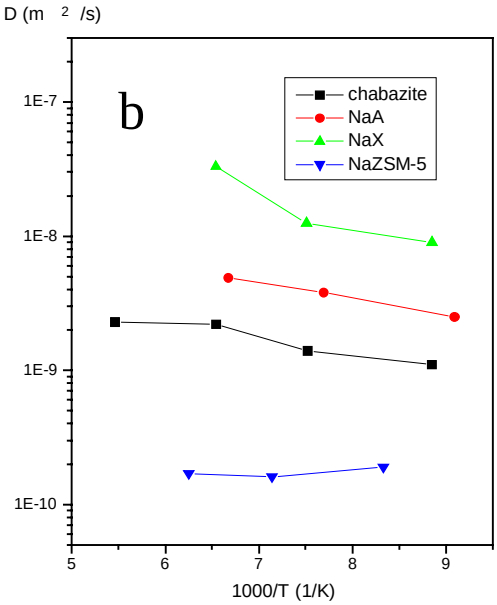

Temperature dependence of hydrogen diffusivities in different zeolites.

The other effect discovered in the PFGNMR studies is the that the influence of co-adsorbed hydrocarbons on the hydrogen diffusivity is essentially zero, even at low temperatures when the pores should be filled with hydrocarbons. This can be seen in Figure 77a where the black and the red line show the hydrogen diffusivity in the presence and absence of co-adsorbed propane. Confirmation of these effects will only come from the further tests planned at IFP/

3.3 Flowsheeting

The primary task of the flowsheeting objective was to take the data generated in the membrane testing programmes and, in combination with the models developed in the fundamentals part of the programme, to carry out detailed flowsheeting studies to establish the viability of the proposed processes taking account of both CAPEX and OPEX savings. In the event the detailed flowsheeting studies could only be accomplished for the palladium membrane systems where a fully functional ASPEN module was developed. It was necessary to use more approximate methods for the microporous membrane processes as the detailed models could not be developed in the time available. Nonetheless the studies still show which processes have potential for further development.

3.3.1 Low Temperature

3.3.1.1 Fluid Cat Cracker Off-gas

A target separation for the FCC application is shown in Figure 78 based on a typical FCC offgas composition and a typical ESC cracked gas composition. The evaluation of the process was based on an ECN polymer membrane model that assumed constant component permeability. For the simulations, a first estimate of the partial pressure difference was used as input for the model, based on feed gas composition and absolute pressures. After the simulation, the calculated partial pressure differences of

the compounds have been compared with that which have been assumed. In case of a larger deviation (> 30 %) the calculation has been repeated with adapted permeabilities.

The simulations were carried out by varying some process parameters over a certain range using counter current flow mode and a feed pressure of 9Bar.

- Permeate side pressure, 1.5 to 4.0 bar
- Membrane surface area, 1,000, 5,000 and 10,000 m² (= 0.062, 0.013 and 0.006 mol/m^{2}s corr. to 226 kmol/h feed gas flow)
- Sweep gas no sweep and 0.1 kmol sweep / kmol feed (N_2)

The key requirement for the process is to maximise the recovery of the C2 and higher components and minimise the recovery of the hydrogen and methane. Typical results in the absence of sweep gas are shown in Figure 79 and demonstrate that these objectives have been met.

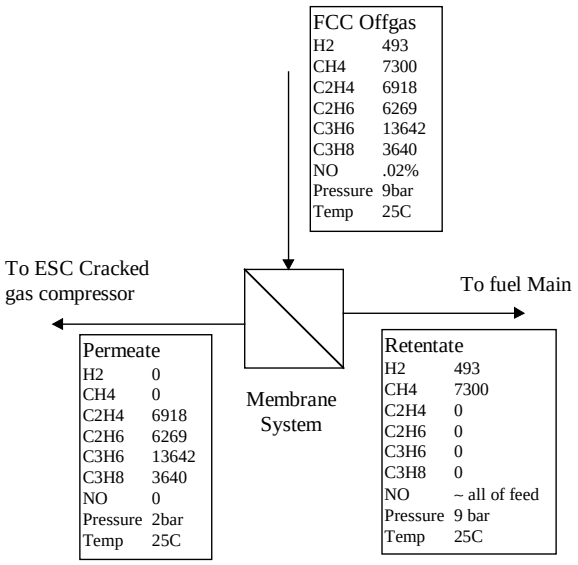

Figure 78: Membrane separation system (component mass flow in [kg/h])

The detailed studies have shown that there is little dependence on the presence or absence of a sweep gas and little dependence upon the permeate pressure. The only limiting factor is that at permeate pressures of greater than 3.0 bar the recoveries will tend to be limited by transmembrane component pressure differentials. The key factor is membrane area where C2 recoveries > 70 % and C3 recoveries > 90 % can be achieved, if membrane surface area is about 10,000 m². The cost effectiveness of the process will therefore depend upon the installed cost vs. the potential savings.

The savings to be made from the membrane installation arise from three sources:-

1. A reduction in firing in the cracker furnace energy costs as the FCC off gas displaces cracked gas product
2. a potential reduction in compression costs if the permeate pressure from the membrane separation exceeds 3.5 bar, the exit pressure from the first stage of the cracked gas compressor. Due to pressure drop considerations this can only be achieved if a sweep gas is used. This however raises the issue as to what sweep gas might be practical.
3. The transfer of value of the FCC offgas from refinery fuel to chemical product

The compositions of the various streams is summarised in Table 30 and are compared to the ethylene furnace exit streams for both a pure C2 and a mixed C2/C3 feed. It can be seen that for the 5000m^2 membrane area case the membrane permeate has a much lower hydrogen+methane content than the ESC stream which will have the additional benefit of reducing costs in the cryogenic de-methaniser column.

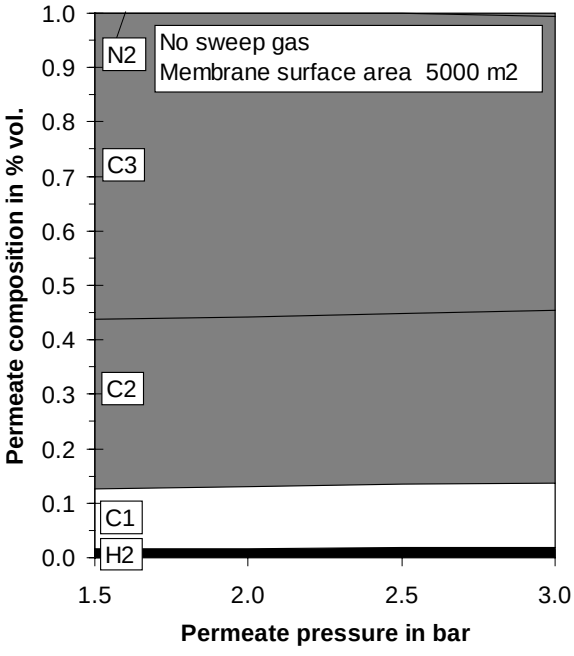

Figure 79:Permeate gas composition without sweep gas

In the main product streams the FCC permeate has a significantly higher C3 content and lower C2 content than the ESC stream with the FCC stream potentially displacing ~12% of the ESC product gas. If the simple assumption is made that this does not then have to pass through the main furnace this would result in a reduction in furnace energy costs of ~12%, equivalent to 86Tj/annum with a net cost of ~ $500,000/year. In addition, if the permeate gas was available at the second stage pressure of the cracked gas compressor, a further 77000kW/h of electricity could be saved. The final saving arises from the transfer benefits of shifting FCC off gas from simple refinery fuel, with a net value of 27.5$/te (1990) to a product gas with a net value varying between 135 and 320$/tonne. Over the course of a year this amounts to a net saving of ~$20million

On the debit side real costs for the zeolite membranes are not available but they will always be higher than the cost of the ceramic substrates used in their preparation. At present the SCT γ-alumina coated tubes that have been used as precursors cost of the order of 15,000ecu/m^2 and it can be assumed that the fully installed cost is likely to be ~x4 higher. If it is assumed that zeolite coating adds a further 5000ecu/m2 to the costs the overall process cost for the 5000m^2 installation is ~4x10^8 ecu. At this cost it is apparent that the membrane installation would not be viable. For a reasonable payback time of say 1 year the maximum allowable cost for the membrane installation would be 5000ecu/m^2 installed or ~1200$/$m^2$ for the membrane tubes. This then provides a clear target for any future programme aimed at this kind of separation.

Table 30:FCC off-gas from vacuum gas oil cracking

	FCC Offgas product		Membrane permeate NO sweep, 5000m2		ESC product C2 feed		C2/C3 feed	
	kmol / h	Mol %	Mol%	Kmol/h	Mol%	Kmol/h	Mol%	Kmol/h
H2S	9.05	4.01						
H2	29.40	13.03	2	22.6	35.8		27.9	
N2	18.09	8.02						
CO	2.26	1.00						
CO2	2.94	1.30						
NO	0.02	0.01						
CH4	54.28	24.06	11.3	67.8	4.7		17.4	
C2H4	29.40	13.03	18.3	77.0	35.3	1683	32.9	1683
C2H6	24.88	11.03	15	63.1	22.2	1058	13.8	706
C3H6	38.67	17.14	42.9	159.4	0.54	25.7	5.44	278
C3H8	9.85	4.37	10	37.2				
C4=	2.71	1.20			0.68	32.4	1.02	61.4
C4	4.07	1.80						
	225.62	100.00						

3.3.1.2 Natural gas Processing

The final low temperature process evaluated was the removal of carbon dioxide from natural gas. This is a key separation as the as-produced natural gas can contain up to around 60% volume of CO_2 depending upon the location of the gas field. The operation is similar to that in the ammonia separation where it is now the CO2 that is the adsorbing gas and methane the non adsorbing. The performance is therefore dominated by the selective adsorption of CO_2. This process is however different to the others considered in this programme in that there are polymeric membranes already in use in the lower CO_2 content fields. The ceramic membranes must therefore offer a considerable improvement in performance if the cost differential between the ceramic and polymeric membranes is to be overcome. This benefit may derived from two sources.

One feature is the minimisation of hydrocarbon loss to the permeate stream along with the carbon dioxide which is quite high in polymer based membranes and limits their use in the high CO_2 environments. To minimise slippage in these operating environments it is then necessary to run polymer membranes in cascade mode with interstage recompression (see Figure 65) which increases both the capital and operating costs. Typical performance of current polymeric membranes is shown in Table 31.

Table 31 Hydrocarbon Slippage with Commercial Polymer Membranes

Case	Area (param.)	Slippage (%)	Permeate CO2 (%)	Permeate CH4 (%)
1	812.9	14.2	39.7	60.3
2	1,071	28.2	77.7	22.3
3	588.7	13.3	86.4	13.6

The "parametric area" quoted is a normalised membrane area in which it is assumed that the permeation coefficient of CH4 is equal to 1 GPU (approx. 3 * 10^{-9} mol/m^2.s.Pa).

The second area where the ceramics should offer a benefit is in mechanical integrity as current polymer membranes cannot operate at the full well head pressures and temperatures found in many fields. This then necessitates cooling and depressurisation prior to processing. Whilst in its own right this is not a problem, the cost arises from increased recompression of the permeate CO_2 to allow reinjection into the gas field.

The final area where ceramics might offer a benefit is in the operating characteristics. A key issue in all CO_2 recovery processes is, as mentioned above, reinjection of the product CO_2. Current polymeric membranes need to operate with a very low permeate pressure to achieve the target CO_2 removal and minimise the methane slippage. In the case of high CO_2 fields this additionally requires cascade operation with interstage compression (see Figure 80). At present it is these compression costs that renders membrane separations non viable. If the ceramic membranes allowed operation at lower trans membrane dP's, i.e. higher permeate pressures this could offer a significant benefit.

Figure 80 Cascade membrane System for High CO2 gas Fields

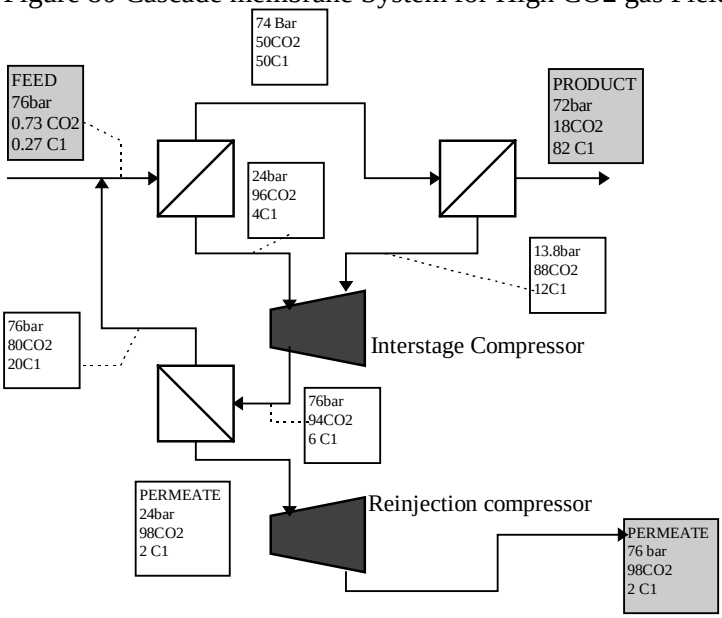

The three cases that formed the basis for the study are summarised below:-

1) 10% CO2 feed gas reduced to 2% in the product gas - i.e. sales gas quality
2) 50% CO2 feed gas reduced to 2% in the product gas
3) 50% CO2 in feed gas reduced to 20% in the product gas - i.e. intermediate export quality for offshore South East Asia.

Estimated performance requirements for the ceramic membranes if they are to achieve the target residual CO2 contents, the low HC losses and run in single stage mode are summarised in Table 19 which then corresponds to the target selectivities which range from 63 to 183 depending on the operating environment.

Table 32 Target Selectivities for Ceramic Membrane

Case	Product CO2 (%)	Slippage (%)	Target selectivity
1	2	3	89
2	2	3	183
3	20	3	63

Comparison with commercial polymeric membranes is difficult as the actual permeation coefficients for commercial polymer membranes are proprietary information, and without this data it is difficult to estimate the cost of commercial separation systems. However, Kvaerner Process Systems have indicated that an installed cost of US $160/m2 would not be unreasonable, which together with an indication in the literature (Desalination, 1988) of a CH_4 permeance of approximately 3 GPU for a cellulose acetate membrane, implies a parametric cost of around US $55/ unit parametric area.

Parametric modelling was carried out to indicate the likely capital equipment cost of a single stage membrane for case 1, by varying the selectivity and the cost per unit parametric area. The result of this study is shown in Figure 81 with the capital cost in US Dollars per million standard cubic feet per day (MMSCFD) of feed gas plotted against selectivity. The costs per unit parametric area, in US dollars per square metre of membrane area , are as designated by the colour codes.

Figure 81

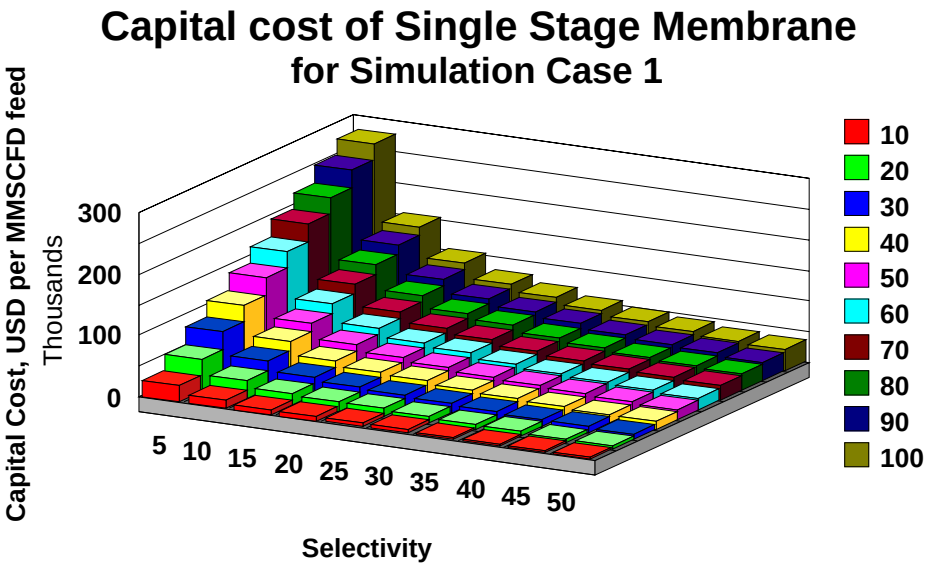

Test data on CO2/CH4 have been disappointing, with permselectivities in mixed environments that are considerably lower than the target values. Accordingly, whilst flowsheets have been developed for natural gas applications, there has been no final process evaluation as it was clear from the test data acquired to date that the permselectivity was insufficiently high to compete with polymeric membranes.

The probability of achieving the target selectivities will hinge on the development of a membrane layer with a much higher CO_2 selective adsorption capability. There have been claims from Japanese workers that such materials have been developed although the primary application has been for CO_2 removal from air at low pressures. Mixed gas selectivities of in the range of 20-100 have been claimed[65] using Y type

65 Morooka S, Kuroda T and Kusakabe K, Studies in Surface Science and Catalysis, 665, 118, (1998)

membranes although similar CO_2:N_2 selectivities have also been achieved with the MAST carbon membranes at low pressures.

As in the other separation processes a key issue will also be cost, particularly as there are already competing polymeric membranes on the market with an installed cost of ~\$150/m^2 compared with the estimated current cost of the zeolite membranes of ~\$15000.m^2 free standing.

3.3.1.3 Ammonia Recovery

A simplified flow sheet for a typical modern ammonia synthesis loop is shown in Figure 82. The normal unit operations which can be seen in this figure comprise:-

- make up gas compression from the feed pressure of ~30 bar to the loop pressure of between 100 and 140bar depending on design (the latest flow processes may now operate down to ~80bar).
- Addition of the make up gas to the recycle loop prior to the cooling/refrig section as any contaminants (water, CO2) are removed in the liquefied ammonia
- Refrigeration to remove the product ammonia as liquid ammonia
- recycle compression
- ammonia conversion

The refrigeration system in the 140bar process runs at ~5C and is both a major energy consumer within the loop and has a significant CAPEX. (In lower pressure plants the refrigeration temperature is considerably lower to keep the ammonia partial pressure in the loop at an acceptable level). The target was the replacement of this process step with a membrane system.

In the simulation a simple separation block has been used for the membrane implementation as it was not possible to develop the microporous membrane model. The separation block splits a given amount of ammonia from the feed stream and adds it to the permeate stream. Specific membrane performance from the test runs at Bath could not be used as the pressure and concentrations were significantly below those in the actual process even though the tests had demonstrated that the separation was possible.

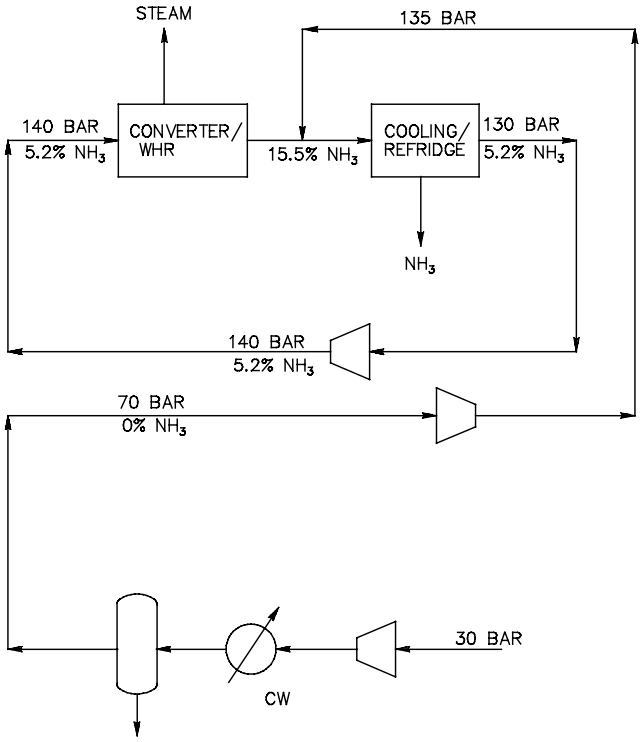

Figure 82 Conventional ammonia synthesis loop

To get an insight into the possible energy savings, which can be realised with a membrane implementation, CE made two assumptions:-

1. a minimum NH_3 partial pressure difference of 1.4 bar. This seems reasonable when the Bath data, which shows a maximum selectivity at a minimum ammonia partial pressure differential is considered (see Figure 68)
2. only NH_3 is permeating through the membrane. This is not the case and represents an oversimplification that was dictated by the absence of the full micropore model. However

as the permeate side of the membrane is purged with the make up gas any slippage will simply add to the purge gas flow and lead to in an increase in the make up gas compression resulting in a decrease in the net energy saving.

CE then implemented the membrane unit in 3 different cases:
Case 3: Sweep/Feed flow pressure 70 bara, including chilling;
Case 4: Sweep/Feed flow pressure 70 bara, no chilling;
Case 5: Sweep/Feed flow pressure 30 bara, no chilling.

The actual process is the subject of a patent application but a summary of the utility consumption for the various cases is presented in Table 33. The utilities that are considered and their units are:
1. Power consumption: power required to drive compressors.[kW].
2. Steam: the net amount of energy for producing steam. [kW]
3. Cool water: the net cooling water duty [kW]

Table 33 Utility consumption and production summary

Equipment		Base case	Case 3 with chilling	Case 4 without chilling	Case 5 low pressure
Power consumption:					
MUG compressor	[kW]	11965	12132	12602	15833
Recycle compressor	[kW]	2588	2265	5079	1904
Refridge compressor	[kW]	5164	5134	0	0
TOTAL	[kW]	19717	19531	17681	17737
Steam production:					
After converter	[kW]	32688	34029	0	36037
Cool water consumption:					
MUG compressor	[kW]	11914	12145	17541	32090
Synthesis loop	[kW]	9271	7916	60188	7910
Refridge loop	[kW]	29860	29734	0	0
TOTAL	[kW]	51045	49795	77729	40000
Overall Consumption	[kW]	38074	35297		21700

The overall energy saving associated with the complete replacement of the refrigeration system amounts to approximately 17000kW, a reduction of nearly 50% in the loop energy costs and 10% in the overall plant energy costs. This represents a major saving in what is already a highly optimised process.

At present the overall costs benefits of the process cannot be assessed as it is not possible to realistically estimate the required membrane area. However it can be seen that the membrane cost is offset both against the complete elimination of the refrigeration compressor and the substantial energy savings. It also seems likely that this process will be even more competitive in the newer low pressure ammonia plants where more severe refrigeration conditions are required to achieve the target recycle ammonia concentrations.

The key requirement will be to assess the membrane performance under real operating conditions to confirm the ammonia recovery/syngas slippage and to provide a realistic assessment of the membrane area. Operation under conditions where liquid ammonia is present could result in substantial changes in membrane performance. It will also be necessary to develop the complete micropore model for the system to allow the development of the fully integrated flowsheet.

3.3.2 High Temperature

3.3.2.1 Hydrogen removal in catalytic processes

The reaction studied, the production of isobutene from isobutane is currently of great importance because of the growing demand of isobutene as an intermediate for the production of methyl-tertiary butyl ether used as a gasoline octane enhancer . A typical flowsheet for butene production is shown in Figure 83 and involves 4 reactors with intermediate feed heating.

Figure 83 Butane dehyrogenation process

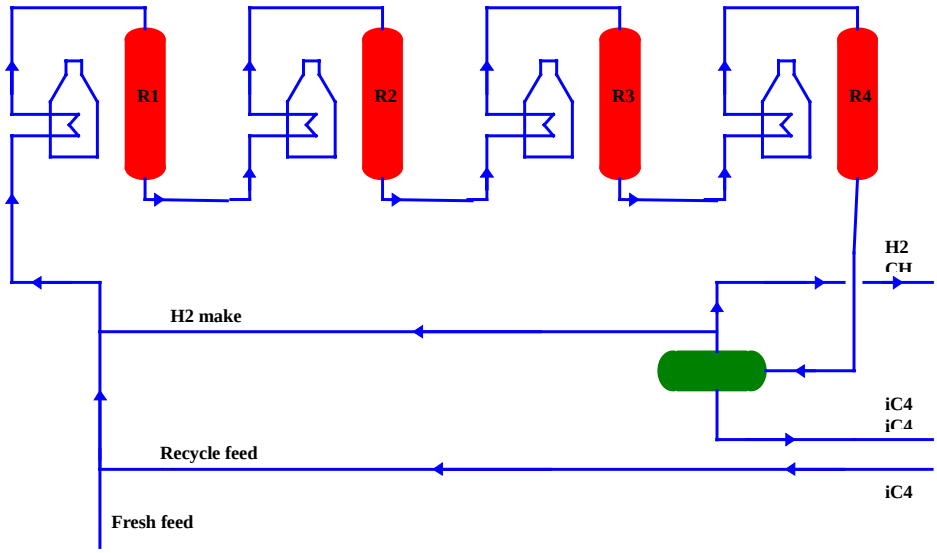

The feed is usually a mixed butane feed with an isobutane concentration of 20 to 40 % (the balance being mostly n-butane). The isobutane is recovered from a deisobutanizer. Dehydrogenation of isobutane to isobutene typically can be accomplished at about 90-92 mol % selectivity depending on operating temperature. In a typical situation for the production of 400000 tons per year of MTBE, 295000 tons of the butane feed is required. The conversion is a function of temperature. For a temperature of 600°C at 1 atm, the equilibrium conversion is 65 % with a selectivity of 92%. Since the reaction is endothermic, conversion is maintained by supplying heat, equivalent to the heat of reaction, through interstage heaters . Since the hydrogen partial pressure increases when increasing conversion, the conversion is generally limited to 45 %. Typical values for the conversions in each reactors are 16 for the first one, 12 for the second one, 10 for the third one and 8 for the last one.

The simplest implementation of a membrane process is then to include a membrane separator before each of the feed heaters to reduce the hydrogen content in the feed to next reactor (Figure 84). This places a lower demand on the membranes than found in the steam reforming and water gas shift processes as the hydrogen in this case is a waste product and does not need to be recompressed to the feed pressure. Lower selectivities can also be tolerated as C4 components lost to the permeate can be recovered and recycled to the feed. The process operating pressure is however much lower, typically between 1 and 5bar and operation with a sweep gas is therefore essential. In principle the lower target selectivities make the use of microporous membranes feasible whilst the high temperature operation, typically ~600C, favours the permeation of the hydrogen relative to the hydrocarbons. However, inhibition of the membrane performance by adsorbed hydrocarbons is an issue.

The addition of a permeator after the first, second and third stages allows the equilibrium to be displaced and thus the conversion increased. Consequently, the second, third and fourth stages are supposed to provide better conversion. However, due to the non ideal selectivity of the membranes, a loss in C4 occurs through the membrane. This loss tends to decrease the conversion gain. The total conversion is

therefore defined as the ratio of the isobutene at the outlet of the last stage to the isobutane at the inlet of the first stage. The limitation of the C4 losses in the membranes requires high selectivity.

Figure 84 Membrane modified process

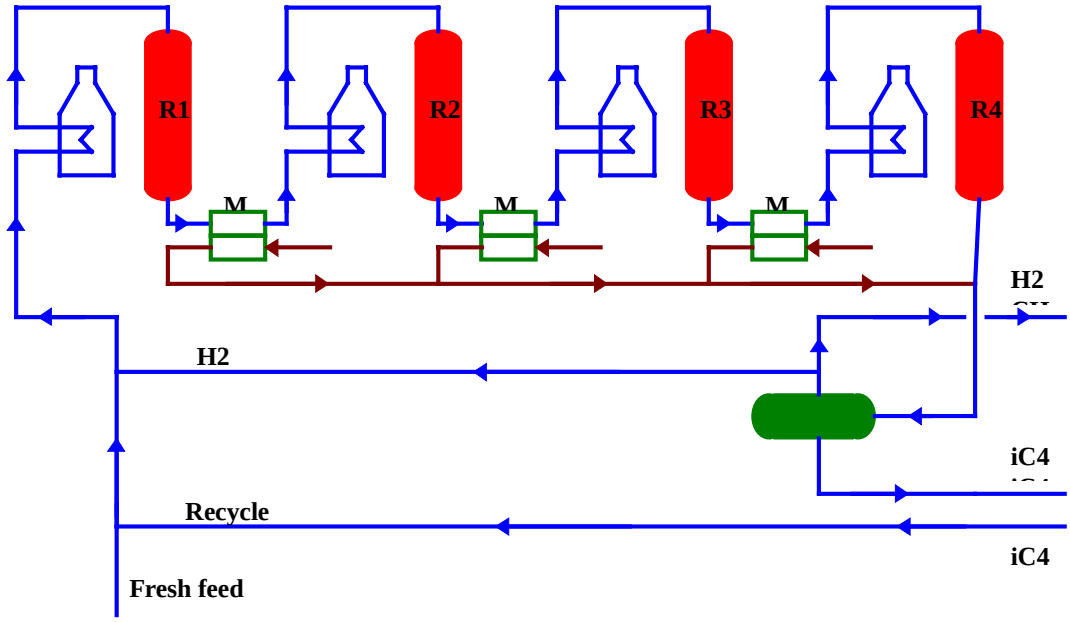

On this basis it was possible to calculate the conversion gain as a function of membrane selectivity and total sweep gas flow. The results (Figure 85) show that a selectivity of at 20-40 is ideally required to maximise the conversion gain and that at this selectivity the impact of sweep gas flow is minimal. However these levels were not achieved with the silicalite (maximum of ~10) and results on he carbon membrane are still awaited.

The performance also requires 2700m^2 of membrane area which, at current costs is non viable. As in the other microporous membrane applications a reduction to around \$1000/m^2 would appear to be essential.

Figure 85: Total conversion gain as a function of selectivity (900 m^2)

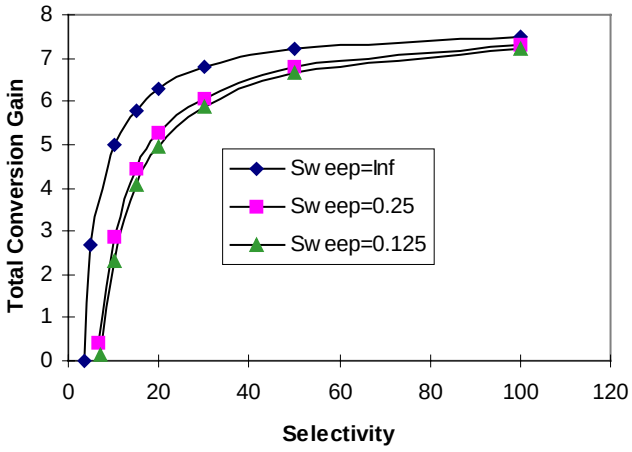

3.3.2.2 Ammonia Synthesis

The flow sheeting studies carried by Continental Engineering for the syngas preparation stages in both the ammonia and methanol flow sheets utilised the Aspen membrane palladium membrane module developed by ECN and as such could use fully integrated ammonia process flow sheet packages.

When during the steam reforming process a part of the produced hydrogen is removed, the equilibrium of the reaction is positively influenced allowing the reaction to be executed at a lower temperature or at a lower steam / carbon ratio. Through this, a recently developed process for steam reforming can be applied. In a Gas Heated Reforming design, approximately 65 to 70 % of the heat required can be provided by the heat recovered from the secondary reformer effluent. When hydrogen is removed during the steam reforming in this process, the equilibrium of the steam reforming reaction is less influenced by the applied pressure. In that case, a higher pressure than normally applied in conventional reforming processes can be used which results in a higher pressure at the suction of the synthesis gas make-up compressor.

Figure 86:block diagram nitrogen membrane case 2 front-end

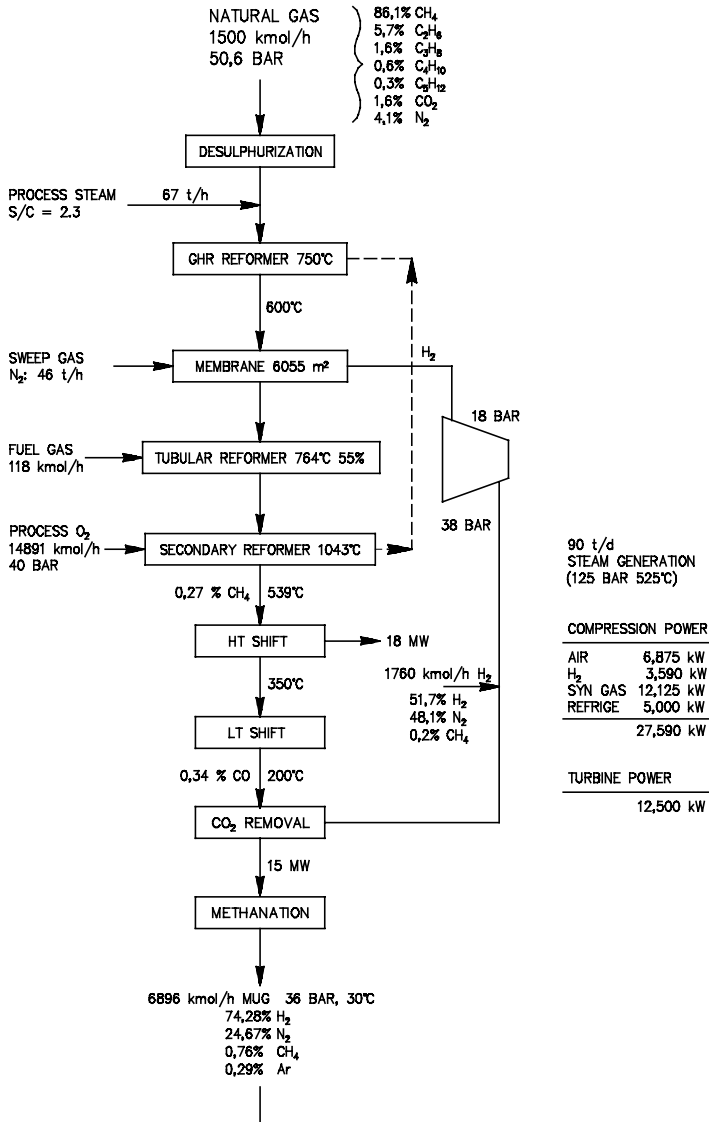

Since nitrogen is introduced with the process air in the secondary reformer, it is not available as sweep gas in the membrane, unless air separation is used. Case 1 therefore uses steam as sweep gas. The amount of steam should be restricted to a minimum, because steam itself can only be produced at the cost of energy. Case 2 is almost similar to the steam sweep gas case except for a few changes. Instead of using steam for sweep gas pure nitrogen is used which is obtained from an air separation unit. The remaining oxygen product is then used for the secondary reforming. The benefit of this option is that the permeate stream can be compressed directly without first condensing the sweep steam and there is no heat/energy involved for sweep steam generation. The disadvantage is that an air distillation will be necessary in this case.

The most economical option is to place a Gas Heated Reactor (GHR) before the existing primary reforming, with a membrane unit between the two reforming units. One of the benefits of this construction is that the

steam carbon ratio can decrease to a value of 2.3 and secondly the outlet temperature of the GHR is 600 °C. A palladium membrane has a temperature limit of approximately 650 °C. A schematic diagram for case 2 is shown in Figure 86.

Natural gas consumption
The natural gas consumption is for both membrane cases 442 kmol/h less than the base case. This is the result of using a GHR in combination with a membrane and a primary reformer.

Power consumption
The power consumption is for both membrane cases about 550 kW more then for the base case. This is due to the extra H_2 compressor after the membrane.

Other consumption's
In the nitrogen case pure oxygen enters the secondary reformer instead of air. This saves about 8500 kW in preheating compared to the other cases.

Steam consumption
The steam / carbon ratio is for both membrane cases 2.3. This saves for both membrane cases about 20.4 t/h steam compared to the base case.
However the steam case (case 1) has the highest steam consumption due to the 33.8 t/h steam necessary for sweep gas.

Steam production
The base case is producing the highest amount of steam. This is the result of placing a waste heat boiler direct after the secondary reformer. Both membrane cases are using this heat for primary reforming in a GHR. The steam production of the steam case is about 30 t/h higher than the nitrogen case. This is due to the latent heat of condensation of the sweep steam.

On balance, although case 2 does appear to offer some benefits this is likely to be offset by the capital and operating costs associated with the air separation plant. The benefits might also be further diminished if a base case was developed that utilised the gas heated reformer. There appears to be little case for pursuing this option further.

3.3.2.3 Methanol Synthesis

The front end of the methanol synthesis process in common with ammonia synthesis requires steam reforming and water gas shift to generate the CO/H_2 mixture. In the case of the methanol plant the incorporation of the membrane system between two reforming reactors leads to two benefits:-

1. Due to the hydrogen removal the steam reforming equilibrium is positively influenced. So that the conversion of this reaction is higher at the same execution temperature.
2. Methanol is produced by the following reaction: $CO + 2\ H_2 \leftrightarrow CH_3OH$. The CO and H_2 necessary for this reaction are obtained from the following steam reforming reaction: $CH_4 + H_2O \leftrightarrow CO + 3\ H_2$. This delivers more hydrogen than necessary for the methanol conversion which is therefore normally not carried out with a stoichiometric feed. When a certain amount of hydrogen is removed by a membrane the reaction can be executed with a stoichiometric feed which results in a higher conversion per pass.

A schematic diagram of the membrane modified flowsheet is given in Figure 87.

Figure 87Block diagram methanol membrane case

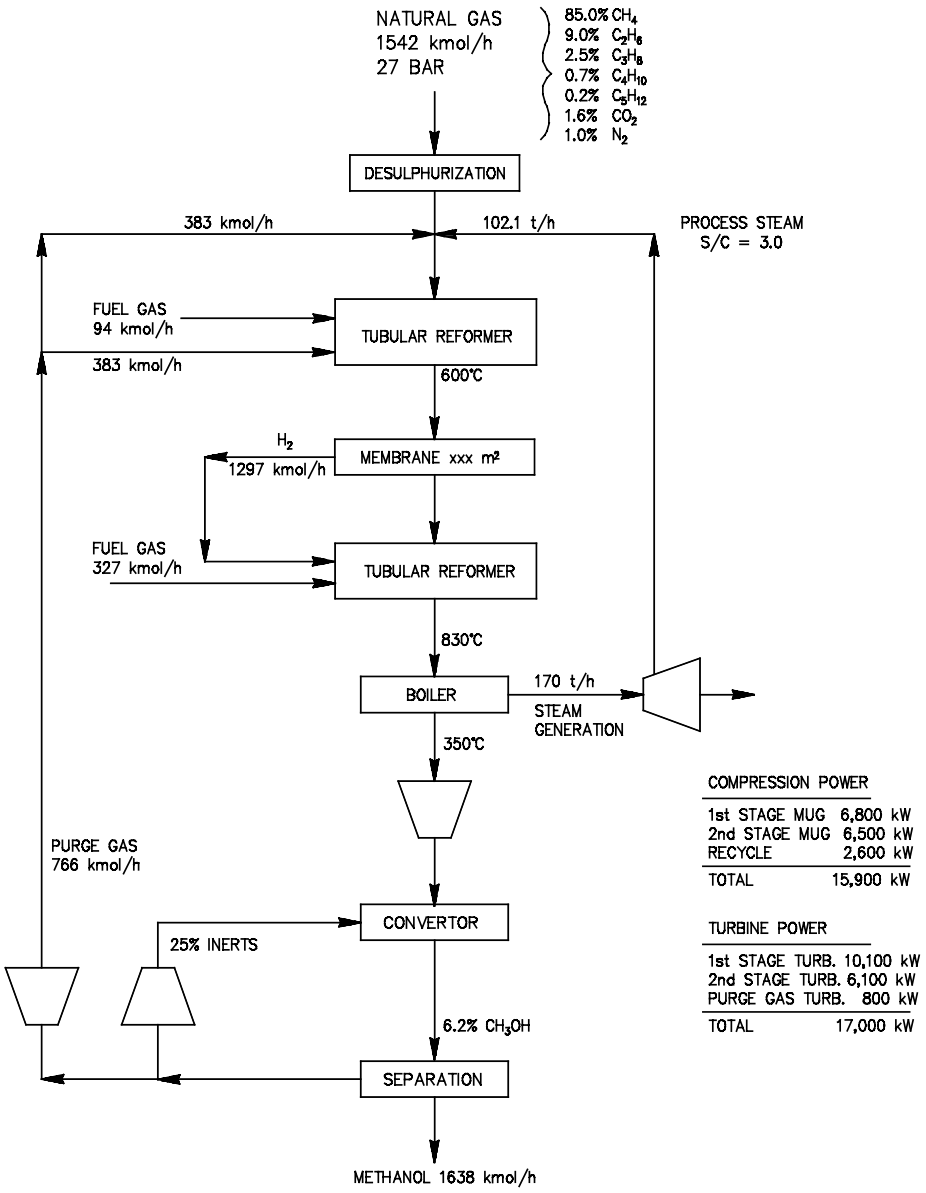

On basis of this flowsheet the direct natural gas saving between the base case and the membrane case amounts up to 3.7 %. However, the base case produces 2225 kW more power than the membrane case because less steam and less purge gas is expanded in the turbines. When making a comparison between the two cases the natural gas saving must be corrected for the less power production. If the heat of combustion of natural gas is assumed to be 1750 kJ/mol with a power generating efficiency of 0.5 the direct natural gas saving is about 2.8 %. These savings can then be equated to an annual cost saving if it is assumed that there is an on stream time of 8000h/yr and a gas price of 0.10 ECU/Nm^3. This amounts to 0.8million ECU/year. However this must remunerate the cost of the membrane installation as there are no other capital cost savings. Based on the membrane model developed at ECN/Salford, which showed a required membrane area of ~6000m^2, and if a payback time of 3 years is assumed, this equates to an installed membrane cost of 650ecu/m^2. As it is generally assumed that the installed cost for simple gas separation ceramic membranes is considerably in excess of ~2000ECU/m^2 it is immediately apparent that the system is not

yet viable. This can also be looked at from the standpoint of the costs associated with membrane production. At present, with Pd layers of around 7micron thickness, the cost of the Pd component alone is ~800ecu/m^2. This compares with the typical costs for the currently available large pore ceramic substrates of at least 1000ecu/m2 (NOT installed). This shows that whilst reducing the amount of Pd used will bring benefits, the key requirement will be to reduce the cost of the substrate and to increase the flux, thereby reducing the area required. If the required area can be reduced by a factor of two this will give an allowable installed cost of ~1300ecu/m^2 which suggests a total membrane cost of around ~400ecu/m^2 (the ratio of membrane to installed cost is typically >3) which will only allow ~200ecu/m^2 for the support.

Nonetheless the system does have potential and shows useful energy savings. The direction of future research must clearly be to reduce membrane costs without compromising stability or lifetime although this also remains a significant issue.

3.3.2.4 IGCC

The Integrated Gasification Combined Cycle (IGCC) is a very clean and efficient process to convert coal and other solid or liquid feedstocks (so-called dirty fuels) into electricity at low contaminant emissions and with a high energetic efficiency. The coal gas from the pressurised gasification contains the combustible compounds carbon monoxide (CO) and hydrogen (H_2) at a high concentration and some methane (CH_4). This offers the interesting possibility to use some of the coal gas for coproduction of various chemical by-products beside electric power generation in the gas and steam turbine combined cycle. Some important feedstocks for chemical syntheses or processes, which are considered here, are hydrogen, ammonia (NH_3) and methanol (CH_3OH). In order to produce them, a slip stream of the coal gas must be conditioned to get the hydrogen out or to adjust the necessary molar ratio between CO and H_2. The conditioning processes as well as the ammonia or methanol synthesis loops are integrated into the IGCC plant, which has the advantage that any "purge" stream or other valuable fuel stream can be burned in the gas turbine and is not lost for the process. Furthermore, process steam to be produced or consumed can be exchanged with the heat recovery steam generator (HRSG).

In conventional synthesis gas treatment plants, the H_2 separation or enrichment is often done by a combination of a CO shift and a CO_2 absorption process. The CO_2 absorption or both processes can be replaced by a ceramic membrane separation process. The hydrogen as the desired product permeates through the pores of the membrane and is enriched at the permeate side. This offers the potential to achieve some primary energy savings via reduced coal input to the gasifier, because the membrane separation process itself consumes less energy than the conventional processes and can improve the overall process design.

Starting point for all process calculations is an IGCC power plant for electricity production only, named Case 0. The design of the plant is similar to the Puertollano demonstration plant, but with state-of-the-art components. An oxygen-blown entrained-flow gasifier with dry coal feed (PRENFLO) delivers a synthesis gas with about 59 % mole CO and 33 % mole H_2. After cooling and removal of dust and gaseous impurities in a conventional wet gas cleaning, the coal gas is saturated, diluted with nitrogen from the air separation unit (ASU) and burned in the gas turbine-generator, a Siemens Model V94.3A with a compressor pressure ratio of about 17. The gas turbine exhaust heat as well as heat from the gas island (gasifier, ASU and gas cleaning) is utilised in the bottoming steam cycle. The base case IGCC has a calculated net electric power output of 383.6 MW and a net efficiency of 50.5 % (based on LHV).

For coproduction purposes, a slip stream of the clean coal gas is extracted after the gas saturator in order to have already some water in the gas stream necessary for the CO shift. In total, seven options for coproduction were considered, the characteristics are listed in Table 34). In all cases the detailed flow sheet optimisation has been carried out using the Aspen palladium module developed by ECN.

Table 34: Selected IGCC processes for coproduction of electricity and chemicals

	By-product	CO shift	$CO_2/CO/H_2$ separation
Case 0	-	-	-
Case 1	Hydrogen	yes	CO_2 Absorption (MDEA)
Case 2	Hydrogen	yes	Pd-Membranes
Case 3	Ammonia	yes	CO_2 Absorption (MDEA)
Case 4	Ammonia	yes	Pd-Membranes
Case 5	Methanol	yes	CO_2 Absorption (MDEA)
Case 6	Methanol	yes	Pd-Membranes
Case 7	Methanol	no	Pd-Membranes

Whilst there are clear technical problems in the implementation of the palladium membranes in free standing methanol and ammonia plants their use in combined cycle plants produces greater benefits due to the integration of the heat management systems and the better utilisation of the waste gases. However the principles found in the free standing plants still apply and it is only the coproduction of methanol that shows substantial benefits. This reflects primarily the problems of recompressing the hydrogen permeate stream to the pressures required for ammonia synthesis.

However the main benefit in the case of methanol synthesis cogeneration arises from a novel flow sheet concept (which is the subject of a patent application by Siemens and Essen) which allows a substantial reduction in membrane area from around $3700m^2$ to ~$1300m^2$.

This also gives rise to an overall increase in plant efficiency with the Primary Energy Utilisation rising from 53.57% o 53.86%. This is equivalent to 610TJ or 20,500 metric tons of coal per annum. This corresponds to a reduction of CO_2 emissions by 53,400 tons per year Whilst this appears to be a small improvement this has to be seen against the highly advanced state of existing co-generation facilities. With this reduced membrane area and the elimination of the CO shift system there is also a reduction in plant CAPEX, even when the membranes are costed at $4000ecu/m^2$. The CAPEX for this flowsheet amounts to 929ecu/kW as compared to 1062ecu/kW for the base case plant when the produced methanol is converted back to an energy output. This is equivalent to a CAPEX saving of ~50million ecu for the 385MW base case plant. With an estimated membrane area of $1300m^2$ this is equivalent to an installed membrane cost of $40,000ecu/m^2$ which should be attainable even at current membrane costs.

This therefore presents a clear option for further development where the key issues will be membrane lifetime and resistance to poisons and thermal cycling along with a direct demonstration of the membrane operation under the desired test conditions. Some further reductions in membrane cost/area will probably also be required to maintain the process benefits.

4. RESULTS AND CONCLUSIONS

As this project was essentially a fundamental study into the potential uses of ceramic membranes in process applications the main target was to provide a clear indication of where process development was a viable future option from both an energy saving a CAPEX reduction standpoint and where further work was not justified. The second target was to comparatively evaluate the different membranes under these process conditions to provide guidance on where future membrane development should be targeted. The final objective was to provide a clearer understanding of the mode of operation of these membranes and to develop fundamentally sound models for their operation.

4.1 Process Applications.

These aims have been achieved and the outcomes can be split into three classifications:-

1. **Further Development Justified** :- The results show clear commercial potential and a further focussed development project is justified
2. **Fundamental Work required**:- the results show some potential but further detailed study is required to confirm the available benefits
3. **No further work Justified**:- The results show that there is little chance of a commercially viable process and no further work is justified

4.1.1 Further Development Justified

FCC Offgas Recovery - Bath University, IRC Lyon, University of Essen
In the low temperature processes only the FCC offgas recovery objective demonstrated clear performance benefits. However the overall cost effectiveness of the process will be dominated by membrane costs. At the current estimated price for the zeolite membranes (~$15000/m2) the process would not be viable It will be necessary to bring the membrane cost down to a maximum of around $1000/m2 or $4000/m2 installed. It seems likely that this will only be achievable through the use of much cheaper supports than the multilayer ceramics in current use and this should be the main aim of any future research. A project is being developed for submission to the next Framework programme (FP5).

It seems likely that any related applications, targeted at separation of the $H_2/C_1/C_2/C_3$ gases will face similar constraints. However there is interest in developing methods for dewpointing natural gas and a project is being prepared for submission to FP5.

Methanol Synthesis in Cogeneration Plants - Siemens, University of Essen, Continental Engineering, ECN, Salford University
In the high temperature processes only the coproduction of methanol in IGCC processes demonstrated a clear benefit showing both CAPEX and OPEX savings even at realistic palladium membrane prices although their use in free standing methanol plants could be viable if the cost of the membranes can be significantly reduced. However whilst JM provided the Pd membranes as a commercial material they have indicated that they have no intention of developing the membranes further for large scale applications. The development of the process will therefore require a committed membrane producer to take the technology further.

A further submission to FP5 is being developed.

4.1.2 Fundamental Work Required

Ammonia Recovery in Synthesis Loops - Continental Engineering, IRC Lyon, University of Bath
The studies demonstrated that the silicalite membranes gave a reasonable performance although the test conditions were limited in both pressure and ammonia concentration. A more detailed assessment of the membrane performance under real test conditions will be required to confirm the performance and provide a better estimate of membrane area. It will also be necessary to develop the micropore membrane model for this application to allow the optimisation of the flowsheet. There is however a reasonable chance that the membranes will show a combination of CAPEX and OPEX benefits. A submission to FP5 is being planned.

CO_2 Removal from natural gas - BG Technology, IRC Lyon, Bath University
Whilst the selectivity of the membranes in this study fell well short of the performance required for a commercial process the prize is sufficiently large to justify further work. It is recommended that this concentrates primarily on the initial development of microporous materials that show enhanced multi-component adsorption for CO_2 in mixed CO_2/Methane gases under the high pressure conditions associated with produced natural gas. This would then be followed by development of membranes based on the optimised adsorbents. Some testing of existing materials under the high pressure conditions

would also be justified to provide a better understanding of the mode of operation of these materials. A proposal to FP5 is planned.

High temperature hydrogen from C4's Institut Francais du petrol, MAST Carbon Ltd
The work completed has demonstrated the limitations of the membranes tested so far (silicalite and silica) both of which failed to give the required selectivity. Further work is ongoing on the carbon membranes which have in the past shown adequate selectivity. A further programme may be justified if the carbon performance is adequate. Alternatively the results have suggested that a zeolitic structure with a similar pore size to the silicalite but with improved hydrogen transfer properties may prove adequate.

Methanol Synthesis - Continental Engineering, ECN, University of Salford
The palladium membranes do give rise to significant energy savings in the production of methanol. This is because a lower permeate pressure is allowable in methanol synthesis compared to ammonia synthesis which removes the requirement for a purge stream. Nonetheless the required membrane area is still very large (~6000m2). Cost benefit analysis has shown that whilst reducing the amount of Pd used will bring benefits, the key requirement will be to reduce the cost of the substrate and to increase the flux, thereby reducing the area required. If the required area can be reduced by a factor of two this will give an allowable installed cost of ~1300ecu/m^2 which suggests a total membrane cost of around ~400ecu/m^2 (the ratio of membrane to installed cost is typically >3) which will only allow ~200ecu/m^2 for the support.

Nonetheless the system does have potential and shows useful energy savings. The direction of future research must clearly be to reduce membrane costs without compromising stability or lifetime.

4.1.3 No Further Work

Environmental Applications
The test work demonstrated clearly that the diffusivity of the larger molecules (aromatics) in any of the microporous membranes was too low under ambient conditions to justify any further work. It is possible that mesoporous membranes could operate.

Water Gas Shift
The production of hydrogen in water gas shift processes using palladium membranes was shown not be feasible. No set of operating conditions was found where the required purity and hydrogen recovery could be achieved in free standing methanol or ammonia plants. No further work is recommended,

Ammonia synthesis processes - Hydrogen Production
The efficient operation of the palladium membranes in the ammonia plant front end is critically dependent upon the use of a sweep gas if the desired hydrogen recovery (>80%) is to be achieved. A further down side is the high cost of recompressing the hydrogen permeate back to the process conditions. Given the high operating pressure of ammonia plants (typically >100bar) this represents a major cost and energy penalty. Under these circumstances it seems unlikely that such an application will be viable.

4.2 Membrane Considerations

The other key objective was to place the different membranes in a comparative evaluation environment to provide guidance on where future membrane development should be targeted in the light of the process studies discussed above. This also then depends critically on the process conditions envisaged. Whilst the studies have provided guidance on this they have also highlighted that at current membrane costs essentially none of the systems offer sufficient benefits to justify larger scale production and process development. A key requirement will be to achieve membrane costs of approximately 1-2000ecu/m^2 if any of the processes is to be viable in the future and this should be one of the key targets of any future programme. Consideration of the production routes to the membranes evaluated in this project shows that this will require a substantial reduction in the cost of the support system used in the production of both the zeolite and palladium membranes.

Considering the membranes in detail the following comments can be made:-

4.2.1 Hydrogen Production Processes - Palladium Membranes - Johnson Matthey, Salford University

Steam reforming and water gas shift flowsheeting considerations have shown that these processes are controlled by hydrogen recovery and selectivity considerations. These can only be met by the palladium membranes although other advanced non porous membranes might also be usable in the future. The microporous silica membranes, which had the highest selectivity of the microporous membranes, do not give adequate selectivity. The critical constraints for the Pd membranes are cost, as discussed above, operability and life. Whilst the tests carried out in this project have shown that the JM membrane can operate for up to 30 weeks there was a continuous decline in performance over this period followed by catastrophic failure. The membranes also required very closely controlled operating conditions if they were subjected to thermal cycling and this could place a major limitation on their use in large scale processes. Future programmes must therefore address these factors as major targets.

4.2.2 Microporous membranes

The uses of the microporous membranes can be split into two main areas of application -

1. low temperature where the performance is dominated by selective adsorption effects but the selectivity is generally reduced by molecular sieving effects
2. high temperature where performance is dominated by molecular sieving but where the selectivity is generally reduced by adsorption effects.

Of the membranes tested only the silicalite membrane (IRC :Lyon) consistently showed good performance in the low temperature separation processes. This appears to reflect that the pore structures of all of the other membranes (silica (ECN), zeolite A (Smart Chemical Company) and Carbon (MAST Carbon Company) were either too small for the processes investigated or that the selective adsorption properties of the materials gave inadequate selectivity. There is clear scope for the further development of the IRC membrane for use in both hydrocarbon and ammonia separation processes with the main target of reducing membrane costs, primarily through a reduced cost support but also possibly through improved permeability. The carbon membranes (MAST Carbon) have shown useful performance in low

pressure CO_2/N_2 separations and this could still justify future development. In natural gas separation none of the membranes showed adequate performance and the main target, if this objective is to be pursued, must be to develop microporous materials with improved selective adsorption capability.

In the high temperature applications (hydrogen from butane) the silicalite membrane showed inadequate selectivity, possibly due to a combination of residual hydrocarbon adsorption and the unusual hydrogen transport characteristics of the silicalite, whilst the selectivity of the silica was apparently inhibited by pore blocking by the residual adsorbed hydrocarbons. Detailed evaluation of the diffusion characteristics of the materials suggests that alternative zeolites with similar pore sizes to the silicalite but improved hydrogen transport properties or the carbon membranes could provide usable membrane performance.

Work is still underway on the carbon membranes (MAST Carbon and IFP) and the possibility of further work on alternative zeolites is under consideration.

4.3 Fundamental Studies

The primary objective was to provide a clearer understanding of the factors controlling both microporous and palladium membrane performance. A key observation for the microporous membranes**, that cannot be too strongly stated**, is the critical requirement to carry out all process evaluations using mixed feed gases. The tendency in the literature to quote membrane selectivity as the ratio of the pure gas permeabilities (ideal selectivity-see appendix 2) will in virtually every circumstance give grossly misleading results due to the presence of both competitive adsorption and competitive transport effects. Only when a detailed and viable microporous membrane model is available will single gas studies be usable in process predictions. However the use of multi-component gases brings its own problem in the shape of surface polarisation phenomena that must then be accounted for.

4.3.1 Micro pore Transport Properties

The investigations into the transport properties of the microporous materials encompassed both theoretical (Imperial College) and practical studies (Leipzig University(PFGNMR) and IRC Lyon(QENS)) and at this stage these have served mainly to demonstrate the extreme complexity of the processes involved. The IC studies have shown that the commonly adopted approach in many modelling studies of either assuming diffusivity to be constant or to use self diffusivity as the constant modified by the Darken correction is seriously flawed. A further term reflecting “viscous” flow characteristics is required although it has not yet been established how this can be obtained from fundamental adsorbate/adsorbent properties. Considerably more work is required in this area. However this only applies to single straight pores when in fact real materials comprise far more complex pore structures.

The practical studies (Leipzig and IRC Lyon) have additionally shown that material properties can have an additional dramatic effect on the diffusive properties. This has been exemplified by the silicalite where the Leipzig and Lyon studies have shown that the channel structure allows hydrogen to be trapped in non transport pores, dramatically reducing the observed diffusivity. As this kind of effect could not be predicted by the simulation studies it will always be necessary to carry out the simulation and practical studies in parallel. Other effects have been the discovery of an apparent parallel diffusion pathway for hydrogen in the presence of more strongly adsorbing molecules. As the hydrogen diffusivity was not inhibited by the presence of e.g. propane in either the carbon or zeolite A materials this would appear to suggest a fundamental process in a single pore rather than the presence of two different pores.

The PFGNMR studies have also shown the severe effect of strong localised site adsorption of one component on the characteristics of the diffusion process - for instance ammonia diffusion in a media with acid surface sites shows an increase with pore concentration whilst a component such as ethane shows a decrease with pore concentration as the diffusivity is dominated molecule-molecule interactions. In a multi-component separation process where diffusion of one component is inhibited by the presence of the other components and where the components may show different concentration dependencies the

modelling of the overall process will clearly become extremely complex. Nonetheless this will be essential for the future development of microporous membrane based processes and considerable further work is required in this area.

Work has also been carried out by MESL Democritos on the transport properties of porous networks from both theoretical and practical standpoints. The theoretical approach has so far been limited to mesoporous networks but has demonstrated the impact of both connectivity and pore shape on transport. Further work will be required to extend this to the microporous systems although the general conclusions appear to be in accord with the practical measurements.

4.3.2 Micro-pore Adsorption Properties

The other parameter underpinning the microporous membrane operation that has been considered in this project is the selective adsorption property of the membrane material (University of Bath, BGGRC and Imperial College). Whilst this is better understood, and less complex, than the transport properties the methodologies for incorporating multicomponent adsorption into the membrane models still requires more detailed assessment. It is anticipated that this would rely on for instance Ideal Adsorption Theory (IAS) although the direct incorporation of this into a model would be potentially very complex. There is therefore a requirement for further work to assess the viability of simpler models such as multicomponent Langmuir and Langmuir Freundlich though both practical and theoretical studies for the gas compositions of interest.

4.3.3 Surface Polarisation Phenomena

The National Technical University of Athens (NTUA) have developed the methodology for examining the effects of surface polarisation phenomena on membrane performance using fluid dynamics (Pheonix™) techniques. These have shown that in membrane studies in mixed gas environments surface polarisation can seriously compromise the data obtained from the membrane test programmes. This can be overcome through either improved practical techniques to minimise the effects (e.g. the “Spider” reactor developed by ECN in this project), although the reactor performance should still be checked against the FD predictions, or by using the FD software to extract the real membrane performance. The work has however shown that there are still some underlying errors in the FD predictions that will need to be resolved in future programmes. These effects will apply equally to the microporous and the non porous palladium membranes.

4.3.4 Module Design

Whilst all of the studies in this project have been limited to single tube systems it is likely that in full scale commercial processes it would become necessary to use multichannel monolith structures to improve the surface:volume characteristics and the mechanical robustness of the membrane systems. MESL Democritos has developed a finite element programme that, through direct measurement of the permeability of the support and membrane layers, allows the impact of moving to multichannel monoliths on the overall monolith flux and the fluxes in the individual channels to be evaluated. At present, with several orders of magnitude difference between the permeability of the support and membrane layers, there is predicted to be little impact in moving from a single tube to a 3 ring, 37 channel monolith. However this will need to be considered in the future if the flux characteristics of the separating layers improves.

5. EXPLOITATION PLANS AND BENEFITS

The exploitation plan is limited to the development of further research programmes as outlined above. Several projects are in the course of preparation that represent either direct development of topics from this project or step-out projects. Whilst the overall benefits from these programmes is difficult to quantify in detail it is believed that the selected projects to offer the potential for viable commercial

processes and the proposed work in these areas will reinforce Europe's current lead in the microporous membrane field.

Projects under consideration are:-

1. **FCC Offgas separation**

The University of Bath and CNRS Lyon will seek to further develop this technology. It is only possible to use the proposed FCC off-gas recovery system when the gas can be passed to the separation system of an existing ethylene plant as the amount of gas available would never justify the construction of dedicated separation facilities. However when the two plants co-exist the financial justification is clear. A survey of refineries and chemical plants on a world wide basis has shown that there are at present 56 possible locations for this technology with an installed FCC capacity of $2.63x10^6$ b/sd with units with capacities ranging from 8,800 to 190,00b/cd. With an estimated current requirement of ~5000m^2 of membrane areas per plant the total membrane demand would be ~280,000m^2 if all plants were eventually retrofitted. The process has the advantage that the installation poses no risk to either of the host plants and should therefore be seen as a low risk option for plant operators.

2. **Natural gas dew-pointing** - CNRS Lyon and the University of Bath will seek to further develop this technology. This is an extension of the above project to treat a specific problem associated with the use of natural gas in gas turbines.
3. **IGCC-Methanol co-production** - this is a direct extension of the topic in the current programme. Siemens believes this has commercial potential and further work is planned. The current study has shown that this combined process offers the best opportunity even at the current price of palladium membranes. If the costs are reduced as production volume increases there will be a significant capex reduction in the overall plant combined with a significant energy savings. Provided therefore that the membrane production can be achieved this could become the standard implementation of IGCC processes in the future. Siemens has estimated that over the next 10 years, 330 IGCC plants of 450 MW (net) average size might be installed world-wide. This would therefore provide a competitive advantage for Siemens and provide a market for approximately 450,000m^2 of palladium membranes.
4. **Ammonia recovery in syn-loops** - Continental believes this has potential and further work is planned. the proposed project is is a direct extension of the topic in the current programme.
   This proposed process is almost certainly restricted to new plant construction as a major part of the benefit derives from the elimination of the refrigeration system. The installation of the facility will be seen as high risk as in the vent of its failure the entire plant will shut down. It will therefore be necessary to demonstrate conclusively the operability and reliability of the process in a significant scale process demonstration unit before it is likely to be installed in new plant. The market opportunity will be limited to approximately 4-6 plants a year, the majority of which are built in third world or far east countries

The possibility of fundamental studies in the following areas is also under discussion:-

1. High temperature hydrogen from hydrocarbons with modified membranes - IFP
2. palladium membranes in methanol synthesis - essentially a membrane development project - Siemens/Continental
3. CO2 recovery targeted initially at the development of microporous material with enhanced CO2 adsorption capability - University of Bath
4. Microporous membrane modelling - there is still a requirement to establish the underlying principles of microporous membrane operation.

6. APPENDICES

6.1 Appendix 1 - Units and Measurement

The nomenclature and symbols are obtained from G H Koops[66].

Asymmetric membrane: A membrane consisting of one material having two or more non identical morphological layers in the direction of transport. This membrane is mostly prepared in a one step process.

Dense membrane: A membrane with no detectable pores.
Synonymous term: nonporous membrane.

Inorganic membrane: A membrane which consists of inorganic materials.
Comment: Four different kinds of inorganic materials frequently used as membrane material can be distinguished: ceramics, glasses, carbon and metals.

Macropores: Pores with a pore diameter larger than 50 nm.

Membrane: A membrane is an intervening structure separating two phases and/or acting as an active or passive barrier to the transport of matter between the phases adjacent to it.

Mesopores: Pores with a pore diameter between 2 and 50 nm.

Metal membrane: A membrane which consists of one or more metals.

Micropores: Pores with a pore diameter smaller than 2 nm.
Comment: the term "nanopores" is also used to define the same pore size. However, the term micropores is preferred to be in accordance with the IUPAC nomenclature.

Permselective membrane: A membrane which separates components of a fluid by differences in one or more properties of the components, such as size and shape, electrical charge, solubility and diffusion rate.
Term to be replaced: Semi-permeable membrane.

Porous membrane: A membrane with pores connecting the two phases separated by the membrane. A foam layer with no interconnecting pores (cellular foam) is generally not considered as being a porous membrane.

Zeolite membrane: Any type of membrane where the separating surface is composed of 100% zeolite.

Bubble-point method: A technique which determines the largest pore in a membrane by bringing a liquid on top of the membrane, while at the bottom side a pressure is applied. When an air bubble penetrates through a pore (the largest pore) the pore size can be calculated using the Laplace equation.
Comment: The air bubble passing through the pore is mostly observed by eye and the membrane is measured in a wet state.

Mercury porosymetry: A technique in which mercury is forced into a dry membrane with the volume of mercury being determined at each pressure. The relationship between pressure and pore size is given by

[66] G-H. Koops, Nomenclature and symbols in membrane science and technology, issued by the European Society of Membrane Science and Technology (ESMST), CIP-DATA, Koninklijke bibliotheek, Den Haag, the Netherlands, 1995, ISBN 90-365-0768-5.

the Laplace equation. This technique determines pore size distribution of the total number of pores (active and inactive).

Permporometry: A technique in which controlled vapour condensation blocks the pores inside a porous membrane while simultaneously a gas flux through the membrane is measured. At relative pressure 1 all pores will be blocked. Decreasing the vapour pressure will empty the pores with a diameter corresponding to the relative vapour pressure given by the Kelvin relation. This technique determines pore size distribution of the total number of active pores.

Gas separation: A pressure driven membrane operation in which gas mixtures are separated by homogeneous, dense membranes or porous membranes. Homogeneous, dense membranes separate due to differences of solubility and diffusivity. Porous membranes separate due to difference in for example Knudsen diffusion and surface flow.

Comment: i) Gas separation membranes are characterised by permeability and selectivity.
ii) Gas permeation is used when the feed consists of one single gas; used in order to determine the gas permeability.

Gas and vapour permeability (coefficient): A permeability (P_i) defined for gas or vapour systems with units of [m^3(STP).m.m^{-2}.Pa^{-1}] or [gmol.m.m^{-2}.s^{-1}.Pa^{-1}].

Comment: Gas or vapour permeability constant is a confusing term as the permeability is not always a constant. The permeability can be pressure dependent in gas separation as well as concentration dependent in vapour permeation.

The gas and vapour permeability (coefficient) is often expressed in Barrer.
1 Barrer = 1 x 10^{-10} cm^3(STP) cm.cm^{-2}.s^{-1}·$cmHg^{-1}$.
Term to be replaced: Gas and vapour permeability constant.

Ideal separation factor: A parameter, α_{ideal}, defined as the ratio of the permeability coefficients of component i to that of component j.

$$\alpha_{ideal} = \frac{P_i}{P_j}$$

The ideal separation factor is to be used in case of pure gas permeation measurements.

Pin hole: A small defect in a dense, selective layer responsible for loss in the membrane selectivity.
Permeability: P_i(mol.m.m^{-2}.s^{-1}.Pa^{-1}).

Permeance (P_i/l) A flux defined for gas or vapour permeation with units of [m^3(ST)m^{-2}.s^{-1}.Pa^{-1}] or [gmol.m^{-2}.s^{-1}.Pa^{-1}]. It is defined as the transport flux, J_i, per unit transmembrane driving force.

Comment: The pressure normalised flux for gases is often expressed in the unit GPU (Gas Permeation Unit) and represents: 10^{-6} cm^3 (STP).cm^{-2}.s^{-1}.$cmHg^{-1}$.

Separation coefficient (factor): A parameter, $\alpha_{i,j}$, defined as the ratio of the composition of components i and j in the permeate stream relative to the composition of these components in the feed stream.

$$\alpha_{i,j} = \frac{\left[\frac{x_i}{x_j}\right]_p}{\left[\frac{x_i}{x_j}\right]_f}$$

The separation co-efficient is to be used when a mixture of gases is concerned. In case of a binary mixture i is the fastest permeating component and j the slower permeating component. In case of a multicomponent mixture again i is the fastest permeating component and j is the sum of the other components, so then the separation coefficient is the ratio of the composition of the fastest permeating component relative to all the other components. However, in some cases it is possible that in a multi component mixture separations coefficients are being calculated for only two components.

Sweep gas: A non condensing gas stream directed along the permeate side of the membrane to reduce the permeate concentration and maximise the driving force for permeation.

Co-current flow: A flow pattern through a membrane module (cell) in which the upstream (feed) and downstream (permeate) fluids move parallel to the membrane surface and in the same directions.

Counter-current flow: A flow pattern through a membrane module (cell) in which the upstream and downstream fluids move parallel to the membrane surface, but in opposite directions.

Cross-flow: A flow pattern trough a membrane module (cell) in which the upstream fluid (or feed) moves parallel to the membrane surface and the downstream fluid (or permeate) moves away from the membrane in the direction normal to the membrane surface.

Comment: Cross-flow is the mode of operation currently used in reverse osmosis and ultrafiltration, and is gaining in importance in microfiltration as an alternative to the traditional dead-end flow.
Terms to be replaced: Parallel flow, Tangential flow.

Feed: The phase (liquid, gas or vapour) in a membrane module or plant from which at least one component is withdrawn by membrane separation.

Flux: A parameter J_i, defined as the number of moles, mass or volume per unit time of a specified component i passing through a unit of membrane surface area normal to the transport direction. Typical units are: molar flux [$mol.m^{-2}.s^{-1}$], mass flux [$kg.m^{-2}.s^{-1}$] or volume flux [$m^3.m^{-2}.s^{-1}$].

Membrane reactor: A device for simultaneously carrying out a reaction and a membrane-based separation in the same physical enclosure.
Comment: Often the reaction takes place, catalysed by catalysts which are immobilised on or in the membrane matrix.

Module: Used to define the smallest practical unit containing one or more membranes, which can be directly manifolded to feed streams to separate a feed stream into retentate and a permeate stream, and supporting structures.
Comment: By supporting structure is meant end caps and other material required so that the resulting unit can operate independently from the rest of the plant, if necessary.
Terms to be replaced: Permeator and Membrane element.

Permeate: The stream leaving a membrane module or plant containing the components from the feed passing through the membrane.
Terms to be replaced: filtrate.

Retentate: The stream leaving a membrane module (cell) that has not passed through the membrane. Term to be replaced: raffinate.

In considering the performance characteristics of microporous membranes some of the terms relating to selectivity are used interchangeably in the literature. It must be remembered when dealing with microporous ceramic membranes that their performance characteristics are very different to those of polymer membranes. Thus, whilst the ideal separation factor, defined as the ratio of the single component permeability's, may be very similar to the separation co-efficient measured in multicomponent feed gases, for polymer membranes the results will be very different for microporous membranes. This reflects that the analysis of polymer membrane performance assumes that adsorption is primarily linear (e.g. Henry's law) and that the adsorbed species diffuse independently of each other which leads to the concept of permeability as a constant, and the ratio of single component permeability's as the selectivity. In microporous membranes the situation is now very different. Adsorption of the feed components within the micropores is controlled by multicomponent adsorption which is a highly non-linear process, whilst the transport mechanism within the confined spaces is highly complex and influenced by the nature of the gases, the surface sites and their interaction with the adsorbing molecules and the nature and interconnectivity of the pore structure. The system for the microporous membranes is shown in Figure 1. This defines much of the fundamental work carried out in this project which was aimed at gaining a greater insight into all of these parameters.

6.2 Appendix 2 Publications

6.2.1 Publications

Bath

Crittenden B, Pererea S, Yang M-Y, Microporous membrane modelling (1999), accepted by J membrane Science

Democritos

Kikkinides E.S., Tzevelekos K.P., Stubos A.K., Kainourgiakis M.E. and Kanellopoulos N.K. "Application of Effective Medium Approximation for the Determination of the Permeability of Condensable Vapours Through Mesoporous Media." *Chem. Eng. Sci*, 52(16) 2837 (1997).
Tzevelekos K.P, Kikkinides E.S., Stubos A.K., Kainourgiakis M.E. and Kanellopoulos N.K. "On the Possibility of Characterizing Mesoporous Materials by Permeability Measurements of Condensable Vapours. Theory and Experiments". *Advances in Colloid and Interface Sci*., in press (1998).
Kainourgiakis M.E., Kikkinides E.S., Stubos A.K. and Kanellopoulos N.K. "Adsorption-Desorption Gas Relative Permeability through Mesoporous Media. Network Modelling and Percolation Theory" *Chem. Eng. Sci.*, in press (1998).

Imperial College

Nicholson, D., *J. Membrane science*, **129**, 209, (1997).
Nicholson, D. *Supramolecular Science*, in press (1998).
Nicholson, D, Carbon, in press (1998).
Nicholson, D., Adams, R. W., Cracknell, R. F. and Papadopoulos, G.K. Proceedings of the 4th IUPAC Symposium on Characterisation of Porous Solids, Royal Society of Chemistry Special Publication No. 213, eds. B. McEnaney, T.J. Mays, J. Rouquerol, F. Rodriguez-Reinoso, K.S.W. Sing and K.K.Unger, 57-64 (1997).
Papadopoulos, G. K. and Nicholson, D, "The concentration dependence of isothermal diffusion in highly confined spaces at very low density" Mol. Simulation
Papadopoulos, G. K. and Nicholson, D. "An investigation of isothermal transport in cylindrical micropores using equilibrium and non-equilibrium molecular dynamics" Mol. Phys.

Leipzig University
Heink, J. Kärger, T. Naylor, U. Winkler: PFG NMR Study of the Transport Properties of A-Type Zeolite Membranes, J. Chem. Soc., Chem. Comm., to be submitted
Heink, J. Kärger, S. Tennison: Pulsed Field Gradient NMR Diffusion Studies with Carbon Molecular Sieves, Carbon, to be submitted
Jobic, H. Ernst, W. Heink, J. Kärger, A. Tuel, M. Bée: Diffusion of Ammonia in Silicalite Studied by QENS and PFG NMR, Microporous and Mesoporous Materials, in press

6.2.2 Presentations

Coordinator
S R Tennison, "Microporous ceramic membranes for energy saving in process industries", ESF network on catalytic membrane reactors - applications and future possibilities, Turnhout October 16017 1997
S R Tennison, "Microporous membranes for gas separation", plenary lecture, European carbon Conference. Newcastle, 7-12July 1996.
S R Tennison, "Ceramic membrane Reactors", plenary lecture - Europacat, Mastricht, September 1996
S R Tennison, "Microporous Ceramic Membranes", CEC Review Meeting, University of Liege, November 1996

Democritos
Kikkinides E.S., Tzevelekos K.P, Romanos G.E., Stubos A.K., and Kanellopoulos N.K. "Theoretical and Experimental Studies on the Permeability of Condensable Vapours in Mesoporous Media" AIDIC Conf. Series, Vol. 3, 109-116 (1997)
Kikkinides E.S., Tzevelekos K.P, Romanos G.E., Stubos A.K., and Kanellopoulos N.K. "Theoretical and Experimental Studies on the Permeability of Condensable Vapours in Mesoporous Media" The First European Congress in Chemical Engineering, Florence, Italy (1997).
Tzevelekos K.P, Kikkinides E.S., Stubos A.K., Kainourgiakis M.E. and Kanellopoulos N.K. "Characterization of Mesoporous Materials by Permeability Measurements of Condensable Vapours. Theory and Experiments" Workshop on Characterization of Porous Materials: from Angstroms to Millimeters, TRI-Princeton, Princeton, NJ, USA (1997).

Imperial College
Conferences attended with material relevant to this project include the following – at least one presentation was given at each of these meetings:
Characterisation of Porous Solids, Bath 1996
Characterisation of Porous materials: from angstroms to millimeters, Princeton, 1997
Nanostructured Materials in Biological and Artificial Systems, (11^{th} Toyota conference, Mikkabi, Japan, 1997
The statistical mechanics of liquids, 6^{th} Liblice conference, Zeledni Rudna, Czechia, 1998
Effects of Surface Heterogeneity in Adsorption and Catalysis, III, Torun , Poland, 1998.
Presentations of aspects of the work have been given at:
The University of Hong Kong,
The University of Chiba,
CNRS, Orleans,
Air Products, Allentown.

The project has also generated collaboration with Prof. S-H Suh (University of Keimyung, Korea) and the following projects:
MSc project ("Effects of adsorbent potential corrugation on diffusion in slit pores") to be completed Sept 1998. (L. Constantini)
Undergraduate project: 1997 "Molecular distributions in confined fluids" (H.L.Windsor)

Leipzig

Bär, H. Jobic, J. Kärger: Diffusion of Hydrogen in Various Zeolites Studied by Pulsed Field Gradient NMR and Quasi-Elastic Neutron Scattering Techniques, Proceedings of the 12th International Zeolite Conference, Baltimore, 1998, in press